THE ROLE OF PYRUVATE DEHYDROGENASE IN CELL GROWTH

APPROVED BY SUPERVISORY COMMITTEE

_____
Ralph J. DeBerardinis, MD, PhD

_____
James F. Amatruda, MD, PhD

_____
Michael S. Brown, MD

_____
Lawrence Lum, PhD

I dedicate this work to my family and friends. These past five years have been very challenging. I couldn't have done it without your support. Thank you so much.

THE ROLE OF PYRUVATE DEHYDROGENASE IN CELL GROWTH

by

KARTIK N. RAJAGOPALAN

DISSERTATION

Presented to the Faculty of the Graduate School of Biomedical Sciences

The University of Texas Southwestern Medical Center at Dallas

In Partial Fulfillment of the Requirements

For the Degree of

DOCTOR OF PHILOSOPHY

The University of Texas Southwestern Medical Center at Dallas

Dallas, Texas

July, 2014

THE ROLE OF PYRUVATE DEHYDROGENASE IN CELL GROWTH

KARTIK N. RAJAGOPALAN

The University of Texas Southwestern Medical Center at Dallas, 2014

Supervising Professor: RALPH J. DEBERARDINIS, MD, PHD

Otto Warburg's observation that tumor cells have increased rates of glucose uptake and lactate secretion in comparison to normal cells spawned his notion that tumors have dysfunctional mitochondria. However, in addition to metabolizing glucose to lactate, tumors *in vivo* exhibit mitochondrial glucose oxidation, indicating activity of pyruvate dehydrognase (PDH), which gates entry of glucose derived carbon into the tricarboxylic acid (TCA) cycle. To test whether cells require glucose oxidation for proliferation, the work in this thesis establishes a model wherein PDH activity is suppressed using RNA interference. Small hairpin RNAs against the transcript encoding the PDHE1α protein were cloned into a retroviral vector which allowed

doxycycline-inducible control of expression. Metabolism of cancer cells was studied *in vitro* using a combination of metabolomics and metabolic flux analysis. Growth in monolayer culture was performed in medium containing lipid-replete serum as well as serum in which lipids had been depleted.

As expected, suppression of PDH activity reduced flow of carbon from glucose to the TCA cycle and to *de novo* fatty acid synthesis. Surprisingly, H460 lung cancer cells could tolerate a 60% reduction of PDH flux without any significant effect on proliferation rate, as long as lipids were present in the medium. Further examination of the effects of PDH silencing on the overall network of central carbon metabolism revealed enhanced channeling of carbon from glutamine to fatty acids and an increase in scavenging free fatty acids. Lipid depletion caused a reduction in growth rate of PDH deficient cells, and this defect was completely rescued by supplying free fatty acids to the medium.

Together the data indicate that proliferating cells exhibit PDH activity that allows transfer of glucose carbon to citrate and the TCA cycle as well as ultimately into fatty acids. Importantly, suppression of PDH activity limits growth in conditions in which cancer cells do not have access to extracellular lipids. This work illustrates that compensatory pathways that sustain cell proliferation are activated during suppression of mitochondrial oxidation of glucose.

TABLE OF CONTENTS

ACKNOWLEDGMENTS

First, I would like to thank the other members of the DeBerardinis Lab. Besides the scientific advice they gave me, their presence in the lab made it a fantastic environment to work in. I would also like to thank the members of the Ge, Morrison, and Zhu Labs and the staff in the metabolomics and FACS core facilities in the Children's Research Institute (CRI) at UT Southwestern Medical Center. They contributed to the energetic environment of the CRI and were always willing to answer scientific questions when asked. Many times all of these people also made it to the CRI First Fridays (social gatherings at a bar conducted on the first Fridays of every month) where I could enjoy a mix of their camaraderie and alcohol to celebrate a scientific breakthrough or mourn a failed experiment (usually the latter).

I would like to begin the work by formally acknowledging everyone who contributed to it. Data and figures from Pei-Hsuan Chen and Christopher Hensley, two other graduate students in the DeBerardinis Lab, were used in the first chapter. Matthew Mitsche created the MATLAB-based software that calculated enrichment in lipogenic acetyl-CoA from palmitate. Maria Calvaruso, a postdoctoral fellow in the DeBerardinis Lab, performed the PDH activity assays. Nicolas Loof, the FACS core facility manager at the CRI, helped me perform many sorts as well as gave me technical advice about sorting. Ajla Wasti, a clinical fellow in the Department of Hematology/Oncology at Children's Medical Center, performed the thin layer chromatography assays. Carlos Rodriguez-Navas, a postdoctoral fellow in the Department of Molecular Genetics, and Jeffrey McDonald, an associate professor in the same department, performed the lipidomics analyses. The delipidated fetal calf serum that was so critical in our

growth assays was given to us by Jin Ye, also an associate professor in the Department of Molecular Genetics. Robert Egnatchik, a postdoctoral researcher in the DeBerardinis Lab, performed the metabolic flux analysis. Jessica Sudderth, the lab manager for the DeBerardinis Lab, helped to isolate the mouse embryonic fibroblasts that are briefly discussed in the closing chapter of this work. Maciek Antoniewicz, an associate professor at the University of Delaware, created the METRAN program used for correction of natural abundance heavy carbon. Last and very importantly, Melih Acar, a postdoctoral fellow in the Morrison Lab, taught me the nuts and bolts of cloning. He also served as a general scientific sounding board, never hesitating to help me or answer one of my questions despite his own busy schedule. This project would not have been possible without his contributions.

I would also like to thank the Medical Scientist Training Program (MSTP) here at UT Southwestern Medical Center. Andrew Zinn, the director of the MSTP, has always been willing to give me career guidance and advice. Robin Downing, the senior administrator for the MSTP, and Stephanie Robertson, a former administrator, have helped me many times with different problems.

Thanks to my thesis committee for all of their advice and guidance. They spent much time and effort attending thesis committee meetings and talking with me about my project. Although all of them manage busy labs, I appreciate their sacrifice in serving on the committee. Thanks Jim Amatruda, Michael Brown, and Lawrence Lum.

Very importantly, I would like to thank my mentor, Ralph DeBerardinis. The past four and a half years spent in Ralph's lab have been very fulfilling. Although it wasn't always easy, I

look in amazement at how much I have learned over this period (both about life and science). This wouldn't have been possible without Ralph's mentoring, guidance, and offering me the opportunity to be a part of his lab. Thanks to Ralph for making my very first step into physician-scientist hood as great as it could have been.

Last and definitely not least, I would like to thank my family and friends. Science is difficult and over the past five years they have offered me an abundance of love and emotional support. They make the energy and time spent searching for a cure to disease worth it. They inspire me to be a better person each day. I am who I am because of them. Thank you.

PRIOR PUBLICATIONS

Marin-Valencia I, Yang C, Mashimo T, Cho S, Baek H, Yang XL, **Rajagopalan KN**, Maddie M, Vemireddy V, Zhao Z, Cai L, Good L, Tu BP, Hatanpaa KJ, Mickey BE, Matés JM, Pascual JM, Maher EA, Malloy CR, Deberardinis RJ, Bachoo RM (2012). "Analysis of tumor metabolism reveals mitochondrial glucose oxidation in genetically diverse human glioblastomas in the mouse brain in vivo." Cell Metab **15**(6): 827-837.

Frezza C, Zheng L, Folger O, **Rajagopalan KN**, MacKenzie ED, Jerby L, Micaroni M, Chaneton B, Adam J, Hedley A, Kalna G, Tomlinson IP, Pollard PJ, Watson DG, Deberardinis RJ, Shlomi T, Ruppin E, Gottlieb E (2011). "Haem oxygenase is synthetically lethal with the tumour suppressor fumarate hydratase." Nature **477**(7363): 225-228.

Rajagopalan, K. N. and R. J. DeBerardinis (2011). "Role of glutamine in cancer: therapeutic and imaging implications." J Nucl Med **52**(7): 1005-1008.

Small EM, Sutherland LB, **Rajagopalan KN**, Wang S, Olson EN (2010). "MicroRNA-218 regulates vascular patterning by modulation of Slit-Robo signaling." Circ Res **107**(11): 1336-1344.

Watanabe M, Yang G, Cao G, Tahir SA, Naruishi K, Tabata K, Fattah EA, **Rajagopalan K**, Timme TL, Park S, Kurosaka S, Edamura K, Tanimoto R, Demayo FJ, Goltsov AA, Thompson TC (2009). "Functional analysis of secreted caveolin-1 in mouse models of prostate cancer progression." Mol Cancer Res **7**(9): 1446-1455.

Yang G, Timme TL, Naruishi K, Fujita T, Fattah el MA, Cao G, **Rajagopalan K**, Troung LD, Thompson TC (2008). "Mice with cav-1 gene disruption have benign stromal lesions and compromised epithelial differentiation." Exp Mol Pathol **84**(2): 131-140.

LIST OF FIGURES AND TABLES

ABBREVIATIONS

3-PG	3-phosphoglycerate
AAA	Amino acid analyzer
ACL	ATP citrate lyase
ALT	Alanine transaminase
AST	Aspartate transaminase
ATP	Adenosine triphosphate
BSA	Bovine serum albumin
CoA	Coenzyme A
DAPI	4’6-diamidino-2-phenylindole
DCA	Dichloroacetate
DFCS	Delipidated fetal calf serum
DHAP	Dihydroxyacetone-phosphate
DMEM	Dulbecco’s Modified Eagle Medium
ETC	Electron transport chain
FACS	Fluorescence Activated Cell Sorting
FBS	Fetal bovine serum
FCS	Fetal calf serum
FDG-PET	Fluorodeoxyglucose positron emission tomography
FH	Fumarate hydratase
GC	Gas chromatography
GLS	Glutaminase
HRP	Horseradish peroxidase
HPLC	High-pressure liquid chromatography

IDH	isocitrate dehydrogenase
INCA	Isotopomer network compartmentalized analysis
ISA	Isotopic spectral analysis
KEGG	Kyoto encyclopedia of genes and genomes
LC	Liquid chromatography
LCFA	Long-chain fatty acid
LDH	Lactate deyhydrogenase
NAD	Nicotinamide adenine dinucleotide
NADP	Nicotinamide adenine dinucleotide-phosphate
MDH	Malate dehydrogenase
ME	Malic enzyme
MEF	Mouse embryonic fibroblast
MFA	Metabolic flux analysis
MID	Mass isotopomer distribution
MS	Mass spectrometry
PBS	Phosphate-buffered saline
PC	Pyruvate carboxylase
PDC	Pyruvate dehydrogenase complex
PDH	Pyruvate dehydrogenase
PDK	Pyruvate dehydrogenase kinase
PDP	Pyruvate dehydrogenase phosphatase
PEP	Phosphoenolpyruvate
PK	Pyruvate kinase
ROS	Reactive oxygen species

SHRNA	Small-hairpin RNA
TCA	Tricarboxylic acid
TLC	Thin layer chromatography

CHAPTER 1

BACKGROUND AND OBJECTIVE

1.1 Introduction

One of the emerging hallmarks of cancer is an altered metabolic state that enables growth and proliferation of the cancer cell (Hanahan and Weinberg 2011) . Glycolysis and the TCA cycle are two metabolic pathways furnish cells with the ability to catabolize glucose both to fuel ATP production and very importantly, to use it as a carbon source to synthesize various macromolecules (DeBerardinis, Lum et al. 2008). Specifically, oxidative metabolism of glucose by the TCA cycle generates ATP more efficiently than glycolysis and also is the major route for the *de novo* synthesis of lipids and certain amino acids (Deberardinis, Sayed et al. 2008). Because proliferation levies increased demands for energy and biomass on the dividing cell (Cantor and Sabatini 2012), robust function of the TCA cycle would seem essential for tumor proliferation. In this introductory chapter, I briefly discuss glycolysis and the TCA cycle and its role in energy generation and macromolecular synthesis. I then focus on PDH and its role in these pathways. I then briefly survey the current literature to discuss the different viewpoints regarding PDH and oxidative metabolism in cancer. I end with discussing my main goal in conducting these studies as well as an outline of the subsequent chapters.

1.2 Glycolysis and the TCA Cycle

The metabolic network in humans is extremely complicated and encompasses various chemical reactions that produce energy and biomass needed for growth. At the core of these

reactions are glycolysis and the TCA cycle, which catabolize glucose in order to generate ATP and carbon backbones for the synthesis of macromolecules. Although difficult to display clearly due to its complexity, glycolysis and the TCA cycle and their location at the core of intermediary metabolism in humans is depicted in figure 1.1.

Glycolysis is the set of reactions that begins with glucose and yields two molecules of pyruvate in addition to net production of two ATP and two molecules of reduced nicotinamide adenine dinucleotide (NAD), or NADH. Besides converting glucose to pyruvate and producing energy, glycolysis generates intermediates that serve as branch points for other important metabolic reactions. In the first step of glycolysis, glucose-6-phosphate is created from glucose by the enzyme hexokinase. Glucose-6-phoshpate can then be metabolized further in glycolysis to yield fructose-6-phosphate or can enter the pentose phosphate pathway, which is important for creating reducing equivalents in the form of reduced nicotinamide adenine dinucleotide-phosphate (NADP), also called NADPH, and 5-carbon sugars to serve as the backbones of nucleotides. Further down the pathway, dihydroxyacetone-phosphate (DHAP) can be converted to glycerol to create the backbone of lipids. Lastly, 3-phosphoglycerate can be converted to serine and glycine, amino acids involved in protein and nucleotide biosynthesis.

The pyruvate that is generated from glycolysis is oxidatively decarboxylated by pyruvate dehydrogenase (PDH) in an irreversible reaction to yield acetyl-CoA, which then condenses with oxaloacetate to yield citrate in the citrate synthase reaction, the first step of the TCA cycle. Very importantly, much like glycolysis, intermediates of the TCA cycle are drawn off for synthesis of different macromolecules. This process is called *cataplerosis.* Citrate is exported from the mitochondria to the cytosol where it undergoes the ATP citrate lyase (ACL) reaction

and yields cytosolic acetyl-CoA and oxaloacetate, which can rejoin the TCA cycle. The acetyl-CoA is used for the synthesis of palmitate, the long chain fatty acid (LFCA) that serves as a precursor to other fatty acids. At another part of the TCA cycle, succinyl-CoA, which is made from α-ketoglutarate in the α-ketoglutarate dehydrogenase reaction is drawn off to synthesize heme. Lastly, oxaloacetate leaves the cycle and can be transaminated by aspartate transaminase (AST) to make aspartate, which is used for protein and nucleotide biosynthesis.

Because so many intermediates in the TCA cycle are drawn off to aid in macromolecule synthesis, glutamine, the most abundant amino acid in the human bloodstream, is converted to α-ketoglutarate through the sequential reactions of glutaminase (GLS) and glutamate dehydrogenase (GDH), alanine transaminase (ALT), or AST. The molecule of α-ketoglutarate that is produced can then join the TCA cycle to replenish lost carbon in a process called *anaplerosis* (Rajagopalan and DeBerardinis 2011). The biosynthetic processes that originate from intermediates of the TCA cycle as well as glutamine anaplerosis that replenishes lost carbon is depicted in figure 1.2.

In addition to synthesizing precursors for different macromolecules, oxidation of acetyl-CoA creates three molecules of NADH, one molecule of $FADH_2$, and one molecule of GTP. Because the NADH and $FADH_2$ donate their electrons to the electron transport chain (ETC), oxidation of each acetyl-CoA molecule ultimately yields a significant amount of ATP.

1.3 Pyruvate Dehydrogenase

Pyruvate dehydrogenase is a multi-subunit enzyme complex (referred to as both PDH and PDH complex throughout the dissertation) that catalyzes the oxidative decarboxylation of

pyruvate to yield one molecule of acetyl-CoA, one molecule of carbon dioxide, and NADH. This enzyme complex and its components will be explored in greater detail in chapter 3.

The importance of the PDH reaction in the context of glycolysis and the TCA cycle is that it is the branch point of aerobic and anaerobic metabolism of the pyruvate molecule. In the absence of oxygen, pyruvate is converted to lactate; and in the presence of oxygen, pyruvate is converted to acetyl-CoA which is oxidized in the TCA cycle. If the pyruvate is converted to lactate by lactate dehydrogenase (LDH), NADH is oxidized to NAD+, which can then serve as an electron acceptor for the reaction catalyzed by glyceraldehyde-3-phosphate dehydrogenase, thus allowing glycolysis to continue in an anoxic environment. In the presence of oxygen, aerobic metabolism of pyruvate takes place and the NADH produced from glycolysis normally donates its electrons to the ETC. Additionally, acetyl-CoA is produced from the PDH reaction and joins the TCA cycle to undergo oxidative metabolism.

As depicted in figure 1.3, the difference between these two fates of pyruvate is not at all insignificant bioenergetically and in terms of macromolecular synthesis. Although conversion of pyruvate to lactate is important for the continuation of glycolysis in the absence of oxygen, it only yields two molecules of ATP per each glucose molecule consumed. However, if the pyruvate molecule undergoes the PDH reaction to yield acetyl-CoA which is subsequently oxidized through the TCA cycle, approximately 30 molecules of ATP are produced and various macromolecules can be synthesized. This makes oxidative metabolism of glucose far more beneficial for the cell in an environment in which the oxygen supply is adequate.

Because the carbon flux through PDH complex is so closely tied to the bioenergetic and biosynthetic needs of the cell, its activity is tightly regulated by substrates and products of the

reaction and also by the cellular energy state. The pyruvate dehydrogenase reaction is almost exclusively regulated post-translationally by a group of four pyruvate dehydrogenase kinases (PDKs), whose isoform expression is tissue specific. The PDKs phosphorylate the E1α subunit of the pyruvate dehydrogenase complex to suppress its activity. Activity of the PDKs are positively regulated by products of the PDH reaction, acetyl-CoA and NADH, which indirectly suppress carbon flux through the complex. On the other hand, activity of the PDKs are inhibited by high levels of pyruvate as well as low energy states, such as high ADP/ATP or NAD+/NADH ratios, which indirectly increase the activity of the complex. There are two isoforms of pyruvate dehydrogenase phosphatases (PDPs), which de-phosphorylate the E1α subunit and increase activity of PDH. The PDPs are upregulated by insulin, calcium ion concentration, and are inhibited by NADH (Patel and Korotchkina 2006). The other major regulation of the PDH complex occurs during hypoxia. Hif1α is stabilized in low oxygen environments and transcriptionally upregulates PDK1, which suppresses PDH activity (Kim, Tchernyshyov et al. 2006) . Thus, low oxygen suppresses PDH and shunts pyruvate towards fermentation rather than oxidation.

1.4 PDH and Cancer

As explained previously, the PDH reaction allows carbons from glucose to enter the TCA cycle. Oxidation of pyruvate by the TCA cycle rather than its fermentation to lactate allows generation of far greater amounts of ATP per glucose molecule consumed as well as use of this carbon to synthesize fatty acids, heme, and amino acids through cataplerosis. Therefore, it would seem advantageous for a proliferating cell, which has greater biosynthetic and energetic demands (Cantor and Sabatini 2012), to oxidize carbon derived from glucose rather than

ferment it to lactate. Specifically, as cancer is a disease of rapid cellular proliferation, it would seem likely that cancer cells have robust PDH activity.

However, Warburg's earliest observations of ascites tumors cells illustrated that they had enhanced glucose uptake and lactate secretion in comparison to their normal counterparts (Warburg 1956). Now dubbed the Warburg effect, this form of metabolism is aerobic glycolysis, or fermentation of glucose to lactate at normal oxygen concentrations (Dang 2012). It has been hypothesized that cancer cells exhibit aerobic glycolysis in an effort to synthesize non-essential amino acids from glucose carbon as well as NADPH for fatty acid biosynthesis, both side reactions upstream of glycolysis (Vander Heiden, Cantley et al. 2009). Certain groups argue that suppression of glucose oxidation is important in resistance to apoptosis in human glioblastomas *in vivo* (Michelakis, Sutendra et al. 2010). Dichloroacetate (DCA), which is an inhibitor of PDK2 that would act to indirectly activate oxidative metabolism of glucose, has been touted as a therapy to decrease proliferation of a variety of cancers (Sutendra and Michelakis 2013). In essence, recent research in cancer metabolism has shifted towards examination of aerobic glycolysis in cancer (Zu and Guppy 2004) with less emphasis placed on other possible fates of glucose, such as its oxidation.

Stable isotope tracing (discussed in the next chapter) in combination with analytical modalities, such as NMR or GC-MS, can identify the fate of the glucose carbon once inside the cell rather than simply being able to track its fermentation to lactate. Observations made by these methods illustrated that rather than complete fermentation of glucose to lactate, both human glioblastomas implanted orthotopically in mice as well as human brain tumors *in vivo* display mitochondrial oxidation of glucose carbon thus indicating activity of the PDH complex

(Maher, Marin-Valencia et al. 2012, Marin-Valencia, Yang et al. 2012). Additionally, unpublished results from the DeBerardinis Lab, depicted in figure 1.4 illustrate that a wide variety of non-small cell lung cancer lines display glucose oxidation. More importantly, other unpublished work from the lab has shown that FDG-PET positive human lung tumors have higher *in vivo* glucose entry into the TCA cycle than surrounding normal lung tissue (figure 1.5). Based on these observations that tumors *in vitro* and *in vivo* display mitochondrial glucose oxidation, it is plausible that PDH is active in cancer and more importantly, might be required for proliferation as the TCA cycle is a source of macromolecules for proliferation (Deberardinis, Sayed et al. 2008).

1.5 Statement of Purpose

Recent studies of tumor metabolism have centered upon the Warburg effect, the observation that cancer cells take up more glucose and secrete more lactate than their counterparts at normoxia. While the Warburg effect, or an upregulation of glycolytic flux, underlies the utility of FDG-PET in localizing tumor growth, it doesn't explain how cancer cells synthesize the macromolecules needed for rapid cell division. Exclusively focusing on upregulation of glycolysis in cancer cell metabolism ignores the role that PDH might play in allowing for glucose to undergo oxidative metabolism. I designed these experiments to further understand the role that PDH plays in rapidly proliferating cells in terms of regulating carbon flux and to determine whether PDH activity is essential for proliferating cells.

To begin this project, I used the cell line H460, a large cell lung cancer cell line, which rapidly proliferates in culture. I performed various metabolic assays, which included metabolomics and stable isotope tracing in combination with GC-MS, during periods of cell

proliferation. Using this technology, I was able to trace carbon flux into lactate as well as the TCA cycle, lipids, and certain amino acids. These experiments were the first in my series of experiments and are described in Chapter 2.

After I determined that glucose carbon could be traced into not only lactate but most importantly, the TCA cycle, as well as lipids, I sought to devise a system whereby I could abrogate PDH activity and then assay the metabolic ramifications. To this end, using molecular biology, I cloned a series of plasmids that contained inducible small-hairpin RNAs against the transcript that encoded for a subunit of PDH. As described in chapter 3, I then studied the metabolic and growth alterations induced in these cells when PDH activity was suppressed.

Because I found that there was no growth suppression in H460 cells with suppression of PDH, I began chapter 4 by determining whether these cells had activated compensatory pathways to sustain proliferation rates. When I determined that free fatty acid uptake was increased when PDH was suppressed, I cultured cells in conditions without lipids to see if I could elicit a growth defect under PDH suppression.

In the last chapter, I determined whether glutamine could supply carbon for fatty acid biosynthesis during PDH suppression. The glucose tracer data from chapter 3 and the glutamine tracer data from were modeled using metabolic flux analysis (MFA) to determine which accessory pathways were active that could shunt glutamine derived carbon to fatty acid synthesis.

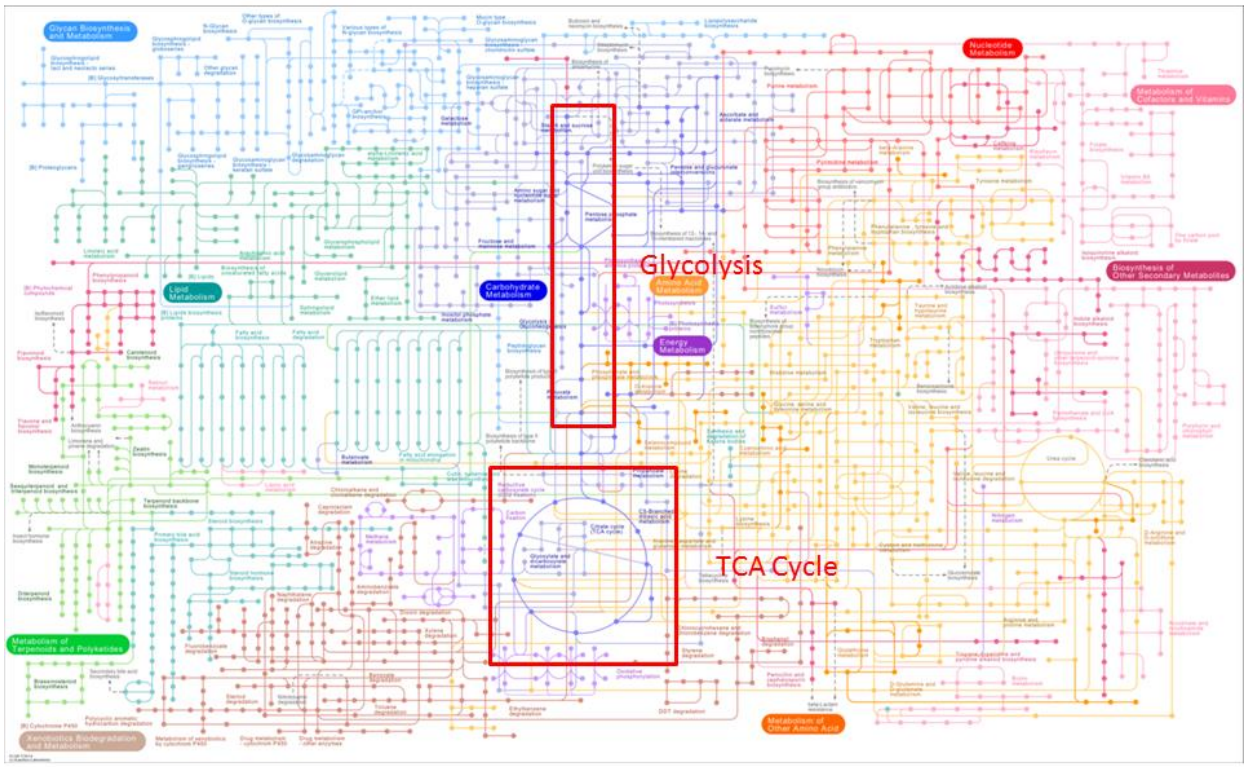

Figure 1.1 Glycolysis and the TCA cycle are at the center of intermediary metabolism. The figure is a map of metabolism in humans. The points represent different metabolites, and the lines represent different metabolic reactions. Glycolysis and the TCA cycle are highlighted by red boxes. Figure adapted from the Kyoto Encyclopedia of Genes and Genomes (KEGG).

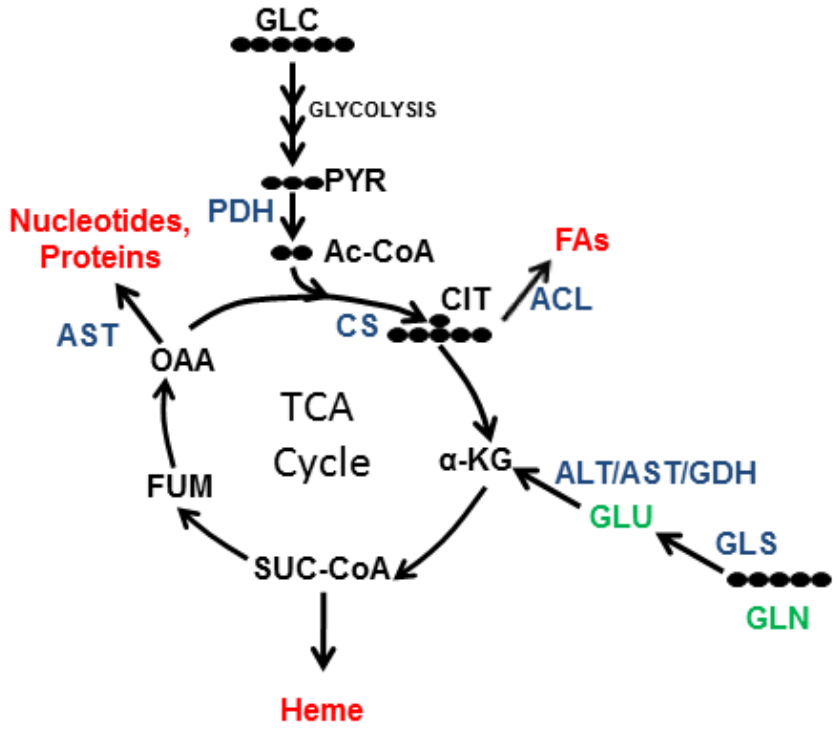

Figure 1.2 Glutamine anaplerosis replaces carbon in the TCA cycle lost to various biosynthetic processes. The schematic shows glucose entering the TCA cycle through the PDH reaction. Citrate, succinyl-CoA, and oxaloacetate are drawn off to participate in fatty acid, heme, and nucleotide/protein synthesis respectively. Carbon derived from glutamine enters the TCA cycle as α-ketoglutarate to replace carbon lost to biosynthetic processes. Enzymes are depicted in blue, products of cataplerotic reactions in red, and anaplerotic substrates are depicted in green. *Abbreviations*: α-KG, α-ketoglutarate; ACL, ATP-citrate lyase; Ac-CoA, acetyl-CoA; ALT, alanine transaminase; AST, aspartate transaminase; CIT, citrate; CS, citrate synthase; FUM, fumarate; GDH, glutamate dehydrogenase; GLN, glutamine; GLS, glutaminase; GLU, glutamate; PYR, pyruvate; SUC-CoA, succinyl-CoA.

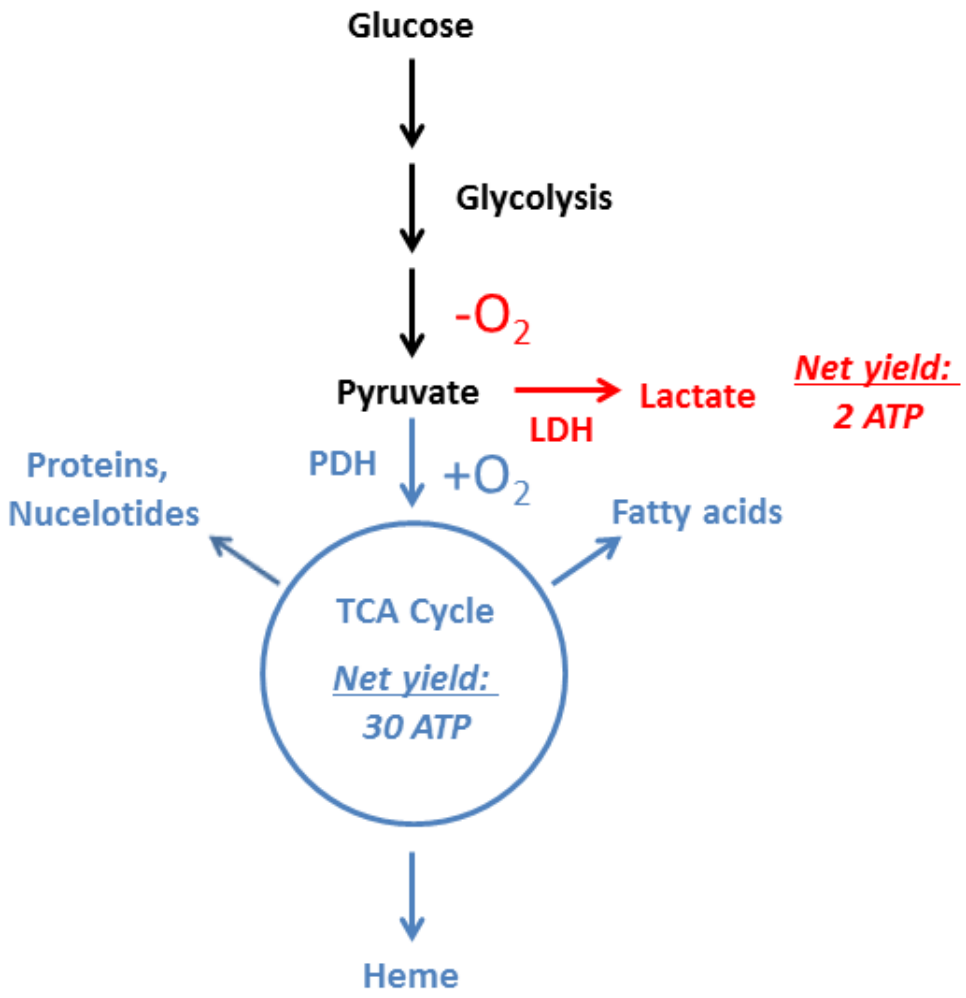

Figure 1.3 The PDH reaction is a major branch point in the metabolism of glucose. The schematic illustrates the PDH complex gating pyruvate's oxidation in the TCA cycle. In addition to the intermediates produced by the TCA cycle for biosynthetic processes, oxidation of pyruvate (blue) is far more energy efficient and allows greater macromolecule production than fermenting it to lactate (red). The path of pyruvate is typically dependent on oxygen availability: high (blue) is oxidation and low (red) is fermentation. *Abbreviations*: ATP, adenosine triphosphate; LDH, lactate dehydrogenase; PDH, pyruvate dehydrogenase; TCA, tricarboxylic acid.

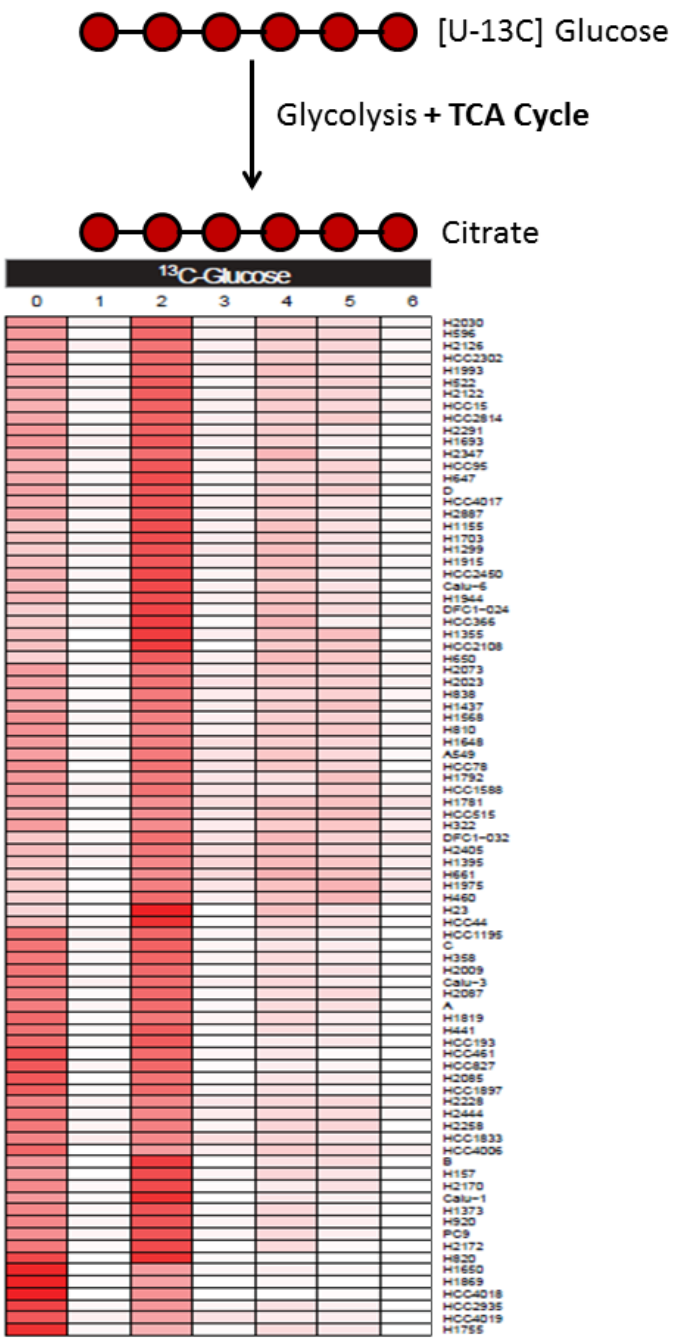

Figure 1.4 Non-small cell lung cancer (NSCLC) cell lines all display derivation of citrate from glucose carbon. The isotope enrichment heat map above displays 6 columns, which are the 6 possible masses of citrate if cells are incubated with [U-^{13}C] (uniformly labeled) glucose. Darker shade of red in the heatmap indicates a larger percentage of a particular weight. As illustrated, all NSCLC lines contain a proportion of two labeled carbons indicating conversion of carbon originally derived from glucose to citrate. Data and figure from Pei-Hsuan Chen.

A

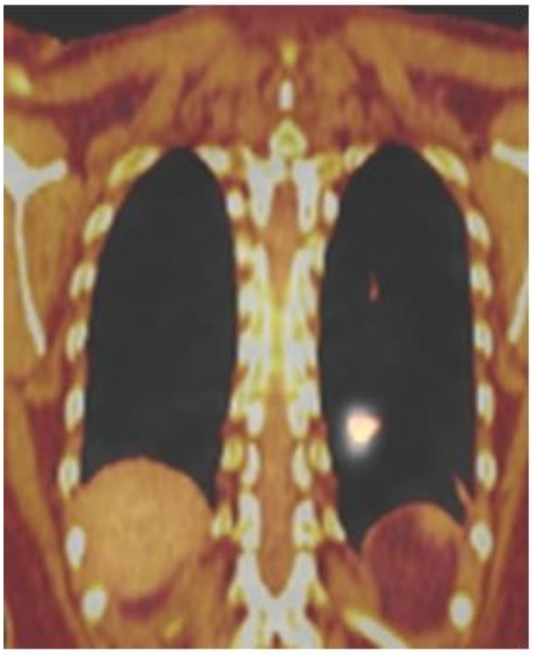

B

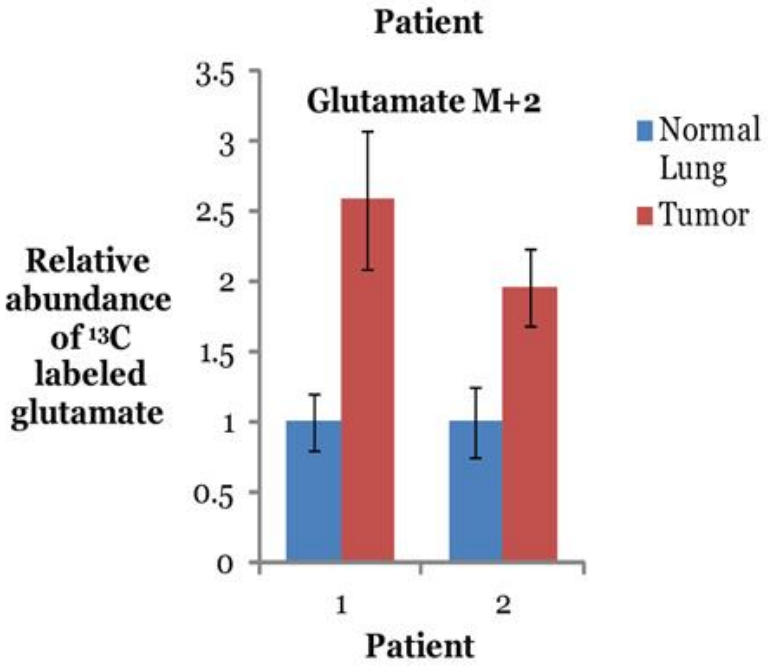

Figure 1.5 Human lung tumors display increased entry of glucose carbon into TCA cycle compared to normal lung. (A) Representative image of FDG-PET positive lung tumor. **(B)** Lung tumors in two patients show increased abundance of glutamate derived from glucose carbon in comparison to normal lung tissue. Data and figure from Christopher Hensley.

CHAPTER 2

ANALYSIS OF GLUCOSE OXIDATION IN PROLIFERATING CANCER CELLS

2.1 Introduction

The main objective of this series of experiments was to determine whether there was a metabolic activity in proliferating cells that could be assigned to PDH. In order to test this, I first performed metabolic flux experiments on H460, a rapidly proliferating large cell lung cancer line, by growing it in the presence of isotopically labeled glucose or glutamine. Then, by analyzing cellular metabolites using GC-MS, I sought to determine the metabolic pathways being used by the cancer cells during periods of proliferation.

To provide a very basic metabolic characterization of the cells, I profiled the cell medium for glucose, lactate, glutamine, and glutamate content. As glucose and glutamine are the carbon sources that are most avidly consumed by cells proliferating *in vitro*, this profiling aids in determining the amount that is consumed. Additionally, byproducts of glucose and glutamine metabolism, lactate and glutamate respectively, are secreted in the process. Profiling consumed and secreted metabolites, as illustrated in the schematic in figure 2.2, is critical for characterizing the metabolic nature of the cell.

Stable isotope tracing uses isotopically labeled carbon substrates, which, in this case, are glucose and glutamine. After cells are incubated with specific tracers for a given period of time, metabolites are extracted from the cells and analyzed. In the GC-MS analysis, cellular metabolites are first separated between mobile (helium) and stationary (fused silica coated

with phenyl-methyl polysiloxane) phases. Based on the affinity of the metabolite for the mobile and stationary phases, the metabolite is eluted from the column into an ion mass detector at a certain time point. The mass detector then fragments each metabolite and determines an m/z (mass/charge) ratio for each ion entering the detector at a specific time. Metabolites whose carbons are derived from heavy glucose or glutamine have an increased m/z ratio. The identity of the metabolite is determined based on the analysis of a pure standard on the GC-MS. An example of a chromatogram and mass isotopomer distribution (MID) of citrate that results when cells are incubated with uniformly labeled glucose is depicted in figure 2.1. By examining the MIDs of various metabolites when cells are cultured with heavy glucose or glutamine, one can understand which metabolic pathways might be active.

Two schematics that illustrate the movement of heavy carbon when cells are labeled with glucose or glutamine are depicted in figures 2.3 and 2.5 respectively. As illustrated by the schematic, an M+2 (increase in two mass units) in citrate when cells are incubated with uniformly labeled glucose (glucose with all ^{13}C) indicates movement of two carbons from glucose into citrate. An M+3 in lactate indicates that three heavy carbons are transferred from glucose to lactate. These MIDs in citrate and lactate are representative of oxidative and fermentative metabolism of glucose respectively. As will become evident, my stable isotope experiments in this chapter illustrated a putative PDH flux of cancer cells proliferating *in vitro*. This then necessitated the creation of genetic tools to manipulate PDH flux to determine metabolic and proliferative changes, experiments which are described in chapter 3.

2.2 Methods

2.2.1 Cell Culture

Cells were passaged in high-glucose D5796 Dulbecco's Modified Eagle Medium (DMEM) supplemented with 2 mM glutamine (to a total of 6 mM), penicillin/streptomycin, and 5% fetal bovine serum (FBS) all from Hyclone.

2.2.2 Metabolic Flux Experiments

2 million H460 cells were plated in 10 cm tissue culture dishes and 12-24 hours later, when cells had reached the appropriate confluence, they were incubated in [U-^{13}C] (uniformly labeled) glucose and unlabeled glutamine at concentrations of 10 mM for glucose and 4 mM for glutamine. Labeling media was formulated from DMEM base powder (purchased from Sigma) supplemented with 5% dialyzed FBS and penicillin/streptomycin. Stable isotope tracing experiments took place for 24 hours, ensuring that glucose and glutamine were in abundant supply. Media was collected to analyze metabolite consumption and secretion. At the end of the experiment, cellular metabolites were extracted using the Bligh-Dyer extraction method using a combination of .1 % Triton-X 100 and 2:2:1 Methanol: Chloroform: Water. Both aqueous and organic phases were isolated. 100 nanomoles of 2-sodium oxobutyrate were added to the aqueous phase to serve as an external standard. Both phases were concentrated at 42 degrees C under blown air.

2.2.3 Protein Content of Cell Extracts

Protein content of cell extracts was measured by a microtiter Pierce BCA protein assay kit purchased from ThermoScientific using bovine serum albumin (BSA) as a standard.

2.2.4 GC-MS Analysis of Organic Phase

After being concentrated, cellular contents from the organic phase were derivatized using acetyl chloride and a 4:1 mixture of toluene and methanol with .01% butylated hydroxytoluene. Samples were heated for 1 hour at 100 degrees C. Organic phase was then re-extracted using 5% potassium carbonate. 1 ul of organic phase was injected into an Agilent -6970 gas chromatograph connected to an Agilent 5973 mass selective detector (hereafter referred to as GC-MS). A method specific for analyzing long chain fatty acids (LCFAs) was used.

2.2.4 GC-MS Analysis of Aqueous Phase

After being concentrated, cellular contents from the aqueous phase were derivatized using 100 uL of trimethylsilane from ThermoScientific. Samples were heated to 42 degrees C for 30 minutes during derivatization. 5 uL of derivatized sample was then injected and analyzed by GC-MS using a method specific to metabolites retained in the aqueous phase.

2.2.5 Software Analysis of Mass Spectra

Mass spectra generated by GC-MS were analyzed by ChemStation from Aglient. METRAN, a program developed by a collaborator, Maciek Antoniewicz, was used to correct spectra for natural abundance of heavy carbon.

2.2.6 Media Analysis

Media was analyzed for glucose, lactate, glutamine, and glutamate content using a NOVA BioProfile Basic-4 Analyzer. Amino acid content of media was analyzed using high-pressure liquid chromatography (HPLC) by an L8900 Amino Acid Analyzer (AAA) from Hitachi.

2.3 Results

2.3.1 Foreword

Metabolic experiments conducted throughout the dissertation were conducted for 24 hours as this was observed to be the approximate doubling time of H460 cells at which most metabolic fluxes would have most likely reached steady state.

2.3.2 Proliferating H460 Cells Consume Glucose and Glutamine and Secrete Lactate and Glutamate

As depicted in figure 2.6(A), over 24 hours of culture H460 cells consume approximately 60 µmoles of glucose and secrete approximately 120 µmoles of lactate. The ratio of µmoles lactate secreted over µmoles glucose consumed is very close to two. Additionally, figure 2.7(A) illustrates that almost 100% of the lactate pool is labeled when incubated with uniformly labeled glucose. This indicates that the lactate is almost exclusively derived from glucose carbon. These data taken together show that the vast majority of glucose consumed by H460 cells is secreted as lactate, as total fermentation of 1 mole of glucose would equal two moles of lactate. The reason for the glucose labeling of lactate being just under 100% is likely because glutamine carbon is also contributing to lactate formation. This conversion occurs through a series of steps beginning with glutamine that is consumed (shown in figure 2.6(B)) being

metabolized by the TCA cycle to malate. The malate then exits the TCA cycle and is acted on by malic enzyme (ME). This converts malate into pyruvate which is then converted to lactate by LDH. This allows for a very small production of lactate from carbon derived from glutamine. Lastly, figure 2.5(B) also illustrates that H460 cells secrete glutamate. Glutamate is produced from deamidation of glutamine by GLS (illustrated in figure 2.1) and also by AST and ALT which transaminate α-ketoglutarate from aspartate or alanine respectively.

2.3.2 Proliferating H460 Cells Display Labeling of TCA Cycle Intermediates from Glucose

H460 cells were labeled with [U-^{13}C] glucose for twenty-four hours. Although the vast majority of glucose carbon goes into lactate production, analysis of TCA metabolites by GC-MS revealed that citrate, succinate, fumarate, and malate all contained carbon that was derived from glucose. In fact, as depicted in figure 2.7(A), almost 80% of the carbon in the citrate pool was derived from glucose. As pyruvate dehydrogenase is the penultimate enzyme that allows derivation of citrate from glucose carbon, these GC-MS data suggest its activity. A smaller portion of the succinate, malate, and fumarate pools were derived from glucose. The decrease in the derivation of these pools from glucose is likely due to glutamine anaplerosis. As depicted in figure 2.1, glutamine derived carbon enters the TCA cycle at the α-ketoglutarate level. These GC-MS data along with the glutamine consumption data from figure 2.6(B) indicate that H460 cells use glutamine as an anaplerotic substrate.

2.3.3 Proliferating H460 Cells Display Labeling of Palmitate from Glucose

As depicted in figure 2.7(B), glucose also labels palmitate during a 24 hour period in H460 cells. The MID of palmitate indicates a wide variety of isotopomers, from M+0

(unlabeled) to M+16 (fully labeled). The significance of this mass isotopomer distribution is illustrated in the schematic in figure 2.4. The ACL reaction cleaves off acetate from citrate which is then used to construct the carbon backbone of palmitate. When cells are incubated in [U-^{13}C] glucose, if labeled acetyl-CoA is condensed with oxaloacetate to make citrate, each acetyl-CoA that is derived from citrate M+2 through the ACL reaction is labeled. As depicted in the palmitate labeling data, only a minority of the palmitate molecules in the H460 cells lack any label. This indicates that the majority of palmitate is synthesized *de novo* and contains at least one acetate molecule that is derived initially from glucose carbon. Also importantly, approximately 5% of the palmitate molecules are M+16. This isotopomer of palmitate is totally derived from glucose carbon through multiple labeled citrates undergoing the ACL cleavage reaction, liberating labeled acetate for palmitate synthesis. This MID in palmitate also indicates PDH activity suggested by the labeling in citrate. The program that mathematically models fatty acid synthesis devised by Matthew Mitsche, calculated that approximately 73 % of the lipogenic acetyl-CoA carbon is derived from glucose.

2.3.4 Proliferating H460 Cells Display Labeling of TCA Cycle Intermediates from Glutamine

As displayed in figure 2.8(A), when H460 cells were incubated with unlabeled glucose and [U-^{13}C] glutamine for 24 hours, the majority of all pools of TCA cycle intermediates were labeled. As discussed earlier, only the minority of TCA cycle intermediates succinate, fumarate, and malate are derived from glucose carbon. The opposite is true for glutamine—this result confirms that glutamine anaplerosis accounts for the vast majority of carbon downstream of α-

ketoglutarate. Additionally, four carbons of the citrate molecule are derived from oxaloacetate (downstream of α-ketoglutarate), which accounts for the high labeling of citrate by glutamine.

2.3.5 Proliferating H460 Cells Display Labeling of Palmitate from Glutamine

As illustrated by figure 2.8(B), glutamine carbon does label palmitate; however, the labeling is far lower than glucose labeling of palmitate. The M+16 ion comprises approximately .1% of the palmitate pool (versus 5% when labeled with [U-^{13}C] glucose. Taking into account the entire labeling distribution, this corresponds to glutamine contributing only approximately 22% of lipogenic acetyl-CoA. This large difference highlights the major derivation of lipogenic acetyl-CoA from glucose carbon, and not glutamine. However, the glutamine that does contribute to palmitate can do so through potentially two avenues: (1) a combination ME and PDH activity or (2) reductive carboxylation. ME converts malate to pyruvate, which is then converted to acetyl-CoA by PDH. The acetyl-CoA would condense with oxaloacetate to make citrate and undergo the ACL reaction. This pathway for palmitate labeling from glutamine would require PDH. The other way would be if α-ketoglutarate derived from glutamine were carboxylated by IDH to citrate. The citrate would then undergo the ACL reaction to make lipogenic acetyl-CoA. This second pathway would not require PDH.

2.4 Discussion

The experiments in this chapter were designed in order to determine whether H460 cells proliferating *in vitro* oxidized glucose. The results in this chapter illustrate that although rapidly proliferating cells ferment a large majority of their glucose to lactate, they transfer glucose carbon to the TCA cycle. This notion is exemplified by the stable isotope tracing experiments in glucose carbon transfers its label to the citrate, succinate, fumarate, and malate pools. Additionally, the results also indicated that proliferating cells synthesize palmitate *de novo* from glucose. ACL is the enzyme that generates lipogenic acetyl-CoA from citrate, which is a product of glucose oxidation. Thus, glucose labeling in palmitate also indirectly indicates oxidation of glucose rather than complete fermentation.

The experiments also indicate that proliferating H460 cells use glutamine for anaplerosis. This is indicated by a minority of the succinate, fumarate, and malate pools being derived from glucose carbon while the vast majority of these pools is derived from glutamine carbon. The TCA metabolites are downstream of α-ketoglutarate, which is the site of entry of glutamine derived carbon. Additionally, glutamine anaplerosis also underlies the small fraction of palmitate that is synthesized from glutamine derived carbon. Malate exits the TCA cycle and is converted to pyruvate by malic enzyme, which then enters the TCA cycle and becomes lipogenic acetyl-CoA.

Irrespective of the result that the vast majority of glucose carbon is fermented to lactate rather than oxidized, it is interesting to test whether oxidation of glucose carbon is required for proliferation. The best characterized enzyme that is involved in conversion of glucose derived

carbon into citrate is PDH. Hence, because the experiments in this chapter illustrate that glucose derived carbon is incorporated into citrate and ultimately palmitate, there is a high likelihood that PDH is active in rapidly proliferating H460 cells. Thus, the experiments in the next chapter describe using genetic methods targeting the PDHA1 transcript that encodes for the subunit that catalyzes the rate-limiting reaction of the PDH complex. These studies are designed to conclusively determine whether the glucose oxidation described in this chapter is mediated by PDH and if so, whether abrogating this reaction has any consequences for cell proliferation.

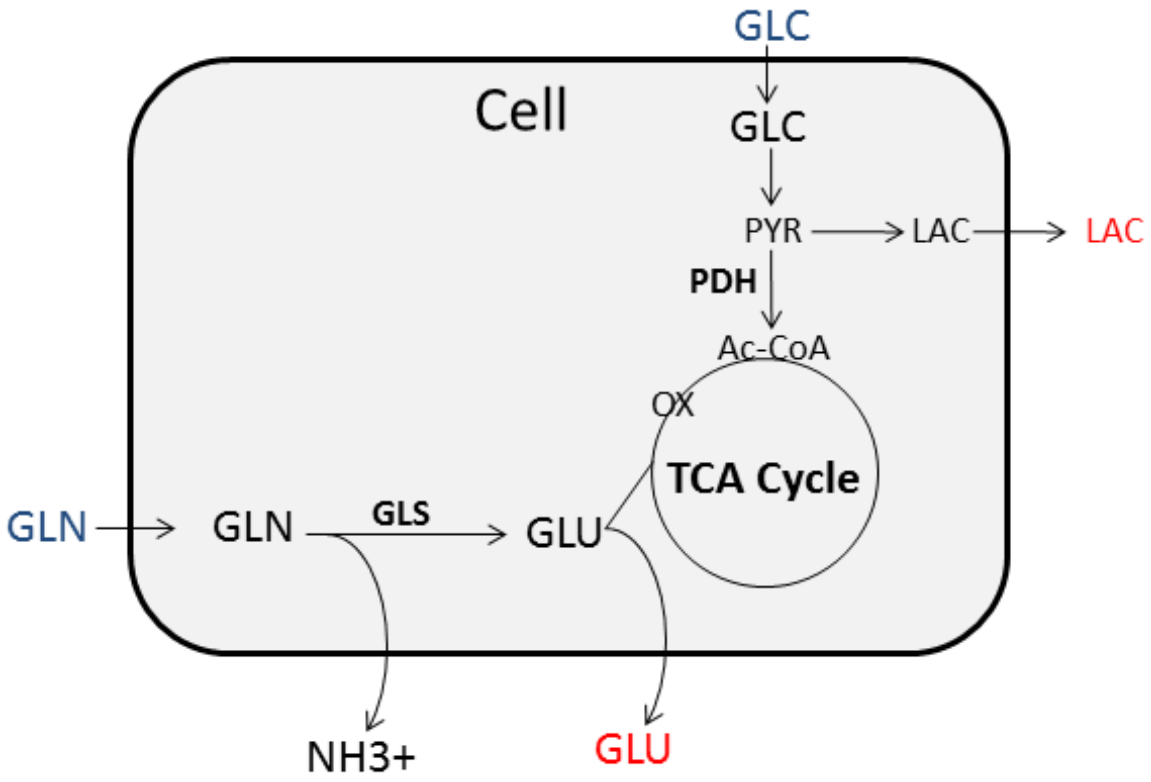

Figure 2.1 Glucose and glutamine metabolism. Glucose that is metabolized to pyruvate can be fermented to lactate by LDH and secreted or decarboxylated by PDH to make acetyl-CoA, which is condensed with oxaloacetate to make citrate in the TCA cycle. Glutamine is deamidated by GLS to make glutamate, which can either be secreted or provide carbon to the Krebs cycle in a process called anaplerosis. Net consumption of metabolites in blue and net secretion of those in red. Abbreviations: Ac-CoA, acetyl-CoA; CIT, citrate; GLC, glucose; GLN, glutamine; GLS, glutaminase; GLU, glutamate; OX, oxaloacetate; PYR, pyruvate; TCA, tricarboxylic acid.

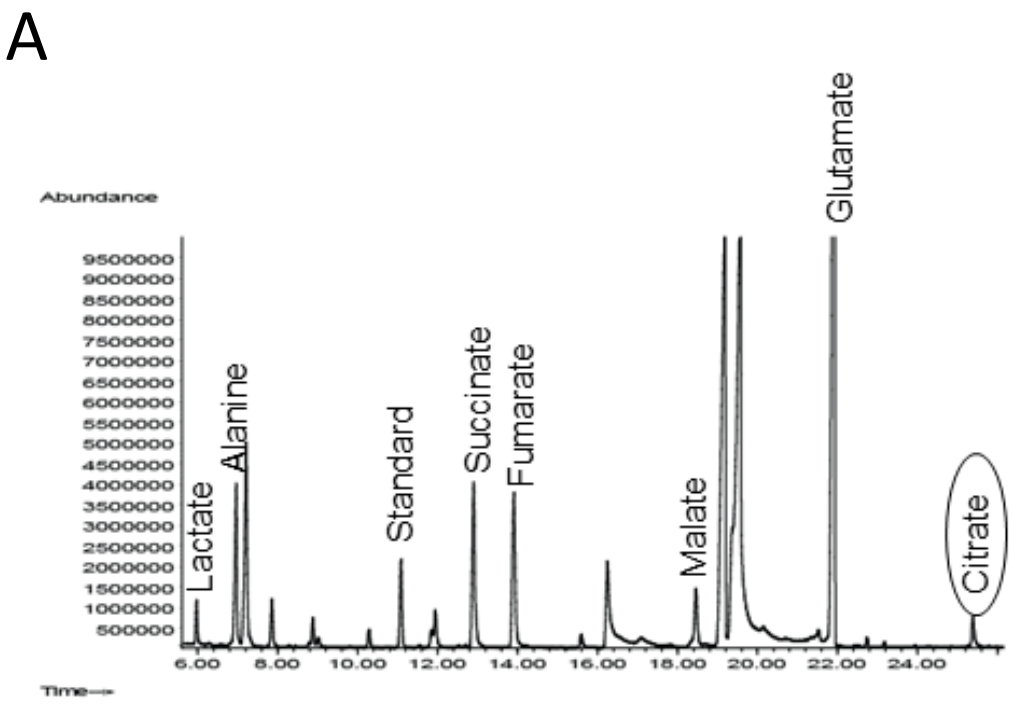

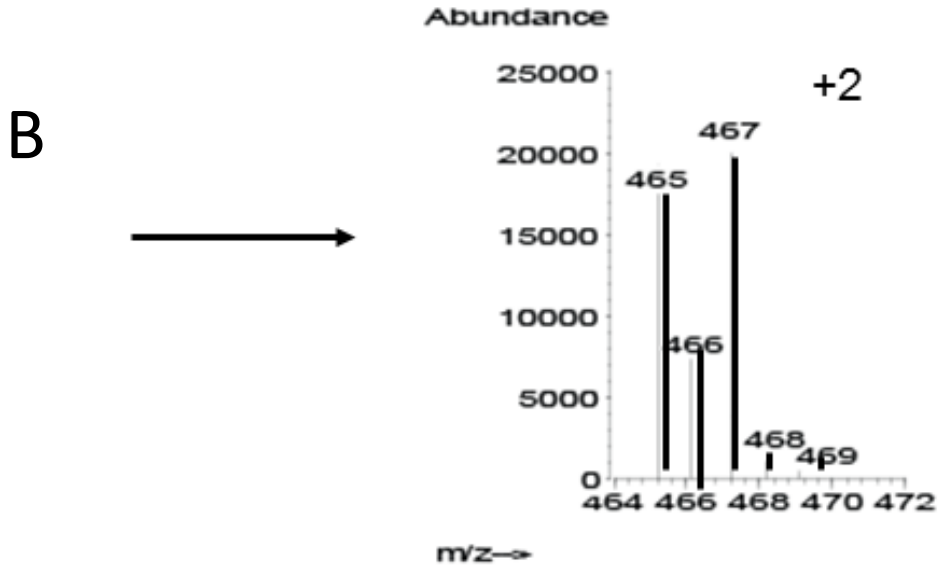

Figure 2.2 Stable isotope tracing using GC-MS illustrates carbon flux. (A) Gas chromatogram displays separation of cellular metabolites based on affinity for mobile and stationary phases. **(B)** MID of citrate. There is an increased abundance of citrate molecules with two heavy carbons, yielding a 467 rather than a 465, which corresponds to an unlabeled citrate with no heavy carbons.

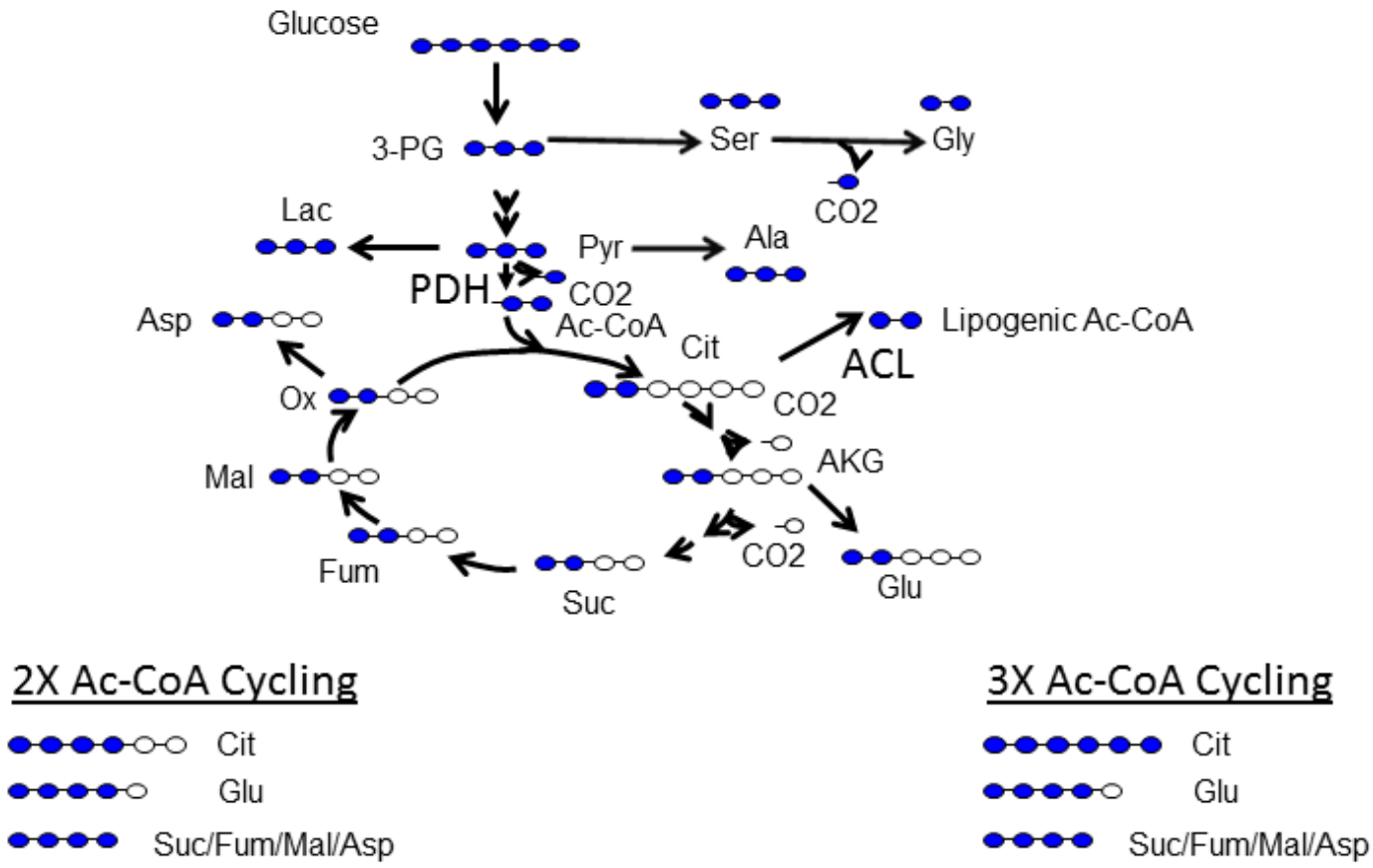

Figure 2.3 Stable isotope tracing with [U-^{13}C] glucose. When cells are incubated with uniformly labeled glucose, products of glycolysis, TCA cycle metabolites, certain amino acids, as well as fatty acids can contain labeled carbon. As the incubation time increases, labeled carbons have circled the TCA cycle and are combined with newly entering labeled acetyl-CoA carbons from glucose, yielding TCA metabolites with increased numbers of labeled carbons. Blue circles represent labeled carbons. *Abbreviations*: 3-PG, 3-phosphoglycerate; Ac-CoA, acetyl-CoA; ACL, ATP citrate lyase; Ala, alanine; AKG, α-ketoglutarate; Asp, aspartate; Cit, citrate; Fum, fumarate; Glu, glutamate; Gly, glycine; Lac, lactate; Mal, malate; Ox, oxaloacetate; Pyr, pyruvate; PDH, pyruvate dehydrogenase; Ser, serine; Suc, succinate.

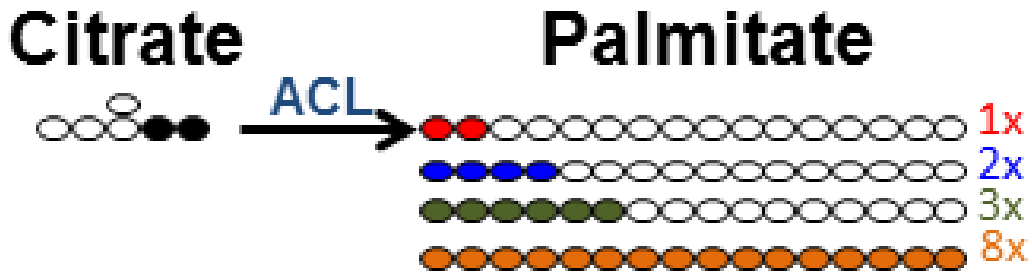

Figure 2.4 Citrate from labeled acetyl-CoA makes labeled palmitate through the ACL reaction. When citrate is derived from labeled acetyl-CoA, it is M+2. This citrate can then be exported from the mitochondrion to undergo the ACL reaction to regenerate a cytosolic labeled acetyl-CoA molecule used for palmitate synthesis. Each time this process occurs it leads to 2 more carbons in palmitate being labeled. *Abbreviations*: ACL, ATP-citrate lyase.

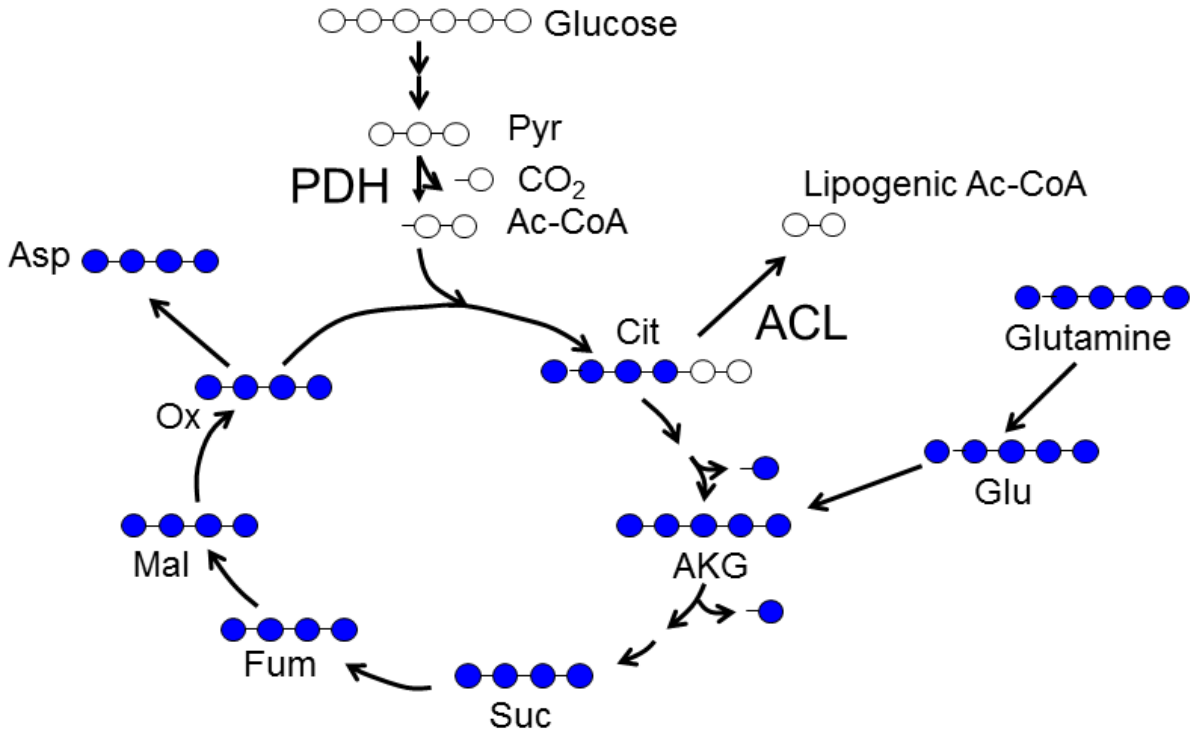

Figure 2.5 Stable isotope tracing with [U-^{13}C] glutamine. When cells are incubated with uniformly labeled glutamine, TCA cycle metabolites and certain amino acids can contain labeled carbon. Blue circles represent labeled carbons. *Abbreviations*: Ac-CoA, acetyl-CoA; ACL, ATP citrate lyase; AKG, α-ketoglutarate; Asp, aspartate; Cit, citrate; Fum, fumarate; Glu, glutamate; Mal, malate; Ox, oxaloacetate; Pyr, pyruvate; PDH, pyruvate dehydrogenase; Suc, succinate.

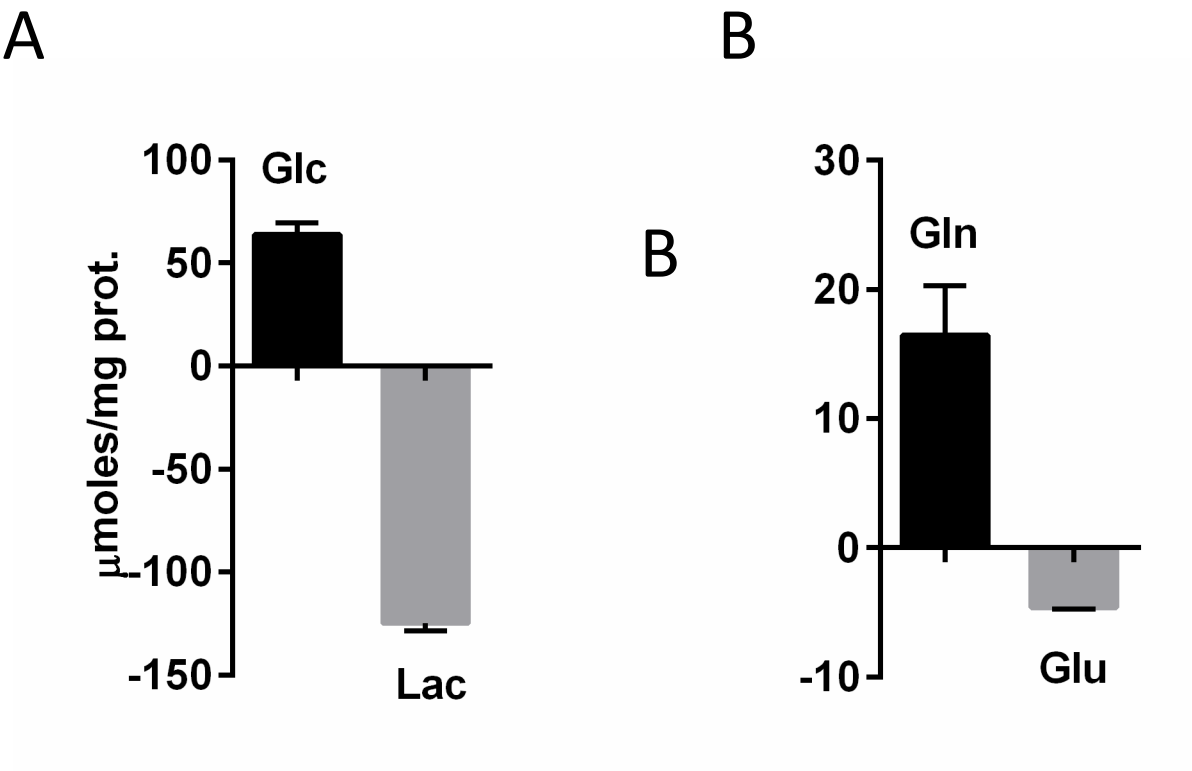

Figure 2.6 H460 cells consume glucose and glutamine and secrete lactate and glutamate. H460 cells were cultured in the presence of 10 mM glucose and 4 mM glutamine for 24 hours. Media was analyzed for metabolite concentrations. Values are an average of biological triplicates with positive values representing consumption and negative values representing secretion. Error bars represent SD. **(A)** Glucose consumption and lactate secretion. **(B)** Glutamine consumption and glutamate secretion. *Abbreviations:* Glc, glucose; Gln, glutamine; Glu, glutamate; Lac, lactate.

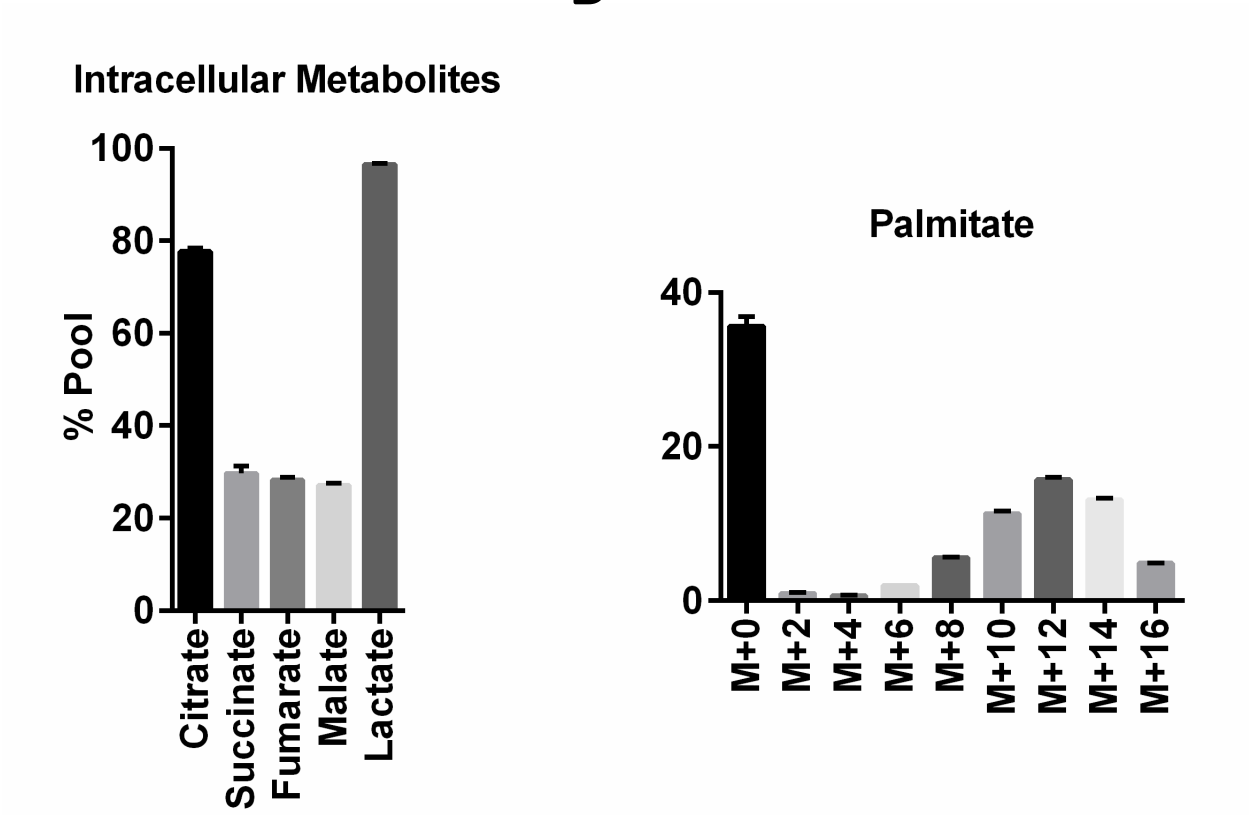

Figure 2.7 H460 cells label TCA metabolites and palmitate with glucose carbon. H460 cells were cultured in the presence of 10 mM [U-^{13}C] glucose and 4 mM glutamine for 24 hours. Intracellular metabolites were analyzed by GC-MS. Values are biological triplicates with error bars representing SD. **(A)** Percentage labeling pools of intracellular metabolites. **(B)** Percentage labeling in even mass isotopomers of palmitate. *Abbreviations:* TCA, tricarboxylic acid.

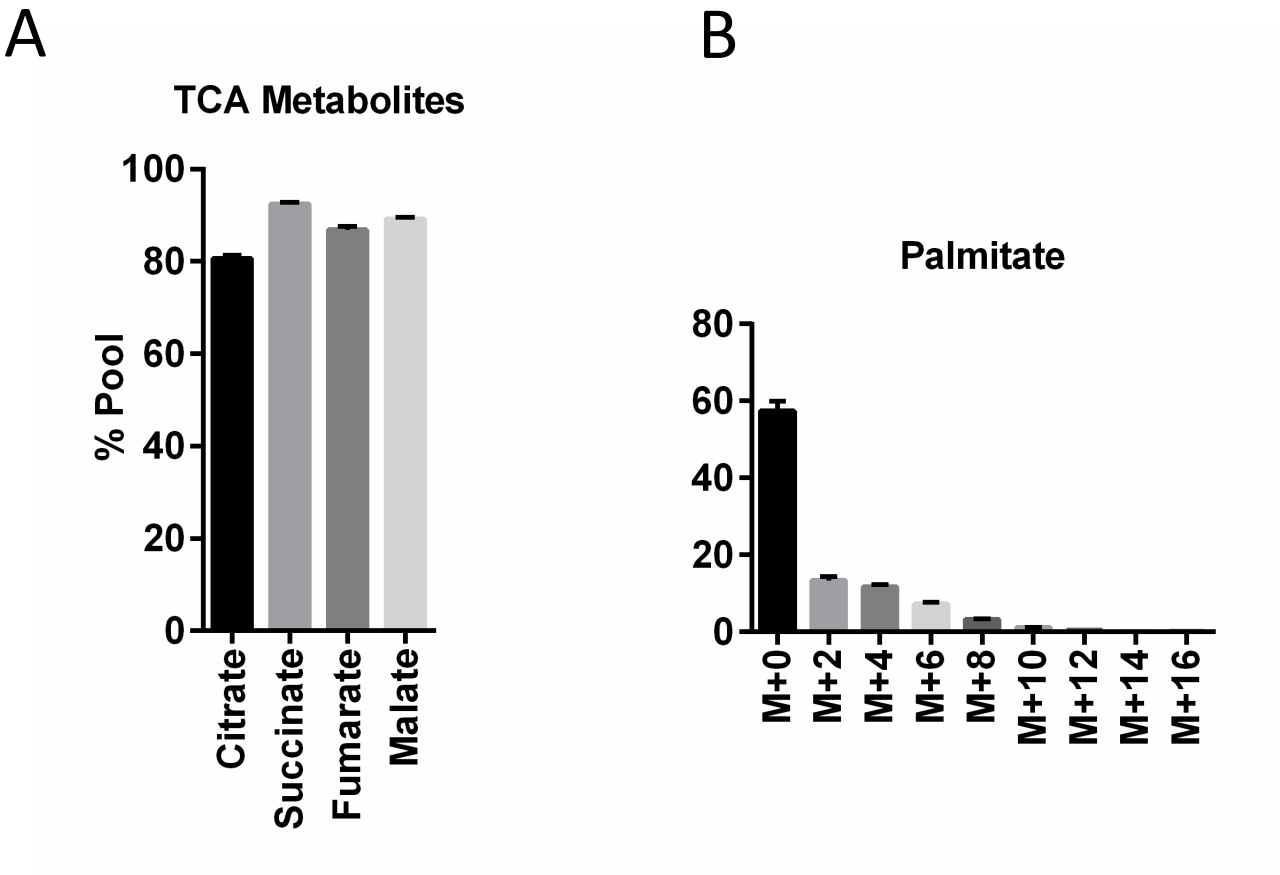

Figure 2.8 H460 cells label TCA metabolites and palmitate with glutamine carbon. H460 cells were cultured in the presence of 10 mM glucose and 4 mM [U-^{13}C] glutamine for 24 hours. Cellular metabolites were analyzed by GC-MS. Values are biological triplicates with error bars representing SD. **(A)** Percentage labeling in pools of different TCA metabolites. **(B)** Percentage labeling in even mass isotopomers of palmitate. *Abbreviations:* TCA, tricarboxylic acid.

CHAPTER 3

SUPPRESSING PDH ACTIVITY IN PROLIFERATING CELLS

3.1 Introduction

The pyruvate dehydrogenase complex (PDC) is a multi-subunit enzyme that is responsible for the oxidative decarboxylation of pyruvate to acetyl-CoA, which can then enter the TCA cycle. The enzyme complex consists of three subunits called E1, E2, and E3. The E1 subunit is a heterotetramer composed of two α and two β subunits. The α subunit is encoded by the *PDHA1* gene in somatic tissues and *PDHA2* in the testes (Dahl, Brown et al. 1990). The β subunit is encoded by the gene *PDHB* located on chromosome 3 (Prasad, Rupar et al. 2011) . These subunits form an interface which is necessary for the binding of thiamine pyrophosphate and a magnesium ion, both cofactors that are involved in the reaction (Ciszak, Korotchkina et al. 2003). The E1 subunit is responsible for decarboxylation of pyruvate and acetylation of the E2 subunit of the complex (Patel, Nemeria et al. 2014). The E2 subunit is encoded by the gene *DLAT* (dihydrolipoamide s-acetyltransferase) and is responsible for transferring the acetyl group derived from the E1 reaction to coenzyme A, thus making acetyl-CoA (Taylor, Hurley et al. 2004). The E3 subunit of the complex is responsible for transferring electrons liberated by the acetylation of coenzyme A to NAD+ (Patel, Nemeria et al. 2014). Overall, PDC is comprised of approximately 96 subunits in humans: 22 E1 subunits, 60 E2 subunits, and 6 E3 subunits, making it the largest multi-enzyme complex known (Zhou, McCarthy et al. 2001). As briefly mentioned in chapter 1, the regulation of the PDC occurs by phosphorylation of the E1α subunit by a combination of 4 pyruvate dehydrogenase kinases (PDKs) and 2 pyruvate dehydrogenase

phosphatases (PDPs). Most importantly, the rate limiting step of the PDC is the E1 reaction (Patel and Korotchkina 2001).

In humans, deficiency of pyruvate dehydrogenase activity has a range of phenotypes from mild to fatal. These phenotypes are both neurological and metabolic in nature. The neurological abnormalities involve anatomical (developmental) abnormalities, mental retardation, and/or seizures while the metabolic finding is usually lactic acidosis. The specific effect of PDH deficiency on the brain is caused by its relative lack of flexibility in glucose as a fuel source and the lactic acidosis is caused by fermentation of the excess pyruvate to lactate. As *PDHA1* is X-linked, the clinical presentation for males is usually very severe, and females have a more varied presentation based on the pattern of X chromosome inactivation. Additionally, based on the mutation, phenotypes can vary dependent on the level of residual PDH activity. Very importantly, the vast majority of mutations occur in the E1 enzyme (Brown, Otero et al. 1994).

A mouse model of PDC deficiency was created by knocking out exon 8 of the *Pdha1* gene. Although all male mice died prenatally, female heterozygotes survived. The model closely resembles the cerebral abnormalities observed in female patients with PDC deficiency. Furthermore, brain homogenate revealed that PDC activity was reduced by 25-50% in knockout mice, indicating that the E1α protein was indispensable for full function (Pliss, Hausknecht et al. 2013).

The preceding information underlies the rationale to genetically manipulate the E1α subunit of the PDC. The E1 reaction is the rate limiting step of the PDH reaction and mutations

in the gene encoding this subunit in both mice and humans causes a diseased phenotype that is associated with a reduction in PDH activity. As described in the subsequent paragraphs, I used RNA interference against the *PDHA1* gene in order to ablate PDH activity in H460 cells to uncover the metabolic and biological significance of glucose oxidation in proliferating cells. Additionally, I did this using a doxycycline inducible system so that reductions in PDH activity were acute and did not cause chronic alterations in cellular metabolism.

3.2 Methods

3.2.1 Cloning Inducible shRNA Vectors Against PDHA1 Transcript

Six different shRNA sequences against PDHA1 were developed using the web-based algorithm developed by the Hannon Lab at Cold Spring Harbor Laboratory. Two other sequences were selected from the siRNA sequences from Dharmacon with the best level of PDHE1α protein reduction on transient transfection. The last sequence was selected from the Open Biosystems shRNA library. A nonsense hairpin sequence that was derived from Janssen Pharmaceuticals was used as a control. Using Infusion, a ligation-independent cloning system purchased from Clontech, these ten sequences were cloned into a doxycycline-inducible mir-30 based shRNA expression system developed by the Lowe Lab at Memorial Sloan-Kettering Cancer Center. A schematic of the vector along with the hairpin sequences is contained in Appendix A.

3.2.2 Fluorescence Activated Cell Sorting (FACS) for Venus

Cells infected with shNS (nonsense), shPDHA1-1 (PDHA1 hairpin #1), or shPDHA1-2 (PDHA1 hairpin #6) were suspended in staining media containing 1 mg/mL BSA, 5 mL .01 M HEPES, penicillin/streptomycin, and 92% v/v Leibovitz's L15 media in water at a concentration of approximately 3 million cells per mL. 1 ug/mL 4'6-diamidino-2-phenylindol (DAPI) was dissolved in this cell suspension to use as an exclusion dye for dead cells. Cells were sorted using a Becton-Dickinson FACSAria III. Cells that were sorted were negative for DAPI and had the top 10% of Venus expression of the pool of cells. In a technique called double-sorting, the

pool of cells was sorted first in the Yield Mode, increasing number of cells sorted at the expense of lower stringency. The cells that were sorted from the pool were then re-sorted using Purity Mode, decreasing number of cells sorted in order to gain higher stringency.

3.2.3 Cell Culture

Methods were similar to those described in section 2.2 except that serum was supplemented with tetracycline-reduced FBS instead of normal FBS. Additionally, cells were maintained in doxycycline-free, un-induced conditions when not involved in experiments.

3.2.4 Inducibly Knocking Down PDHA1

The appropriate cells were treated with doxycycline at a concentration of 100 ng/mL for 96 hours before plating cells for experimentation. Media with fresh doxycycline was added at 72 hours, one day before plating cells for experimentation. Protein was extracted at the beginning of the assay to ensure that knockdown had occurred effectively. A schematic of the infection, sorting, induction, and plating processes are illustrated in Appendix B.

3.2.5 Western Blotting for PDH E1α

The cell lines were plated in culture medium described in section 2.2 and 12-24 hours later protein was extracted using RIPA buffer with protease inhibitor from Roche. Protein was run on a 4-12% gradient, Bis-Tris Invitrogen gel and transferred using Invitrogen western blot apparatus. Primary antibodies were dissolved in 5% BSA with .01% sodium azide as a preservative. Mouse anti-PDH E1α was obtained from Invitrogen and used at 1:1,000; rabbit anti-cyclophilin B was obtained from Abcam and used at 1:10,000. Horseradish peroxidase

(HRP)-conjugated anti-mouse and anti-rabbit secondary antibodies were dissolved in 5% milk and used at 1:5,000 for PDHE1α and 1:10,000 for cyclophilin B respectively. Detection was performed using peroxide and luminol enhancer solutions from ThermoScientific.

3.2.6 Determination of PDH Activity

Determination of PDH activity was performed by Maria Calvaruso, a postdoctoral fellow in the DeBerardinis Lab. After cells had been under doxycycline induction for approximately 96 hours, cells were treated with 5 mM DCA for 1 hour to activate all PDH enzyme complexes. Mitochondria were then isolated by centrifugation and suspended in buffer containing .1% Triton-X-100, 1 mM $CaCl_2$, 5 mM $MgCl_2$, 50 mM KCl, 250 mM sucrose, and 20 mM Tris HCl. Protein content was determined by BCA assay and .1 mg mitochondrial suspension was added in triplicate for each sample. The reaction began when the reaction mixture containing 50 mM KPi, .1% Triton-X-100, 1 mM $MgCl_2$, 1g/L BSA, 5 mM L-carnitine, 2.5 mM NAD+, .2 mM thiamine pyrophosphate, .1 mM Coenzyme A, 5 mM pyruvate, .6 mM MTT, 6µM phenazine methosulfate, was added to each of the wells. PDH activity was determined by following the reduction of the MTT dye. The nanomoles of pyruvate oxidized was calculated from the absorbance change in MTT dye at 570 nM using the ε=13 mM^{-1} cm^{-1} at 25 degrees C. Non-specific reduction of the dye was determined by adding 5 mM 3-bromopyruvate (a PDH complex inhibitor) and was subtracted away to achieve the final measurement.

3.2.7 Metabolic Flux Experiments

Methods were similar to those described in section 2.2.except that stable isotope tracing media contained 100 ng/mL doxycycline for the appropriate cells.

3.2.8 Protein Content of Cell Extracts

Methods were similar to those described in section 2.2.

3.2.9 GC-MS Analysis of Organic Phase

Methods were similar to those described in section 2.2

3.2.10 GC-MS Analysis of Aqueous Phase

Methods were similar to those described in section 2.2

3.2.11 Software Analysis of Mass Spectra

Methods were similar to those described in section 2.2

3.2.12 Media Analysis

Methods were similar to those described in section 2.2.

3.2.13 Radiolabeling of Lipids by Glucose and Separation by Thin Layer Chromatography (TLC)

4.5 million cells were plated in 15 cm tissue culture dishes and 12-24 hours later, when cells had reached appropriate confluence, they were incubated in 10 mM [U-^{14}C] glucose and 4 mM unlabeled glutamine for 24 hours. Lipids were isolated using the Bligh-Dyer extraction method detailed in section 2.2. After being dried down, lipids were re-suspended in 500 uL chloroform and separated using TLC. Reference standards, which were purchased from Nu-chek Prep, Inc. were also included. The solvent used for separation was an 80:20:1 mixture of hexane: ethyl ether: acetic acid. Plates were developed in iodine and bands were cut and

scintillated. Phospholipids were extracted from the band corresponding to the original sample after the separation had been completed.

3.2.13 Growth Rate Assays

100K cells from each cell line were plated in triplicate in wells of a 6-well dish in medium used for metabolic flux experiments described in 2.2, except that glucose and glutamine were unlabeled. After 4 days, cells were trypsinized and counted using a Beckman-Coulter Vi-Cell XR Cell Viability Analyzer. Cells were then re-plated and counted again after 4 days. The growth assay lasted for a total of 12 days during which 3 data points after the initial plating were collected.

3.3 Results

3.3.1 Foreword

Schematics of glucose metabolism and glutamine metabolism in the context of stable isotope tracing are contained in the last chapter in figures 2.1 and 2.3-2.5 respectively. For this chapter as well as the subsequent ones, readers should refer back to these schematics for proper interpretation of the data. Additionally, rather than monitoring the entire molecule for alanine, I monitored a two carbon fragment due to interference from another metabolite on the MS for the three carbon fragment. In the subsequent figures that depict alanine, the MS data is based on this two carbon fragment.

3.3.2 Doxycycline Induction of H460 Cells with shRNAs Against PDHA1 Reduces PDHE1α Levels

The gene *PDHA1* encodes for the E1α of the PDH complex. By cloning an shRNA against the PDHA1 transcript into an inducible vector, doxycycline treatment causes reduction of PDHA1 transcript levels by inducing expression of the shRNA. Thus, the level of PDHE1α protein is also reduced. This is depicted in the western blot in figure 3.1(A), where doxycycline treatment of H460 cells that have been infected with a small hairpin against the PDHA1 transcript causes reduction in PDHE1α levels. A hairpin expressing a nonsense targeting sequence serves as the control.

3.3.3 Reduction of PDHE1α Levels By RNAi Causes an 80% Decrease in PDH Enzymatic Activity

PDH activity in H460 cells was measured by providing substrates of the PDH reaction to isolated mitochondria and determining rate of the reaction by analyzing reduction of an MTT dye. The assay determined that the level of protein silencing depicted in figure 3.1(A) corresponded to an 80% reduction in enzymatic activity.

3.3.4 Reduction of PDHE1α Does not Affect Glucose and Glutamine Consumption or Lactate and Glutamate Secretion

As in chapter 2, the NOVA Bioprofile was used to determine the consumption of glucose and glutamine consumption and secretion of glutamate and lactate secretion that accompanied PDHE1α reduction. As illustrated in figure 3.2(A), it is surprising that PDHE1α reduction does not increase lactate secretion as availability of pyruvate for the LDH reaction has increased. Reasons as to why this might be the case will be discussed in the "Discussion" section of this chapter. Additionally, as depicted in figures 3.2(A) and 3.2(B), glucose and glutamine consumption and glutamate secretion also do not change with reduction in PDHE1α levels.

3.3.5 Reduction of PDHE1α Decreases Proportional Contribution of Glucose Carbon to TCA Cycle Metabolites

Cells were incubated with uniformly labeled glucose and unlabeled glutamine for 24 hours and the mass isotopomer distributions (MIDs) that result from GC-MS analysis of TCA cycle metabolites citrate, succinate, fumarate, and malate are depicted in figures 3.3 and 3.4. The figures indicate that there is an increased M+0 ion in all of the aforementioned metabolites when PDHE1α levels are reduced. However, there is lack of any significant difference between the M+2 ions, as might have been expected. This is probably due to steady state of the M+2 ion

of the citrate pool in both the control and the PDH-suppressed cells at the 24 hour time point. It is likely that in shorter tracing experiments, the PDH suppressed cells would have exhibited a lower M+2 ion in citrate. Ions higher than M+2 are decreased in cells with suppressed PDH activity. An ion greater than M+2 in citrate requires PDH adding a labeled acetyl-CoA to an already labeled oxaloacetate which has made its way around the TCA cycle—two iterations of PDH activity per molecule of citrate. The M+2 ions in succinate, fumarate, and malate are decreased due to reduced entry of labeled acetyl-CoA from glucose. And additionally, similar to citrate, all of the ions higher than M+2 in the previously mentioned TCA metabolites are decreased due to a reduction in "repeat" PDH reactions adding labeled acetyl-CoA to an already labeled oxaloacetate. Figures 3.4(A), 3.4(B), and 3.5(B) show that the abundance of the M+3 ion, although statistically significant, is similar between control cells and those with PDHE1α reduction. This is potentially due to an upregulation of PC activity in cells which have suppressed PDH activity. PC converts fully labeled (M+3) pyruvate into oxaloacetate. The transamination product of oxaloacetate, aspartate, contains the same label. Additionally, the reversibility of the MDH and FH reactions transfer this oxaloacetate label to malate and fumarate.

3.3.6 Reduction of PDHE1α Decreases Proportional Contribution of Glucose Carbon to Glutamate and Aspartate

AST reversibly transfers an amine group from glutamate to oxaloacetate, producing α-ketoglutarate and aspartate in the process. Because the contribution of glucose carbon to α-ketoglutarate and oxaloacetate are decreased because of decreased glucose derived acetyl-CoA

entering the TCA cycle, the transamination products of α-ketoglutarate and oxaloacetate that are derived from glucose carbon are also decreased. Hence, as depicted in figure 3.5(A) and 3.5(B), there is a decreased M+2 in glutamate and aspartate when PDHE1α is reduced and cells are labeled with uniformly labeled glucose.

3.3.7 Reduction of PDHE1α Increases Proportional Contribution of Glucose Carbon to Serine and Glycine but does not Change Contribution to Alanine

As depicted in figures 3.7(A) and 3.7 (B), proportional contribution of glucose carbon to serine and glycine increases when PDHE1α levels are reduced, as indicated by the percentage increase in the M+3 and M+2 ions respectively. Both serine and glycine can be produced *de novo* from the glycolytic intermediate 3-PG by phosphoglycerate dehydrogenase. It is possible that the aforementioned pathway is causing the increase in serine and glycine labeling from glucose due to an accumulation of 3-PG caused by a reduction in pyruvate oxidation when PDH activity is abrogated. The accumulation of 3-PG then upregulates the branch pathway that synthesizes serine and glycine. As depicted in figure 3.6, reduction of PDHE1α does not change labeling in alanine. However, although labeling in alanine does not change, the amount of secreted alanine increases under reduction of PDHE1α, as explained in a subsequent section.

3.3.8 Reduction of PDHE1α Decreases Intracellular Citrate and Increases Intracellular Aspartate

Acetyl-carnitine is generated from acetyl-CoA by carnitine acetyltransferase (CAT). Thus, reduction in PDHE1α protein levels causes a decrease in acetyl-CoA levels which is

reflected in decreased acetyl-carnitine levels depicted in figure 3.8(A). Additionally, as reduction in PDHE1α protein levels decreases the amount of acetyl-CoA generation from pyruvate, there is reduced acetyl-CoA for the citrate synthase reaction. Therefore, as depicted in figure 3.8(B), intracellular citrate levels decline when PDHE1α levels are reduced. Additionally, since there is an increase in the ratio of oxaloacetate to acetyl-CoA required for the citrate synthase reaction, the excess oxaloacetate is transaminated to aspartate by AST. As illustrated in figure 3.8(C), the intracellular pool size of aspartate increases.

3.3.9 Reduction of PDHE1α Increases the Secretion of Aspartate and Alanine

As discussed in the previous section, reduction of PDHE1α levels increases the levels of intracellular aspartate due to excess oxaloacetate which undergoes transamination by glutamate. Increased intracellular aspartate levels leads to increased secretion, which is portrayed in figure 3.9(A). Additionally, as PDH activity is suppressed due to reduction in the PDHE1α protein level, pyruvate is not converted to acetyl-CoA and engages the ALT reaction. ALT transaminates pyruvate to alanine, which is secreted from the cell, as shown in figure 3.9(B).

3.3.10 Reduction of PDHE1α Decreases the Amount of Glucose Labeling in Palmitate

The ATP citrate lyase reaction produces acetyl-CoA from citrate for synthesis of fatty acids, such as palmitate. As this acetyl-CoA is derived from glucose carbon, it is informative to determine the MID of palmitate to determine glucose contribution to *de novo* fatty acid synthesis. When one acetyl-CoA unit is produced *de novo* from glucose for the purpose of fatty acid synthesis, the resulting palmitate molecule is mass shifted by M+2. If the palmitate

molecule has two acetyl-CoA units that are synthesized *de novo* from glucose, the mass shift is M+4. As depicted in figure 3.10(A), when PDHE1α levels are reduced, the number of acetyl-CoA units incorporated into palmitate that derived from glucose is reduced, i.e., the mass shift of the palmitate pool is reduced. This reduction in lipogenic acetyl-CoA derived from glucose is illustrated in figure 3.10(B), which shows, using an algorithm developed by Matt Mitsche, that the percentage of glucose contribution to lipids has been reduced when PDHE1α levels are reduced.

3.3.11 Reduction in PDHE1α Levels Decreases Glucose Contribution to Various Lipid Pools

The data illustrated in figure 3.10 represents all palmitate in the cell, both free and esterified. In order to more accurately determine which lipid pool was most affected by this decrease in *de novo* synthesis of palmitate from glucose caused by reduction of PDH activity, Ajla Wasti, a clinical fellow in the lab, incubated cells with radiolabeled glucose and separated lipids by TLC. As depicted in figure 3.11, in H460 cells, the phospholipid pool accounts for the vast majority of lipids derived from glucose. Thus, when PDH activity is abrogated, the glucose entry into this pool is most affected. However, glucose entry into all of the lipid pools were decreased when PDH activity was suppressed.

3.3.12 Reduction in PDHE1α Levels Does Not Affect Proliferation

In order to determine if there was a change in growth rate caused by reduction in PDHE1α levels, growth curves were established with the control cells as well as cells in which levels of PDHE1α were reduced by shRNA knockdown. The cells were then re-plated and the procedure was repeated to establish a 12 day growth curve. Surprisingly, as depicted in figure

3.12, proliferation rate and doubling time are, at most, only marginally affected by reduction in PDHE1α levels.

3.4 Discussion

The data that is presented in this chapter illustrates the metabolic changes that accompany a reduction in PDHE1α levels as determined by stable isotope tracing with glucose. As discussed previously, PDHE1α comprises a subunit of the rate limiting E1 reaction of the PDH enzyme complex. Thus, reducing levels of PDHE1α effectively abrogates PDH enzymatic activity, as illustrated in the 80% decrease in activity in figure 3.1(B). This is most evident in reduction of intracellular citrate which is derived from the product of the PDH reaction, acetyl-CoA. The labeling changes that occur in the TCA cycle intermediates citrate, succinate, fumarate, and malate illustrate that carbon derived from glucose comprises these TCA cycle intermediates and most importantly, that this conversion requires PDH activity. Similarly, the amino acids glutamate and aspartate also contain carbon that originates from glucose and is dependent on PDH activity.

Additionally, the abrogation of PDH activity causes an increase in the percentage of labeling in serine and glycine in the M+3 and M+2 ions respectively. This is potentially due to an accumulation of glycolytic intermediates causing an increase in flux through branch pathways, such as serine and glycine biosynthesis. However, this cause for an increased labeling in serine and glycine is suspect because of the irreversibility of the pyruvate kinase (PK) reaction. Even if pyruvate accumulated due to a reduction in PDHE1α levels, the pyruvate would be unable to be converted to phosphoenolpyruvate by PK due to the irreversibility of the reaction. Additionally, the data in this chapter shows that some amount of excess pyruvate that accumulates due to the reduction of PDH activity is transaminated by ALT and secreted from the cell as alanine. In essence, although the glycolytic side reaction is a possible

explanation for the increased MID in serine and glycine when PDH activity is reduced it is not completely corroborated by knowledge of glycolytic pathways and other experimental observations.

Pyruvate cannot be readily converted to acetyl-CoA due to suppression of PDH activity. Under this circumstance, it is interesting that this doesn't lead to a noticeably increased formation of lactate. Pyruvate engages a carrier to gain access to the mitochondrion where is undergoes oxidative decarboxylation by PDH (Halestrap, Scott et al. 1980). Unpublished results from the DeBerardinis Lab indicate that when this carrier is blocked by a chemical inhibitor, cellular alanine secretion is reduced. As my data indicates that reducing PDH activity increases alanine secretion, a portion of the excess pyruvate likely enters the mitochondrion where it is processed by ALT. Since cellular lactate secretion is two magnitudes larger than alanine secretion, the small increase in lactate secretion that is caused by reduction of PDHE1α might not be detectable by our methods. Lastly, because acetyl-CoA levels are reduced with reduction of PDHE1α, the stoichiometric ratio of oxaloacetate to acetyl-CoA rises which causes an increase in substrate for the AST reaction. This causes an increase in aspartate secretion.

The "left-shift" of palmitate labeling from glucose when PDH activity is reduced illustrates that PDH enzymatic activity underlies the cells ability to convert glucose carbon into acetyl-CoA needed for fatty acid synthesis. As illustrated by figure 3.10, the amount of glucose contributing to lipogenic acetyl-CoA significantly decreases when PDHE1α levels are reduced. A downstream consequence of the reduction of glucose derived lipogenic acetyl-CoA is demonstrated in figure 3.11, which illustrates that glucose incorporation into phospholipids is

reduced by approximately half. This illustrates that PDH activity is important for glucose contribution to phospholipids, which are required for cell membranes. Despite this reduction in glucose incorporation into phospholipids, the cell growth rate does not change.

One interpretation of this data is that the fatty acid and phospholipid biosynthesis from glucose is in surplus to the amount needed for cell proliferation. Another interpretation of this data is that when PDHE1α levels are reduced, there are compensatory pathways that are upregulated that circumvent the need for *de novo* synthesis of lipids from glucose. In the next chapter, I will attempt to determine which, if any, compensatory pathways are upregulated when PDH activity is reduced.

A

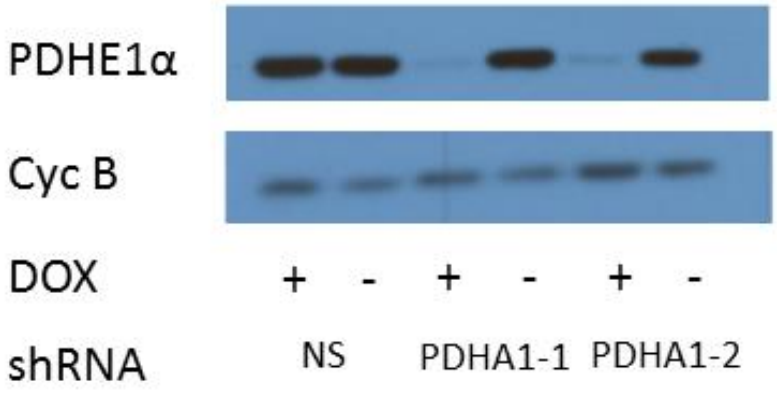

B

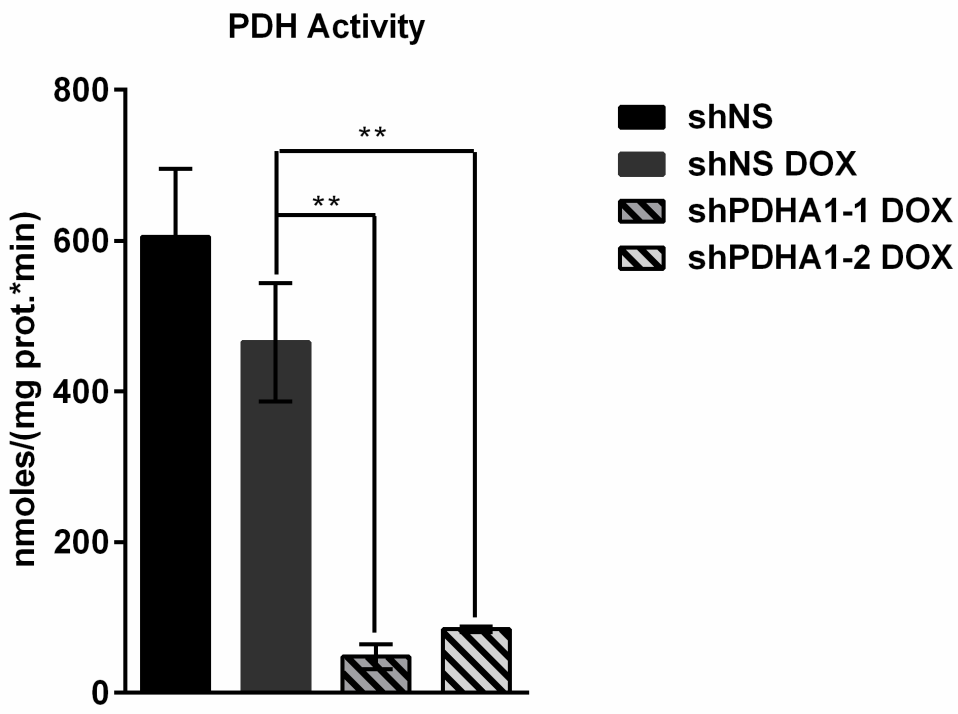

Figure 3.1 H460 cells infected with vectors carrying shRNAs against PDHA1 have reduced PDHE1α levels and PDH activity after induction with doxycycline. (A) H460 cells were sorted for high YFP expression. Cells were then induced with 100 ng/mL doxycycline for 4 days and protein was extracted subsequently and probed for PDHE1α by western blot. Cyclophilin B serves as a loading control. **(B)** PDH activity in each cell type was measured using a dye reduction assay. Values are an average of technical triplicates with error bars representing SD. *P, <.05; **P<.005. *Abbreviations:* Cyc B, cyclophilin B; DOX, doxycycline; NS, non-sense.

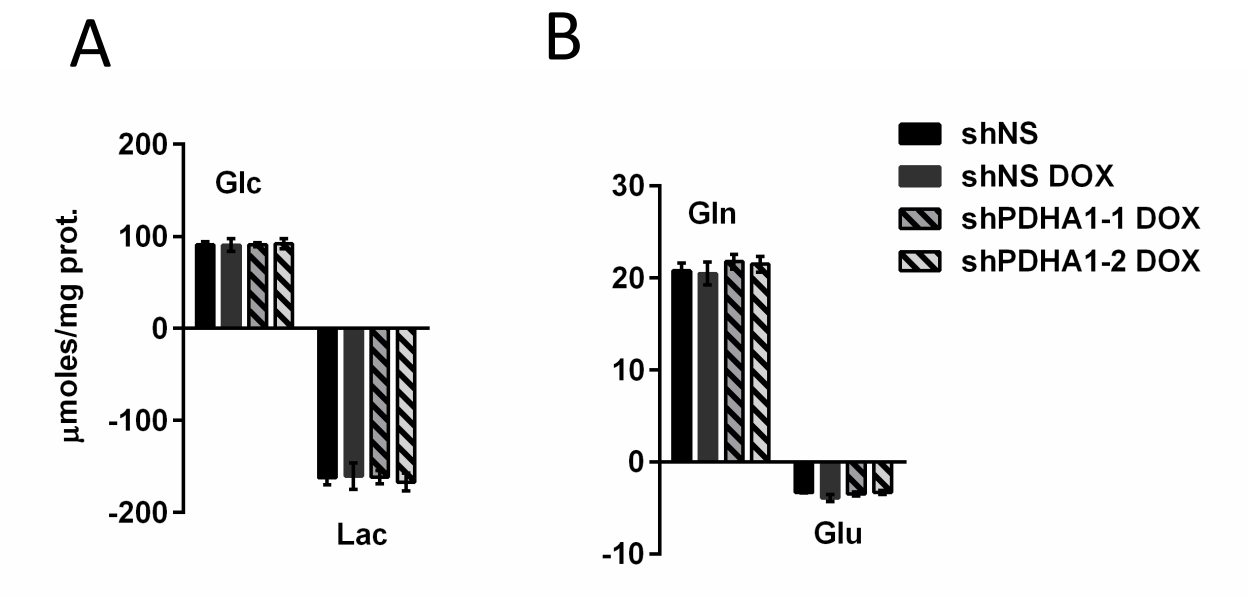

Figure 3.2 Reduction of PDHE1α in H460 does not affect glucose and glutamine consumption or lactate and glutamate secretion. H460 cells were incubated for 24 hours with 10 mM glucose and 4 mM glutamine and media metabolite concentrations were analyzed by the NOVA Bioprofile. **(A)** Glucose consumption and lactate secretion. **(B)** Glutamine consumption and glutamate secretion. Values are biological triplicates with positive values representing consumption and negative values representing secretion. *Abbreviations:* Glc, glucose; Gln, glutamine; Glu, glutamate; Gln, glutamine.

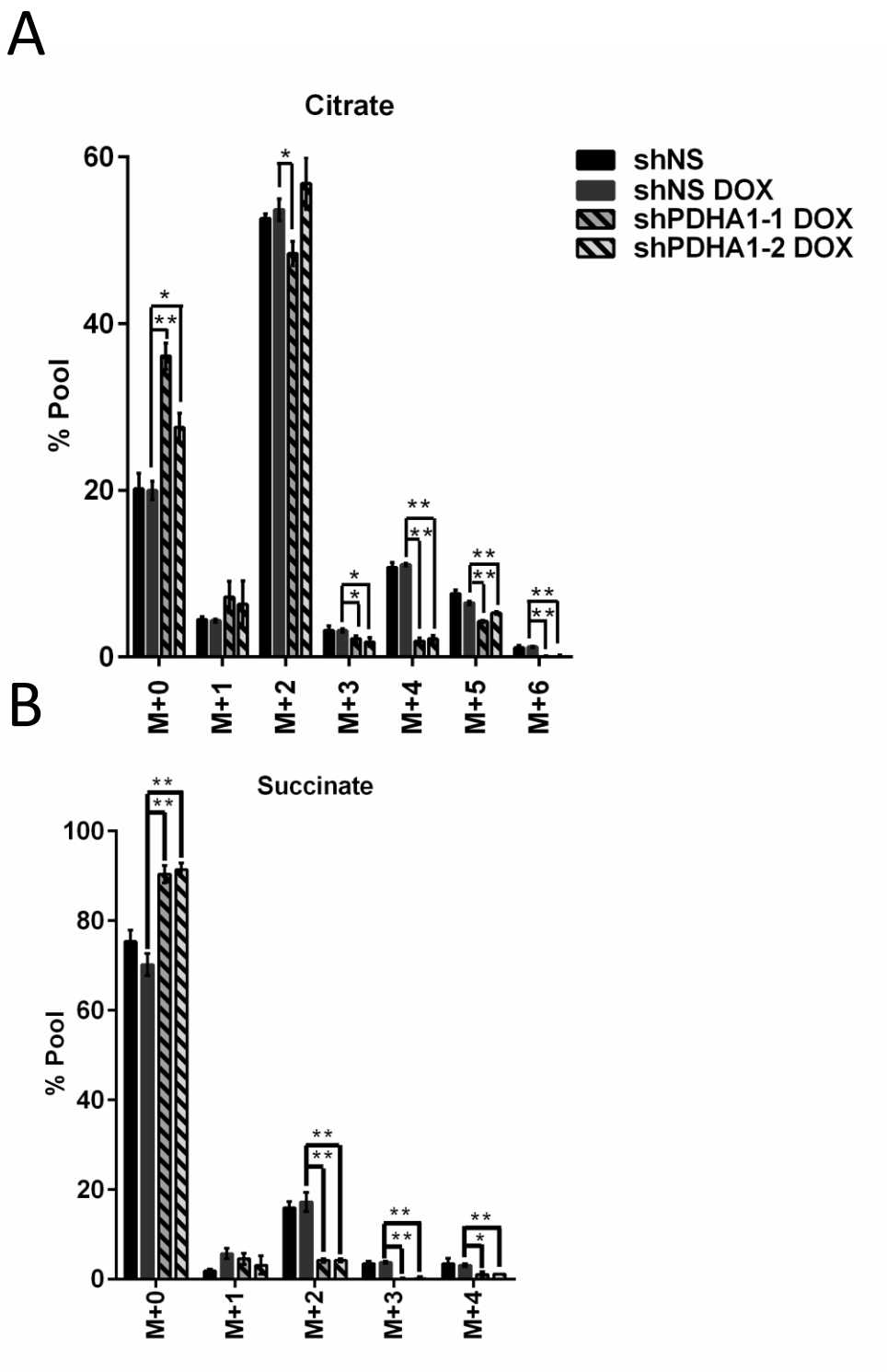

Figure 3.3 Reduction of PDHE1α decreases contribution of glucose carbon to TCA metabolites citrate and succinate. H460 cells were incubated with 10 mM [U-^{13}C] glucose and 4 mM glutamine for 24 hours and metabolites were analyzed by GC-MS. **(A)** MID of citrate is depicted, and **(B)** MID of succinate is depicted. Values are an average of biological triplicates with error bars representing SD. *P, <.05; **P<.005.

A

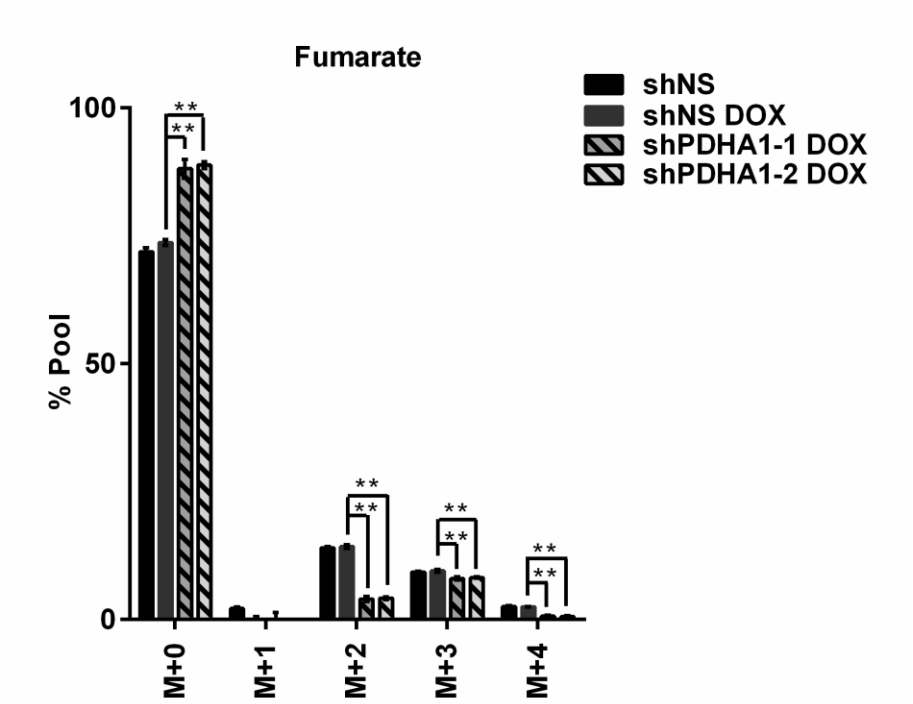

B

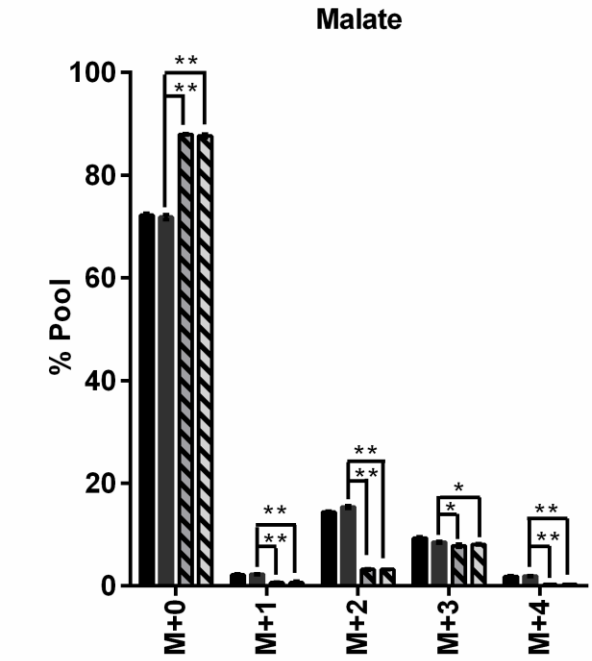

Figure 3.4 Reduction of PDHE1α decreases contribution of glucose carbon to TCA metabolites fumarate and malate. H460 cells were incubated with 10 mM [U-^{13}C] glucose and 4 mM glutamine for 24 hours and metabolites were analyzed by GC-MS. **(A)** MID of fumarate is depicted, and **(B)** MID of malate is depicted. Values are an average of biological triplicates with error bars representing SD. *P, <.05; **P<.005.

A

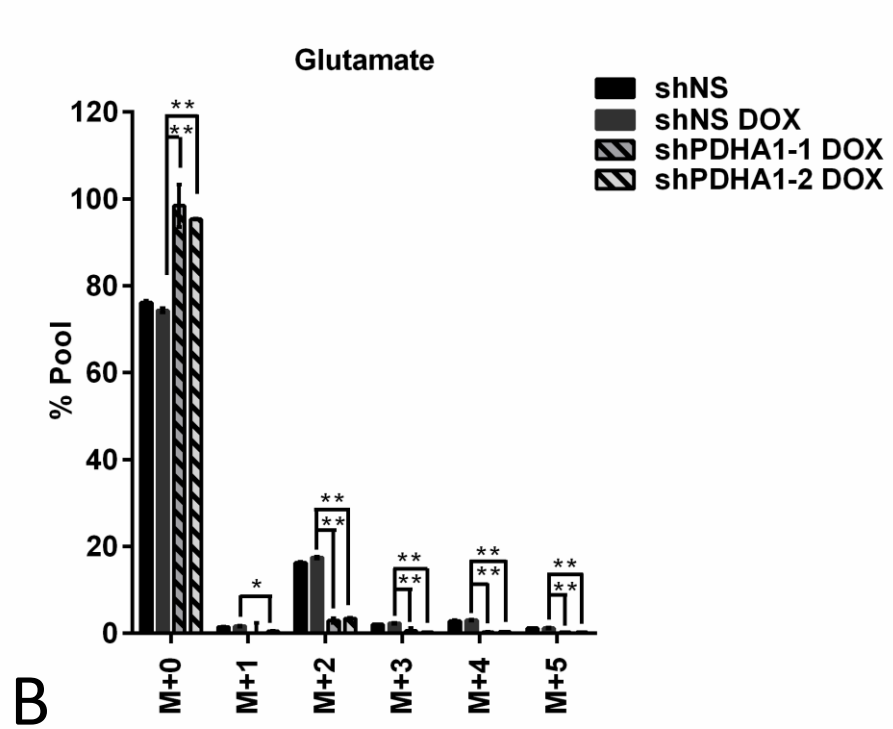

B

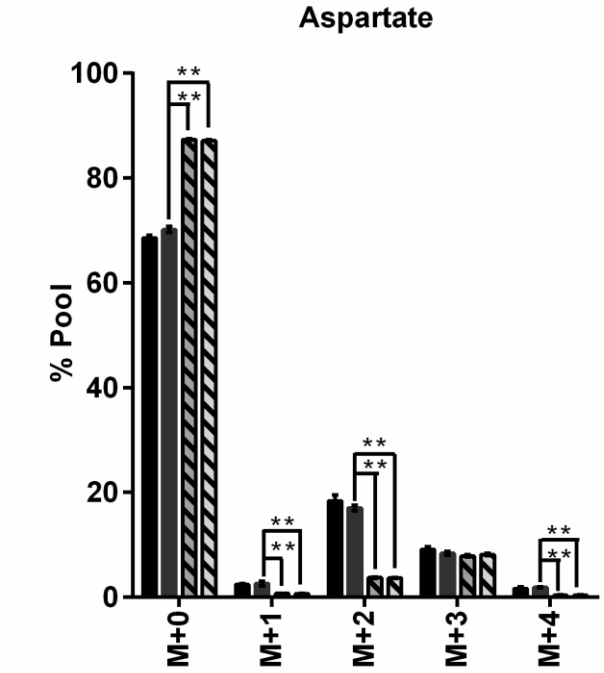

Figure 3.5 Reduction of PDHE1α decreases contribution of glucose carbon to amino acids glutamate and aspartate. H460 cells were incubated with 10 mM [U-^{13}C] glucose and 4 mM glutamine for 24 hours and metabolites were analyzed by GC-MS. **(A)** MID of glutamate is depicted, and **(B)** MID of aspartate is depicted. Values are an average of biological triplicates with error bars representing SD. *P, <.05; **P<.005.

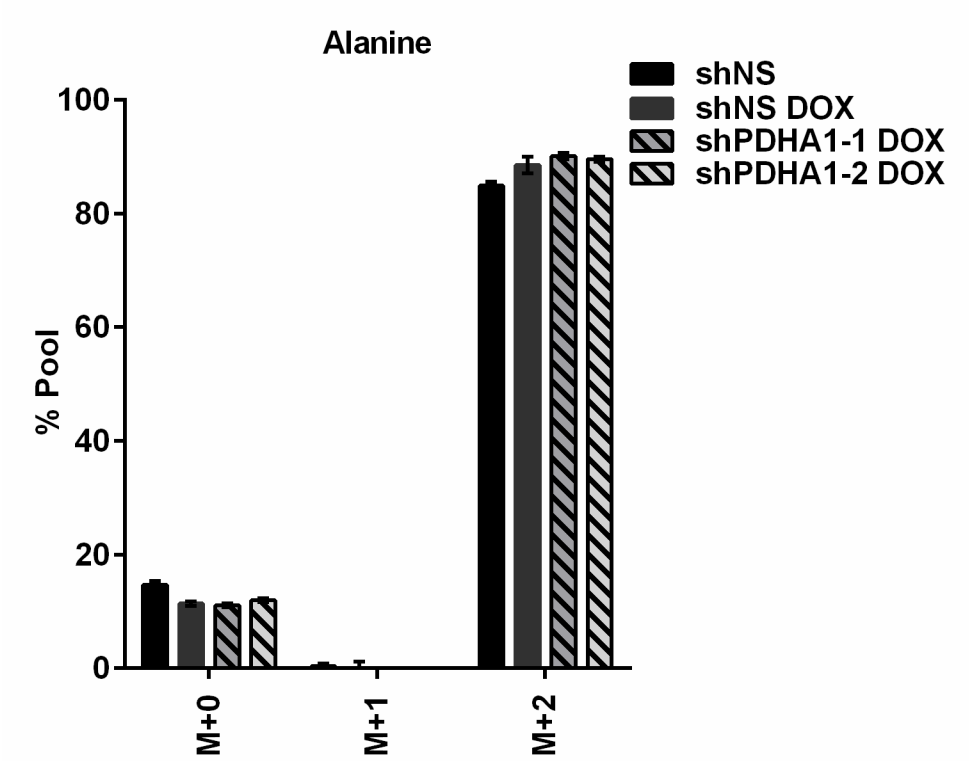

Figure 3.6 Reduction of PDHE1α does not affect contribution of glucose carbon to amino acid alanine. H460 cells were incubated with 10 mM [U-^{13}C] glucose and 4 mM glutamine for 24 hours and metabolites were analyzed by GC-MS. MID of alanine is depicted. Values are an average of biological triplicates. Two carbon fragment of alanine was selected for analysis due to MS interference for analysis of the entire molecule.

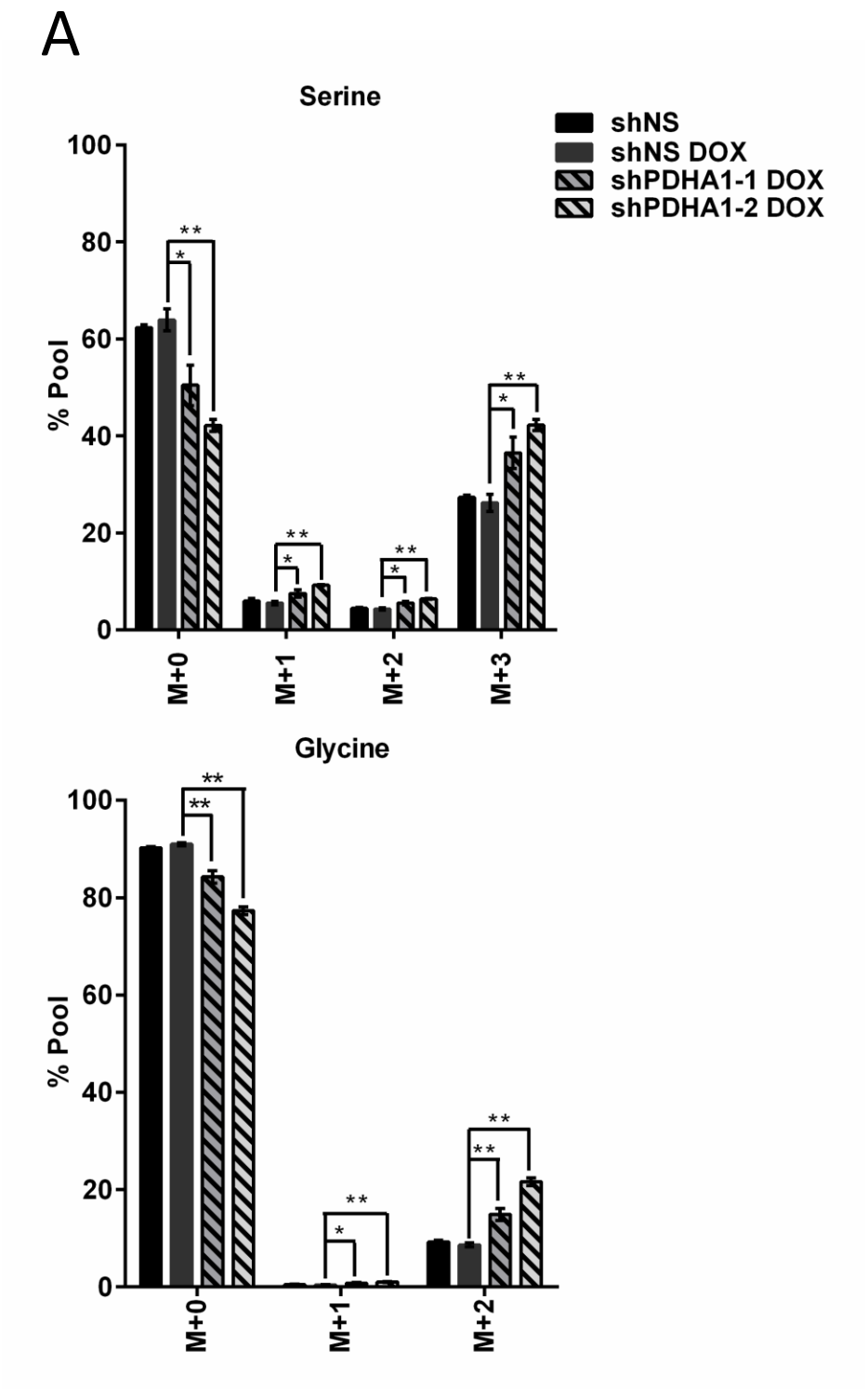

Figure 3.7 Reduction of PDHE1α increases contribution of glucose carbon to amino acids serine and glycine. H460 cells were incubated with 10 mM [U-^{13}C] glucose and 4 mM glutamine for 24 hours and metabolites were analyzed by GC-MS. **(A)** MID of serine is depicted, and **(B)** MID of glycine is depicted. Values are an average of biological triplicates with error bars representing SD. *P, <.05; **P<.005.

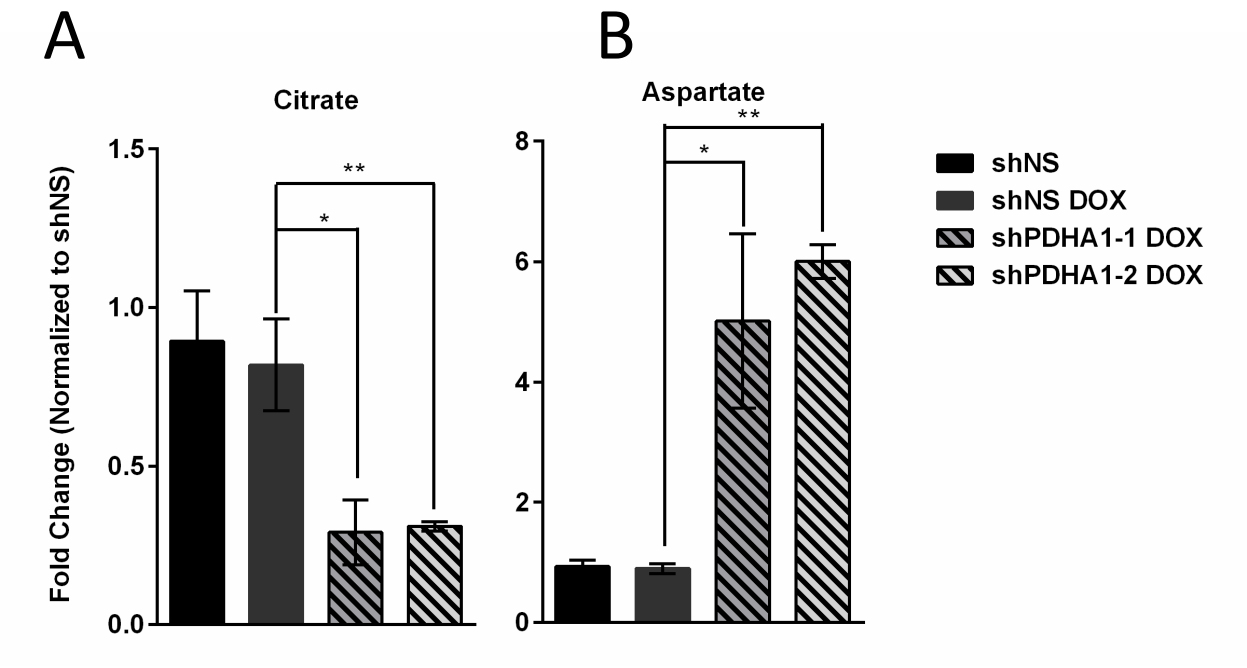

Figure 3.8 Reduction of PDHE1α decreases citrate levels and increases aspartate levels. H460 cells were incubated with 10 mM glucose and 4 mM glutamine for 24 hours and metabolites were analyzed by GC-MS. Pool size under each condition is relative to shNS sample. Relative pool sizes of **(A)** citrate and **(B)** aspartate. Values are an average of biological triplicates with error bars representing SD. *P, <.05; **P<.005.

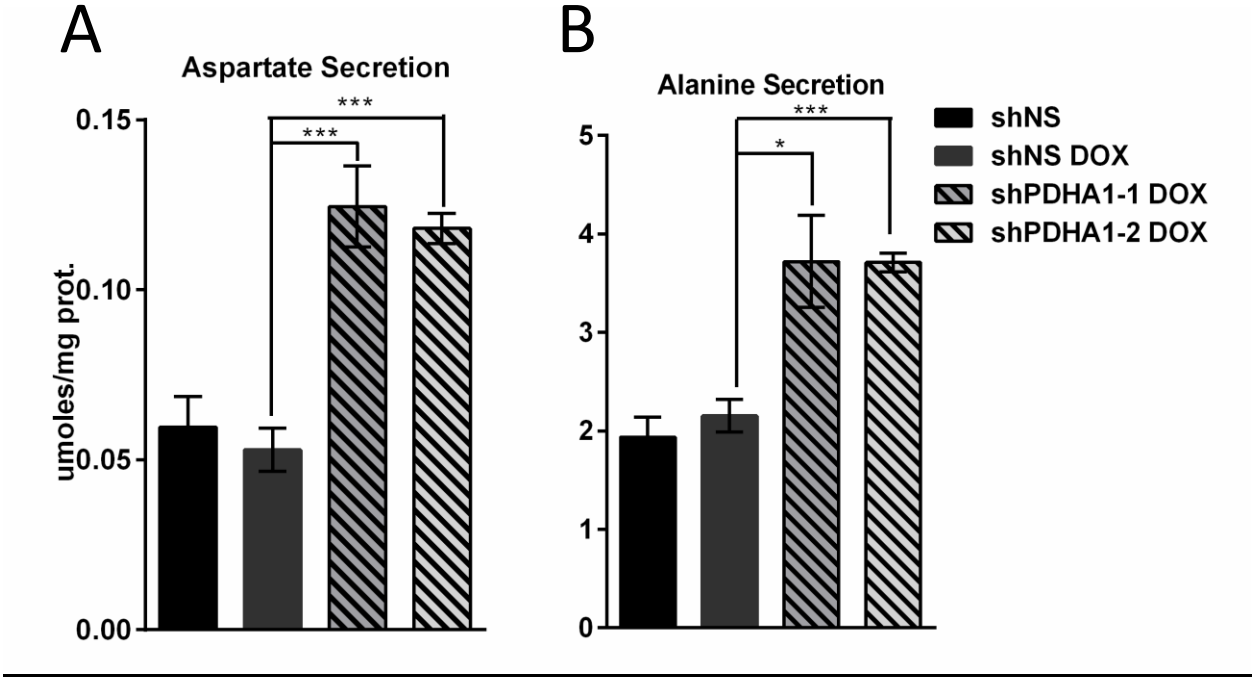

Figure 3.9 Reduction of PDHE1α increases aspartate and alanine secretion. H460 cells were incubated with 10 mM glucose and 4 mM glutamine for 24 hours and at the end of the experiment, media was analyzed by HPLC for amino acid content. Values are an average of biological triplicates with error bars representing SD. **(A)** illustrates secretion of aspartate in medium and **(B)** illustrates secretion of alanine. *P, <.05; **P<.005.

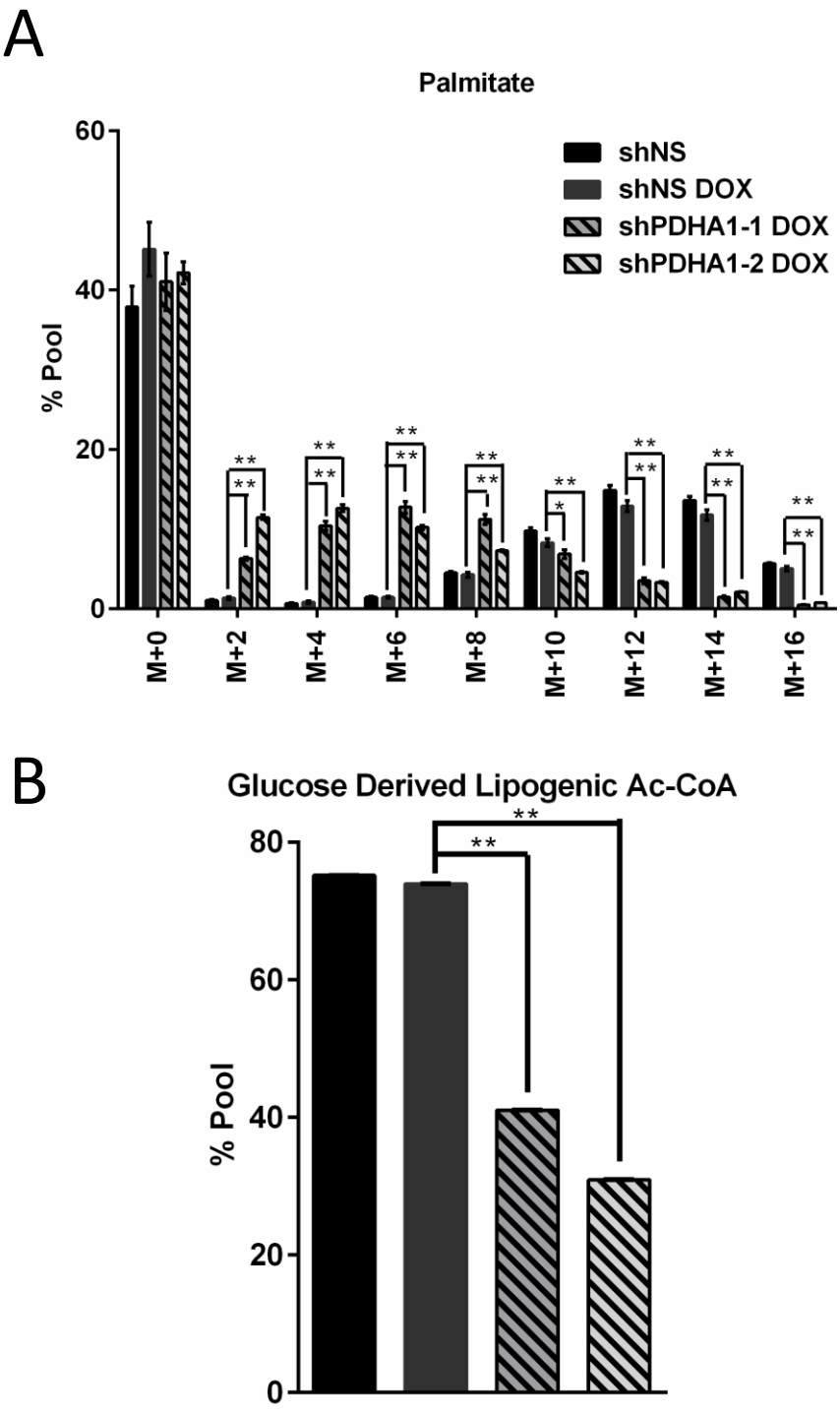

Figure 3.10 Reduction of PDHE1α decreases contribution of glucose carbon fatty acid palmitate. H460 cells were incubated with 10 mM [U-^{13}C]glucose and 4 mM glutamine for 24 hours and metabolites were analyzed by GC-MS. **(A)** MID of palmitate is depicted. **(B)** Percent lipogenic acetyl-CoA derived from glucose for palmitate synthesis. Values are biological triplicates with error bars representing SD. *P, <.05; **P<.005. *Abbreviations:* Ac-CoA, acetyl-CoA.

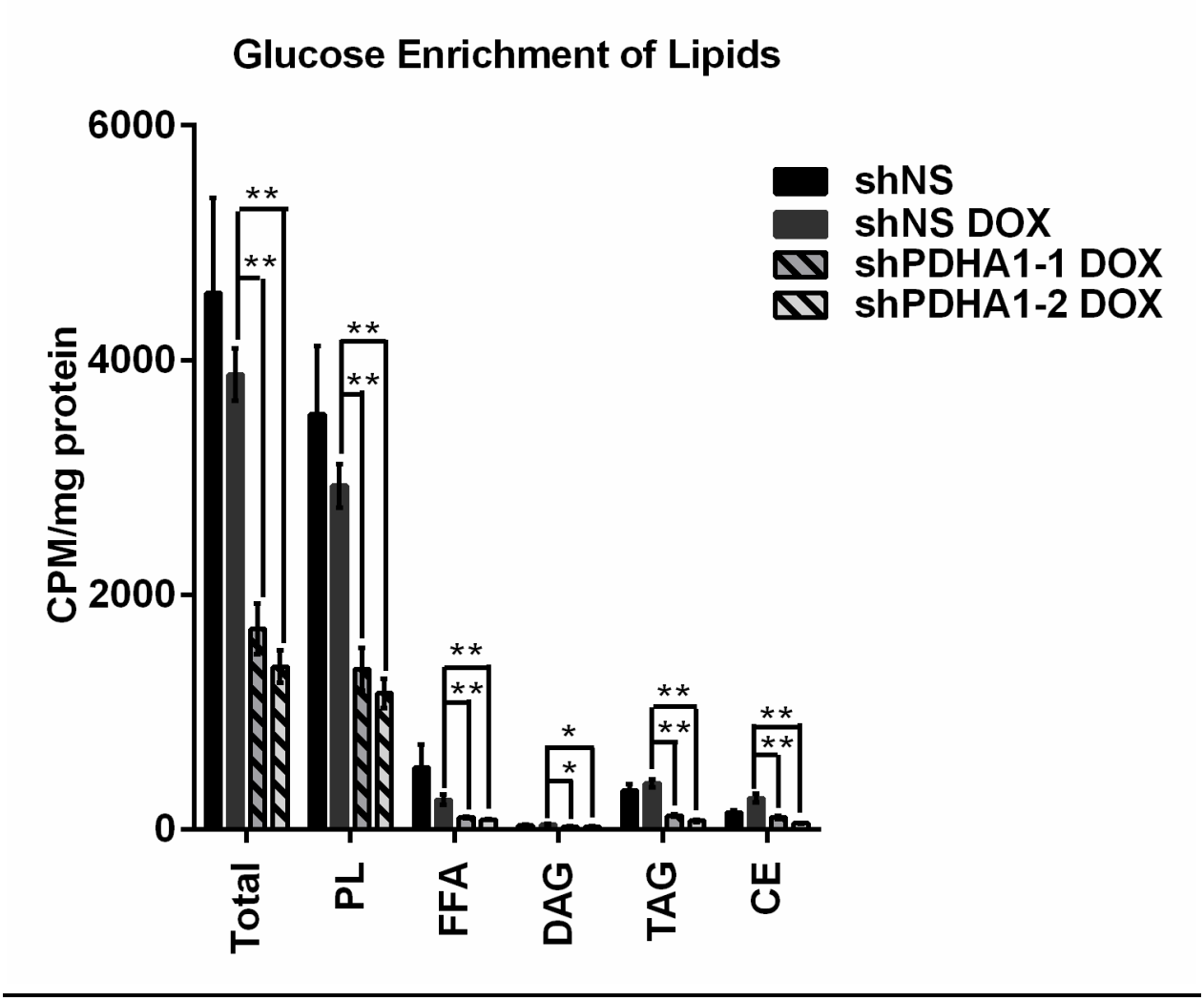

Figure 3.11 Reduction of PDHE1α profoundly decreases glucose contribution to various lipid pools. H460 cells were grown in media that contained 10 mM [U-^{14}C] glucose for 24 hours. Lipids were isolated from cells and various classes of lipids were separated using TLC and then scintillated. Values are biological triplicates with error bars representing SD. *P, <.05; **P<.005.

A

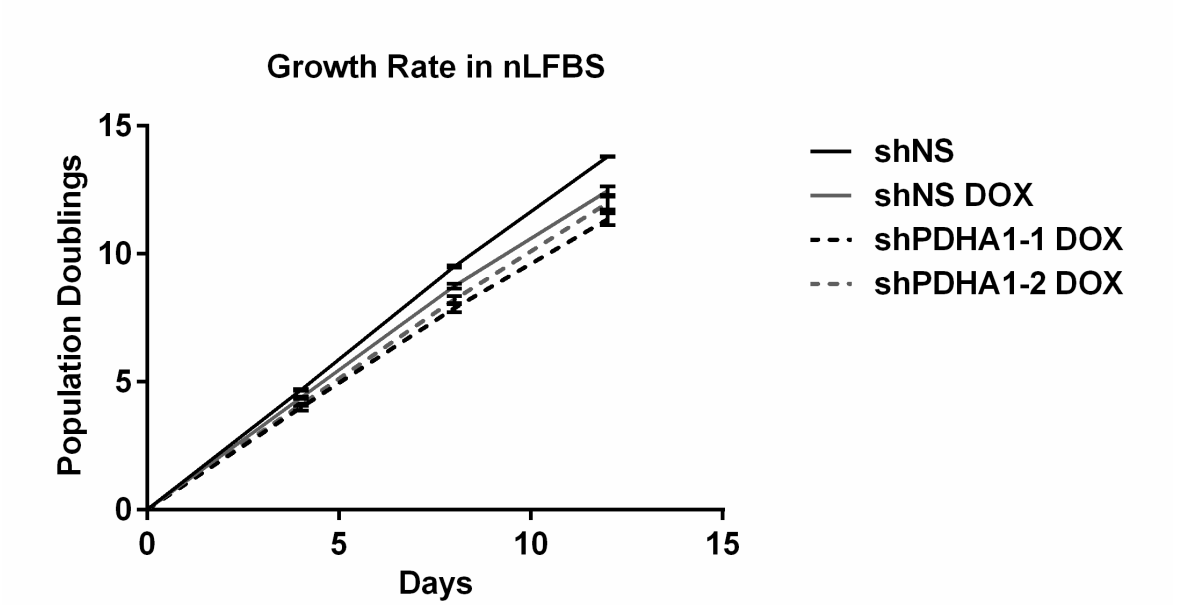

B

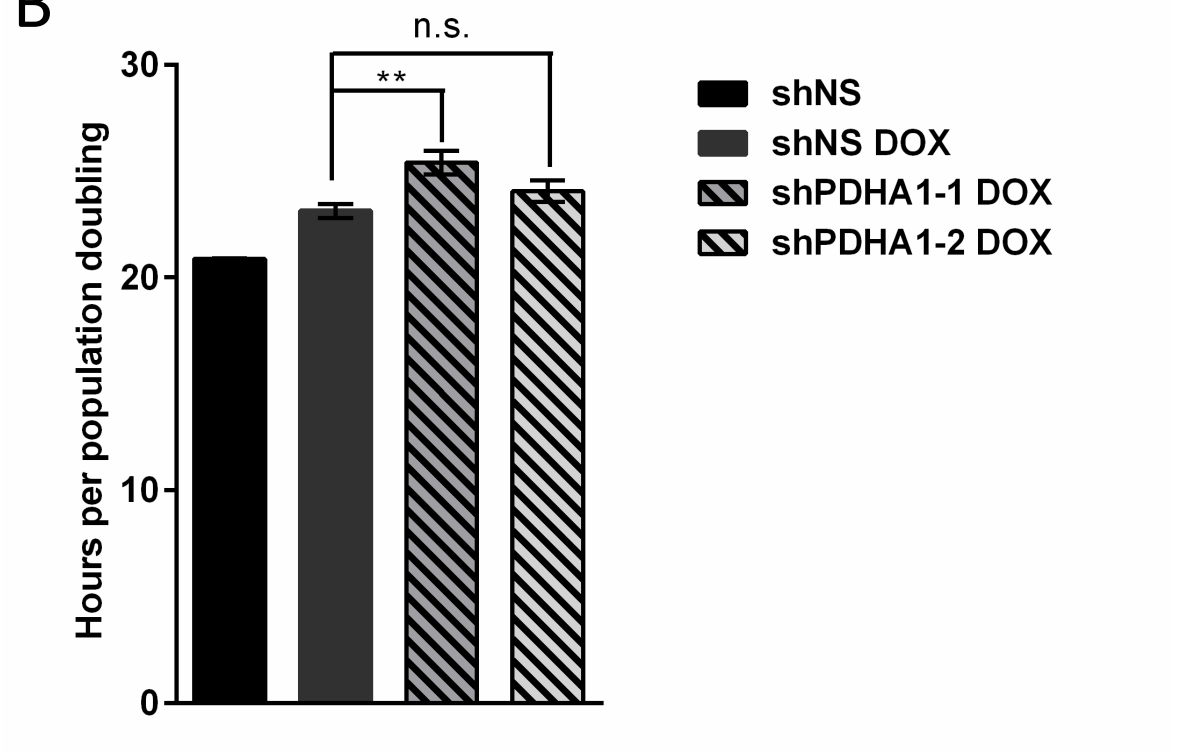

Figure 3.12 Reduction of PDHE1α does not significantly alter proliferative capability. H460 cells were grown in media that is identical to labeling conditions (10 mM glucose and 4 mM glutamine). Cells were counted every 4 days, and 100 K cells were re-plated each time and allowed to proliferate. **(A)** is a scatter plot of cell growth and **(B)** represents the hours per population doubling from the same experiment. Values are biological triplicates with error bars representing SD. *P, <.05; **P<.005.

CHAPTER 4

PDH REQUIREMENT FOR OPTIMAL GROWTH IN LIPID POOR CONDITIONS

4.1 Introduction

The results in the last chapter illustrated that despite decreasing *de novo* lipogenesis from glucose by suppressing PDH activity, H460 cells were able to proliferate normally. It was imperative to look for compensatory pathways that might be upregulated to provide fatty acids, which are necessary for membrane synthesis during proliferation. Both *KRAS* mutations and hypoxia causes cells to shift from glucose derived acetyl-CoA for lipogenesis to scavenge lipids from the extracellular milieu (Kamphorst, Cross et al. 2013). Inhibition of monoacylglyerol lipase in cancer cells, which serves to liberate stored fatty acids, could be rescued by addition of exogenous fatty acids (Nomura, Long et al. 2010). This indicates that cell scavenging of fatty acids can circumvent the need for endogenous production. Injection of Ras protein is sufficient to increase pinocytosis in fibroblasts, thus implicating oncogene expression in scavenging nutrients (Bar-Sagi and Feramisco 1986).

Based on data from the Cancer Cell Line Encyclopedia, H460 cells express a canonical oncogenic mutation in *KRAS* (Piva, Ganzinelli et al. 2014). The data in the paragraph above illustrates that not only do cancer cells rely on an exogenous fatty acid supply for growth but also, very importantly, *KRAS* mutations upregulate this scavenging ability. Thus, determining whether H460 cells relied on fatty acid import when PDH activity was suppressed was very pertinent. Furthermore, HIF1α metabolic response, which is a transcription factor that governs the hypoxic response, transcriptionally upregulates PDK1, ultimately suppressing PDH activity

(Kim, Tchernyshyov et al. 2006). It is plausible that when PDH activity is suppressed by RNAi in H460 cells, pathways that are part of the Hif1α, such as fatty acid import, are upregulated. The experiments in the following chapter attempt to elucidate whether H460 cells are dependent upon exogenous lipid sources for proliferation when PDH activity is suppressed. I used a combination of lipidomics profiling of media fatty acids and viability assays to illustrate that H460 cells are dependent on exogenous lipids when PDH activity is suppressed.

4.2 Methods

4.2.1 Cell Culture

Methods were similar to those used in section 3.2.

4.2.2 Inducibly Knocking Down PDHA1

Methods were similar to those used in section 3.2.

4.2.3 Delipidation of FCS

Delipidated FCS (DFCS) was made by Jin Ye's lab according to a standardized protocol developed by Cham and Knowles (Cham and Knowles 1976). Briefly, lipids are extracted from 500 mL of fetal calf serum by mixing it with 400 mL of n-butanol and 400 mL of isopropyl ether at room temperature for 20 minutes followed by a 20 minute incubation on ice. Then samples are centrifuged, the aqueous layer is extracted, and mixed with another 200 mL of isopropyl ether. The samples are re-centrifuged, the aqueous phase is separated, and evaporated under nitrogen gas. The lyophilate is dissolved in 200 mL of distilled water and dialyzed against phosphate-buffered saline (PBS). The average concentrations of free fatty acids, triglycerides, and cholesterol typically before and after the delipidation protocol are as follows: 840 to 7.7 uM for free fatty acids, 280 to 7.5 ug/mL for cholesterol, and 600 to 23 ug/mL for triglycerides (Hannah, Ou et al. 2001).

4.2.4 Fatty Acid Uptake Experiments

2 million H460 cells were plated in 10 cm tissue culture dishes and 12-24 hours later, when cells had reached the appropriate confluence, unlabeled glucose and glutamine at 10 mM and 4 mM respectively were provided in DMEM supplemented with 5% dialyzed FBS and penicillin/streptomycin. Uptake experiments took place for 24 hours at which point media was collected. Cellular protein was extracted using .1% Triton-X 100. Media was collected and given to Jeffrey McDonald and Carlos Rodriguez-Navas for profiling of free fatty acids by lipidomics, explained in the next paragraph.

4.2.5 Lipidomics Analysis of Medium for Free Fatty Acids

Free fatty acids contained in the medium were analyzed using a method adapted from Quhenberger, *et al* (Quehenberger, Armando et al. 2008). Free fatty acids were extracted from medium using 50:50 mixture of methanol and isooctane. After extraction, samples were dried down by vacuum evaporation. Samples were derivatized using 1% pentafluorobenzyme bromide (PFB). Samples were then re-evaporated and the lyophilate was re-constituted in isooctane and analyzed by electron capture negative ion GC-MS using internal standards for calibration.

4.2.6 Protein Content of Cell Extracts

Methods were similar to those described in section 3.2.

4.2.7 Growth Rate Assays

Procedure is identical to growth rate assays described in section 3.2. The only exception is that medium was made with 5% delipidated FCS rather than normal (lipid-replete) FBS used for the growth assay in section 2.2.

4.2.8 Fatty Acid Rescue Assays

100K cells were plated in triplicate in wells of a 6-well plate. Plating occurred in DMEM base with 10 mM glucose, 4 mM glutamine, and 5% DFCS, with 100 ng/mL doxycycline as appropriate. Cells that were plated in rescue wells were also given a 50 µM mixture of palmitate and oleate complexed to essentially fatty-acid free BSA (Sigma). Cells were counted after 4 days of growth using a Beckman-Coulter Vi-Cell XR Cell Viability Analyzer.

4.3 Results

4.3.1 Suppression of PDH Activity Causes Increased Consumption of Palmitate and Oleate

As mentioned in the previous chapter, although *de* novo lipogenesis from glucose was decreased when PDH activity was abrogated, cell proliferation was not affected. It was possible that cells were scavenging fatty acids to maintain proliferation. In order to test this, I worked with Jeff McDonald and Carlos Rodriguez-Navas in the Department of Molecular Genetics. Lipidomics was performed on cell medium to determine consumption of which, if any, free fatty acids increased upon abrogation of PDH activity. As depicted in figure 4.1, both palmitic and oleic acid consumption were upregulated under loss of PDH activity.

4.3.2 Suppression of PDH Activity in Lipid Poor Conditions Causes Growth Retardation

Because cells with loss of PDH activity upregulated fatty acid uptake, cells were challenged to grow in medium containing serum that had been delipidated using chemical procedures. Although medium containing delipidated serum caused a growth disadvantage even in control cells, cells with reduced PDHE1α were more affected, as illustrated in the growth curve in figure 4.2(A). Using the growth rate, the doubling time of all the cell types grown in medium containing delipidated serum was calculated. Depicted in figure 4.2(B), the doubling time increases by approximately 30-40% when cells with suppressed PDH activity are grown in medium containing delipidated serum. This illustrates that cells that have reduction in PDH activity rely on extracellular lipids to sustain normal proliferation rates.

4.3.3 Cells with Suppressed PDH Activity Grown in Delipidated Medium Can Be Rescued with Long Chain Fatty Acids

As discussed above, cells with reduced PDH activity exhibited a growth defect when grown in media supplemented with delipidated serum rather than normal serum. Although this observation illustrated that access to lipids is necessary for optimal growth during reduction of PDH activity, I wanted to determine whether LCFAs alone were sufficient to restore growth under delipidated conditions. Thus, a 50 μmolar mixture of palmitate and oleate were added to the delipidated medium. As depicted in figure 4.3, the mixture of fatty acids provided a complete rescue of growth in cells that had reduced PDH activity. Remarkably, supplementation with 50 μmolar palmitate and oleate not only completely rescued growth but also caused increased growth compared to control cells. The implications of this observation will be discussed in the discussion section.

4.4 Discussion

The experiments performed in this chapter were designed to uncover whether alternative pathways required for growth maintenance were engaged when PDH activity was suppressed. Based on the results illustrated in figures 4.1 and 4.2, when PDH activity is suppressed in H460 cells, they rely on extracellular lipids for maintenance of growth. Importantly, this suggests that the availability of extracellular fatty acids might define the requirement for maximal PDH activity in tumors. However, very importantly, these results do not indicate that glucose oxidation is suppressed in proliferating cells within a tumor; the data only indicate that if a tumor does suppress glucose oxidation, that nutrients in the extracellular milieu might be sufficient for growth. Moreover, it is plausible that import of extracellular nutrients is possible in cells proliferating *in vitro* due to the nutrient-rich extracellular environment but is impossible for tumors growing *in vivo* due to factors such as poor perfusion. Xenograft models of PDH suppression are necessary to determine whether maximal PDH activity is required for tumor growth *in vivo.* Additionally, the experiments determined that addition of the LCFAs palmitate and oleate were sufficient to completely rescue growth, indicating that cell is able to utilize these two fatty acids to circumvent a requirement for maximal PDH activity.

As illustrated in figure 5.2, it is interesting that addition of fatty acids rescued and increased proliferation of cells with PDHE1α reduction above control cells. Based on this data, it is possible that as PDH activity is reduced, cells begin to upregulate alternative pathways to maintain a supply of lipids. Thus, if these pathways were upregulated in cells with reduced PDH

activity, this might cause them to more readily utilize exogenous lipids than control cells in which alternative pathways have not been upregulated. This is an interesting possibility because if tumor cells in some instances suppress mitochondrial oxidation of glucose for evasion of cell death, these cells might be exquisitely dependent on nutrients in their environment. This would make therapeutics that target these import pathways more toxic to cells with suppressed glucose oxidation, potentially cells in certain tumors.

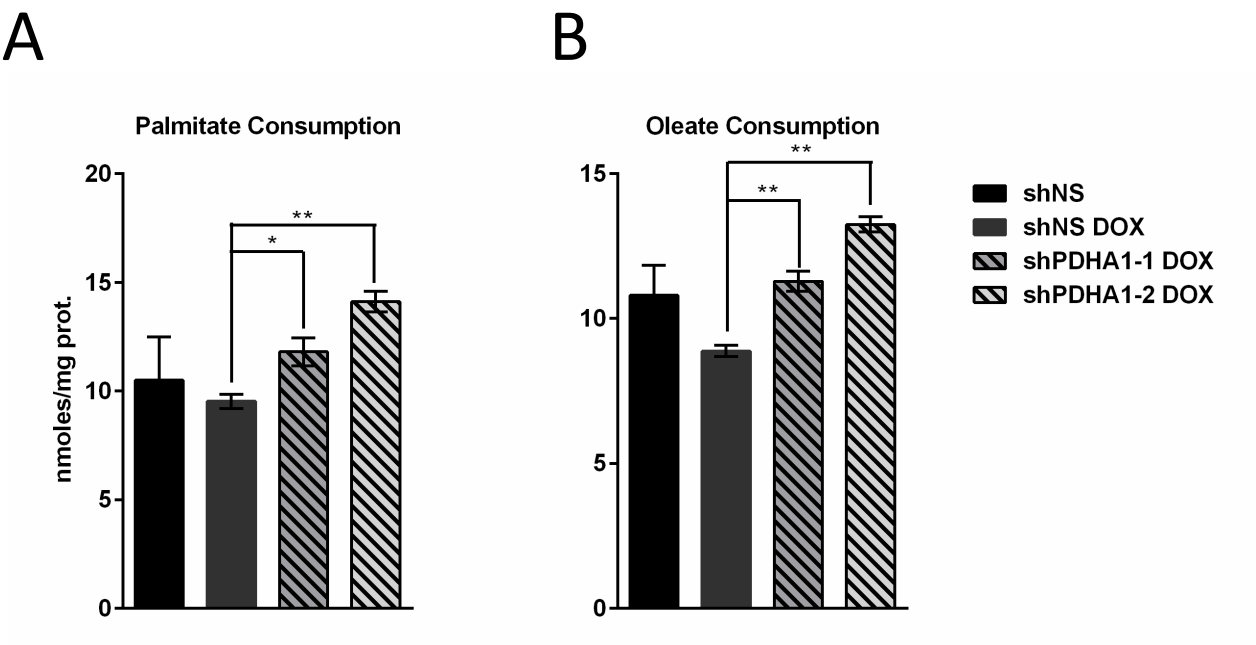

-

Figure 4.1 Reduction of PDHE1α increases cellular consumption of long chain fatty acids palmitate and oleate. H460 cells were incubated with 10 mM glucose and 4 mM glutamine for 24 hours and media was collected and analyzed by LC-MS/MS. **(A)** Consumption of palmitate is depicted and **(B)** consumption of oleate is depicted. Values are biological triplicates with error bars representing SD. *P, <.05; **P<.005.

A

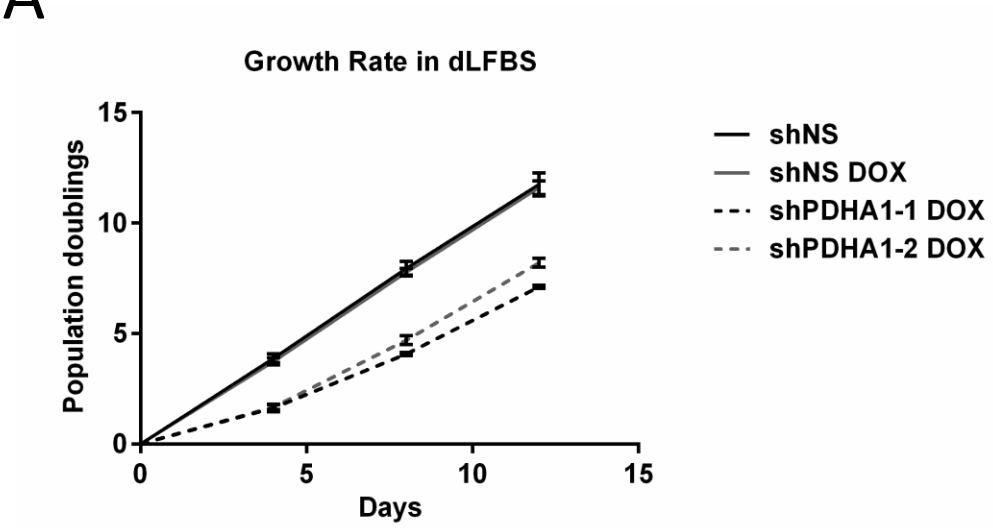

B

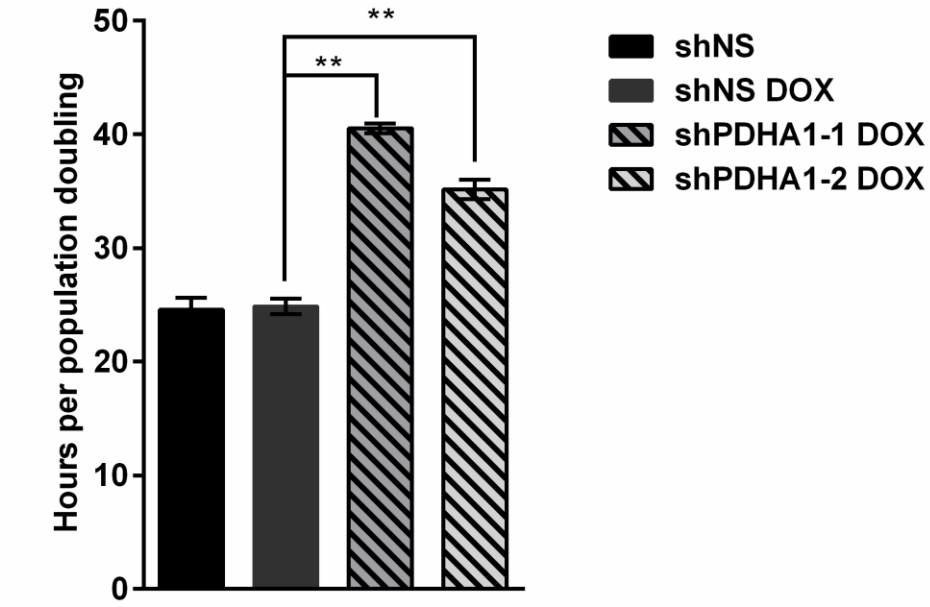

Figure 4.2 Reduction of PDHE1α retards growth in delipidated conditions. H460 cells were grown in media that is identical to labeling conditions (10 mM glucose and 4 mM glutamine) except that the serum had been delipidated. Cells were counted every 4 days, and 100 K cells were re-plated each time and allowed to proliferate. **(A)** is a scatter plot of cell growth and **(B)** represents the hours per population doubling from the same experiment. Values are biological triplicates with error bars representing SD. *P, <.05; **P<.005.

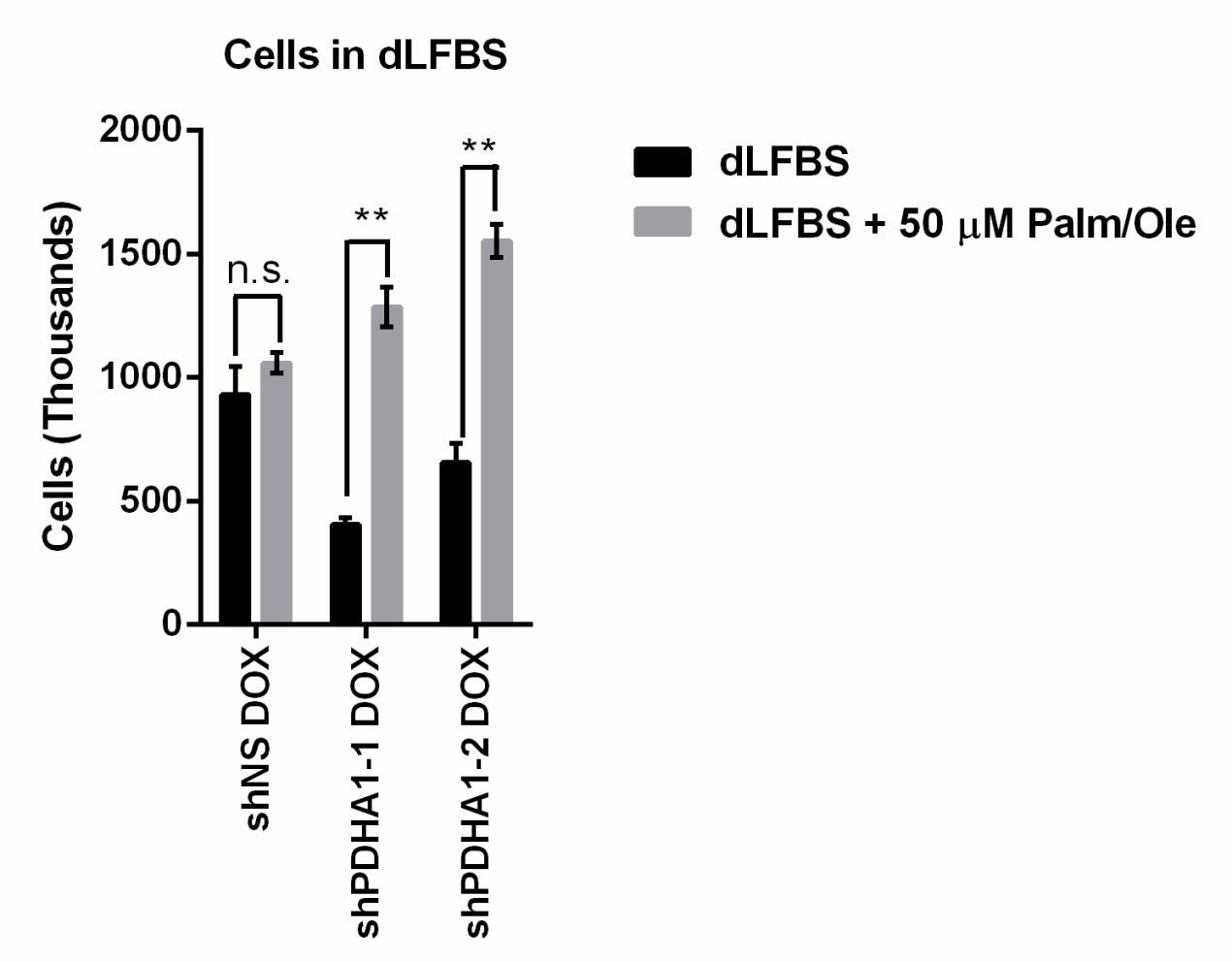

Figure 4.3 Adding back a combination of palmitate and oleate is able to fully rescue growth retardation caused by loss of PDH activity in delipidated conditions. Both control cells and cells with reduction of PDHE1α levels were plated in delipidated conditions and conditions where a 50 μM mixture of palmitate and oleate were added back. Cells were counted after 4 days of growth. Values are the average of a biological triplicate with error bars representing SD. *P, <.05; **P<.005.

CHAPTER 5

ALTERNATIVE LIPOGENIC PATHWAYS

5.1 Introduction

Although the experiments performed in the last chapter led to the discovery that H460 cells that have PDH suppression rely on lipids in the medium for maintenance of growth, these cells still proliferated in delipidated conditions. Based on this finding, I decided to use stable isotope tracing with the second most abundant carbon source in growth medium, glutamine. Experiments conducted in the DeBerardinis Lab have illustrated that glutamine-derived carbon (rather than glucose-derived) comprises the majority of lipogenic acetyl-CoA under conditions such as ETC dysfunction and FH deficiency. Glutamine dependent fatty acid biosynthesis occurs through reductive carboxylation of α-ketoglutarate to citrate that is dependent on isocitrate dehydrogenase (IDH), isoforms 1 and 2. The citrate then undergoes cleavage by ACL to make acetyl-CoA for palmitate biosynthesis (Mullen, Wheaton et al. 2012). Osteosarcoma cells that are deficient in cytochrome B are unable to dissipate their high NADH/NAD+ ratios. The reducing equivalents are transferred to NADPH whose abundance then allows both IDH1 and IDH2 to run in the reverse direction, creating lipids from glutamine in the process (Mullen, Hu et al. 2014).

Another group has shown that under hypoxia or loss of the Von Hippel Lindau (VHL) tumor suppressor, an enzyme responsible for degrading Hif1α, that glutamine dependent fatty acid synthesis increases, this time by reductive carboxylation of α-ketoglutarate by IDH1. The study also showed that by treating cells in hypoxic conditions with DCA, that glutamine

dependent fatty acid synthesis could be decreased (Metallo, Gameiro et al. 2012). This result indicates that suppression of PDH activity by hypoxia is responsible for causing synthesis of fatty acids from glutamine. Additionally, this implicates PDH activity as having an effect on glutamine dependent fatty acid biosynthesis as DCA would inhibit PDK1 mediated phosphorylation (inactivation) of PDH.

Another group illustrated that it was actually the citrate pool size to α-ketoglutarate pool size ratio that caused glutamine to be reductively carboxylated and feed into fatty acid synthesis. They showed that even when cells were treated with drugs that inhibited complexes of the ETC, increasing the citrate pool size could suppress reductive carboxylation of α-ketoglutarate (Fendt, Bell et al. 2013).

This collection of studies illustrates that there might be two distinct causes of reductive carboxylation of glutamine-derived carbon contributing to fatty acid synthesis: (1) a reductive potential causing the IDH reactions to run in the reductive direction and (2) a decrease in the abundance of citrate leading to a decrease in isocitrate levels causing a net reductive flux. Suppression of PDH activity led to a 70% reduction in citrate levels illustrated in figure 3.8(A). It is plausible that the shift in this ratio is causing H460 cells to undergo reductive carboxylation of α-ketoglutarate to synthesize lipids. This flux is promoting cell proliferation even in the face of suppression of glucose derived lipogenesis and lack of access to media fatty acids. The subsequent experiments were performed using [U-^{13}C] glutamine to uncover whether H460 cells relied on glutamine for lipogenic acetyl-CoA during suppression of PDH activity.

5.2 Methods

5.2.1 Cell Culture

Methods were similar to those described in section 3.2.

5.2.2. Inducibly Knocking Down PDHA1

Methods were similar to those described in section 3.2.

5.2.3 Metabolic Flux Experiments

Methods were similar to those described in section 3.2 except that cells were incubated with 10 mM unlabeled glucose and 4 mM [U-^{13}C] glutamine.

5.2.4 Protein Content of Cell Extracts

Methods were similar to those described in section 3.2.

5.2.5 GC-MS Analysis of Organic Phase

Methods were similar to those described in section 3.2.

5.2.6 GC-MS Analysis of Aqueous Phase

Methods were similar to those described in section 3.2.

5.2.7 Software Analysis of Mass Spectra

Methods were similar to those described in section 3.2.

5.2.8 Metabolic Flux Analysis (MFA) and Isotopic Spectral Analysis (ISA)

These methods were performed by Robert Egnatchik, a postdoctoral fellow in the DeBerardinis Lab. The INCA (Isotopomer Network Compartimentalized Analysis) software package allows users to take into account the stoichiometry and atom transitions of glycolysis, the TCA cycle, and biomass generation and simulates mass isotopomer distributions in metabolites (Young 2014). Flux estimations of the metabolic pathways are made using steady state MFA according to the best fit of the simulated MIDs to experimental MIDs.

5.3 Results

5.3.1 Foreword

A schematic of stable isotope tracing with [U-^{13}C] glutamine is illustrated in figure 2.5 in order to aid the reader with interpretation of the data in this section

5.3.2 Reduction of PDHE1α Alters Glutamine Labeling in TCA cycle Intermediates

As depicted for glucose labeling in the previous chapter, the MIDs that result in the TCA metabolites citrate, succinate, fumarate, and malate when H460 cells with reduced PDH activity are labeled with uniformly labeled glutamine are depicted in figures 5.1 and 5.2. Very importantly, reducing PDHE1α does not increase the percentage of the M+0 ion of any of the TCA metabolites as it did when glucose labeling was performed. This indicates that reduction in PDH activity does not decrease the ability of glutamine-derived carbon to enter the TCA cycle. However, reduction in PDHE1α levels causes a decrease in the M+2 that is due to a reduction in incorporation of unlabeled carbon from glucose which would normally undergo PDH mediated conversion to acetyl-CoA before entering the TCA cycle. Because PDHE1α levels have been reduced, there is less incorporation of unlabeled carbon from glucose in TCA metabolites, thus decreasing the M+2. In figures 5.1 and 5.2, the MIDs of the TCA metabolites are shown as having a slightly increased M+3 ion when PDH activity is reduced. The reasons for the increased M+3 are interesting and will be explored based on MFA in a subsequent section. The increase in the M+6 ion of citrate, depicted in figure 5.1(A), is potentially due to an increased proportion of fully labeled M+4 oxaloacetate being condensed with an M+2 acetyl-CoA molecule originating from pyruvate. This pyruvate is potentially derived from malic enzyme (ME) activity,

which would form a fully labeled pyruvate from an M+3 or M+4 (fully labeled) malate. This indicates ME activity in both the control and PDH-reduced conditions.

As illustrated in figure 5.1(B), one potential explanation of the increased M+4 in succinate when PDHE1α is reduced is due to the same reason that there is a decreased M+2--that in the succinate pool there is a greater proportion of carbon that has not undergone TCA cycling under PDH-reduced settings. This translates to a higher proportion of M+4 succinate and a lower proportion of M+2 succinate. A robust source of acetyl-CoA is required for carbon to circle the TCA cycle.

5.3.3 Reduction of PDHE1α Alters Glutamine Labeling in Glutamate and Aspartate

With respect to glutamate, reduction in PDHE1α levels causes a decrease in the M+3 ion with an increase in the M+5 ion. Again, because PDHE1α levels are reduced, entry of unlabeled acetyl-CoA derived from glucose is decreased. Therefore, carbon undergoing TCA cycling is decreased which causes a reduction in the M+3 ion. The increase in the M+5 ion is because a larger portion of glutamine in the cells that have reduced PDHE1α has only entered the cycle by deamidation and has not undergone cycling. This is very similar to the mass ion enrichment of the succinate pool mentioned in the last section.

As mentioned earlier, aspartate is the transamination product of oxaloacetate. Therefore, the aspartate MID, which is depicted in figure 5.3(B), reflects the labeling pattern of oxaloacetate. The reduction of M+2 in aspartate is due to lack of entry of unlabeled acetyl-CoA into the cycle thus diminishing TCA cycling and decreasing the M+2 in oxaloacetate. Additionally, the increase in aspartate M+3 is due to the same reaction that causes an increased

M+3 in fumarate or malate, as these metabolites all interconvert in reversible reactions. Very importantly, there is not an increase in the M+0 in glutamate or aspartate because glutamine is able to enter the cycle and be converted to aspartate without PDH activity.

5.3.4 Reduction in PDHE1α Slightly Increases Percentage M+2 in Alanine

As depicted in figure 6.4, there is a very small increase of M+2 alanine when PDH activity is reduced. This occurs due to ME activity which converts malate into pyruvate. An M+3 or M+4 malate would be converted to pyruvate. The reduction in PDH activity would then cause increased substrate for the ALT reaction, increasing transamination of pyruvate to alanine. Thus the combination of ME with reduction in PDH activity causes in an increase in M+2 alanine.

5.3.5 Reduction in PDH Activity Causes Increased Contribution of Glutamine to Palmitate Synthesis

As discussed in chapter 3 and depicted in figure 3.10, reduction in PDH activity causes a 30-40% decrease in glucose contribution to lipogenic acetyl-CoA. This is exemplified by the "left-shift" of palmitate MID when H460 cells with reduced PDH activity are labeled with [U-^{13}C] glucose. However, as depicted in figure 5.5, reduction in PDH activity increases glutamine contribution to lipogenic acetyl-CoA as illustrated by the "right-shift" that occurs when H460 cells with reduced PDH activity are labeled with [U^{13}-C] glutamine. This corresponds to an increase of 20% to 60% lipogenic acetyl-CoA derived from glutamine when PDH activity is reduced.

5.3.6 Metabolic Flux Analysis Indicates 60% Suppression of PDH Flux with Reduction of E1α Protein

Metabolic flux analysis used cellular growth rates, nutrient consumption and secretion, and MID from labeling experiments with [U-^{13}C] glucose and [U-^{13}C] glutamine and determined suppression of PDH flux under reduction of PDHE1α. As illustrated in figure 5.6, the PDH flux was calculated to be decreased by roughly 60% when PDHE1α was reduced. The fact that there is a small discrepancy between this calculation of reduction of PDH flux and the enzymatic assay potentially rests in the fact that activity is higher for control cells in the enzymatic assay due to mitochondrial protein isolation and maximal activation of the PDH complex with DCA. Higher activity in control cells would increase the percentage reduction of activity in the PDH suppressed cells.

5.3.7 Metabolic Flux Analysis Indicates Reductive Isocitrate Dehydrogenase 1 Flux During PDH Suppression

Surprisingly, when attempting to fit the measured fluxes with the simulated fluxes, the MID measured in palmitate could only fit the simulated flux correctly if a cytosolic IDH1 reaction was added to the network in the PDH suppressed cells. As depicted in figure 5.7, addition of this enzyme allowed the simulated MID in palmitate to match the measured MID. As depicted in the reaction network in figure 5.8(B), the IDH1 reaction added to the control H460 cells network (5.8(A)), would carboxylate glutamine derived α-ketoglutarate to citrate. The citrate would then cleaved by ACL to generate acetyl-CoA for lipogenesis. Interestingly, the M+3 ions of fumarate, malate, and aspartate (figures 5.2 and 5.3(B)) are all increased in cells

with suppressed PDH activity when labeled with [U-^{13}C] glutamine. Based on the modeling, this is potentially occurring because an M+5 citrate generated by IDH1 mediated reductive carboxylation of α-ketoglutarate is being cleaved by ACL to form acetyl-CoA and oxaloacetate. While the acetyl-CoA contributes to fatty acid synthesis, the oxaloacetate rejoins the TCA cycle. This would increase the M+3 in oxaloacetate and its transamination product aspartate as well as the malate and fumarate which can be interconverted by reversible reactions.

5.4 Discussion

The experiments described in this chapter examined glutamine metabolism during reduction of PDH activity by labeling H460 cells with [U-^{13}C] glutamine. A very important finding was that the M+0 ion of the TCA metabolites citrate, succinate, fumarate, and malate were not increased as they were when H460 cells with reduction in PDH activity were labeled with [U-^{13}C] glucose. This is important because it illustrates that metabolism of glutamine by the TCA cycle can be uncoupled from metabolism of glucose, such that entry of glutamine carbon into the TCA cycle appears to be irrespective of entry of glucose. However, in all TCA metabolites, there was significant suppression of the M+2 due to a lack of entry of glucose into the TCA cycle thus decreasing the cycling of glutamine derived carbon. The suppression of the M+2 reinforces the observations made when the cells were labeled with [U-^{13}C] glucose that there was suppression of the higher mass isotopes in the TCA metabolites due to reduced entry of glucose carbon caused by suppression of PDH activity.

An interesting finding in this chapter is the significant "right-shift" of the MID during suppression of PDH activity. These data indicate that the cell shifts its lipogenic acetyl-CoA source to glutamine when PDH is suppressed and glucose can no longer readily contribute to lipogenic acetyl-CoA. These data illustrate that an accessory pathway might allow for formation of lipogenic acetyl-CoA during suppression of glucose oxidation.

As illustrated in figures 5.7 and 5.8, the metabolic flux modeling indicated an interesting possibility: reductive carboxylation of glutamine derived α-ketoglutarate to generate fatty acids during suppression of PDH activity. Other studies have highlighted this pathway for lipogenesis

during hypoxia or when the citrate/α-ketoglutarate ratio is decreased (Metallo, Gameiro et al. 2012, Fendt, Bell et al. 2013). However, unlike my observations, the aforementioned groups had an increased citrate M+5 ion when labeling with [U-^{13}C] glutamine when reductive carboxylation is induced. If reductive carboxylation by IDH1 is occurring during PDH suppression, it is unclear why the citrate M+5 ion is not elevated when cells are labeled with [U-^{13}C] glutamine.

Therapeutically, this finding could be significant because if certain tumors suppress glucose oxidation, perhaps this pathway is active in providing fatty acids for proliferation *in vivo*. This possibility is translatable for therapeutic reasons as tumors that rely on glutamine for lipogenesis might be selectively vulnerable to therapeutics aimed at this pathway sparing normal cells that use glucose for production of fatty acids.

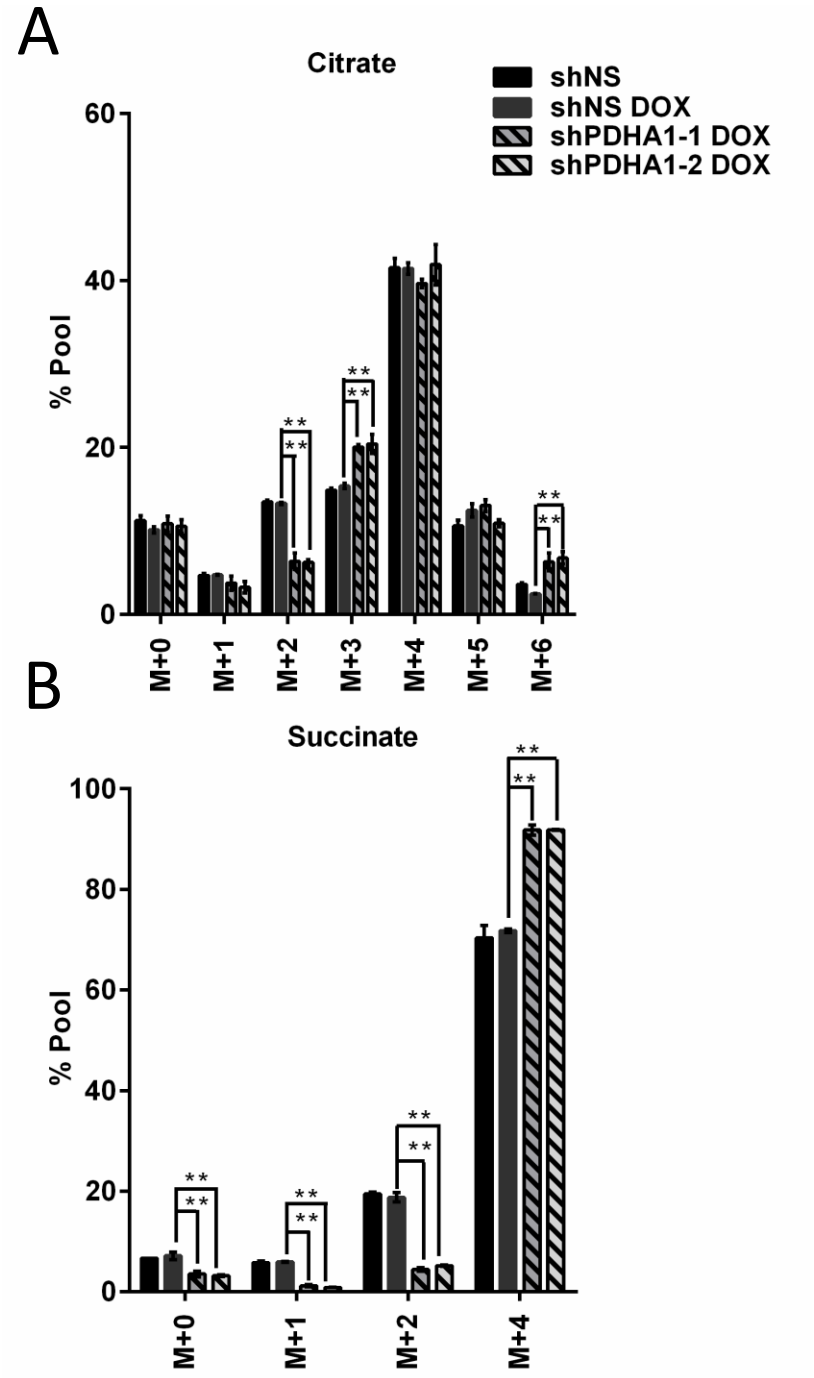

Figure 5.1 Reduction of PDHE1α alters MID of TCA metabolites citrate and succinate when labeled with [U-^{13}C] glutamine. H460 cells were incubated with 10 mM glucose and 4 mM [U-^{13}C] glutamine for 24 hours and metabolites were analyzed by GC-MS. **(A)** MID of citrate is depicted, and **(B)** MID of succinate is depicted. Values are biological triplicates with error bars representing SD. *P, <.05; **P<.005.

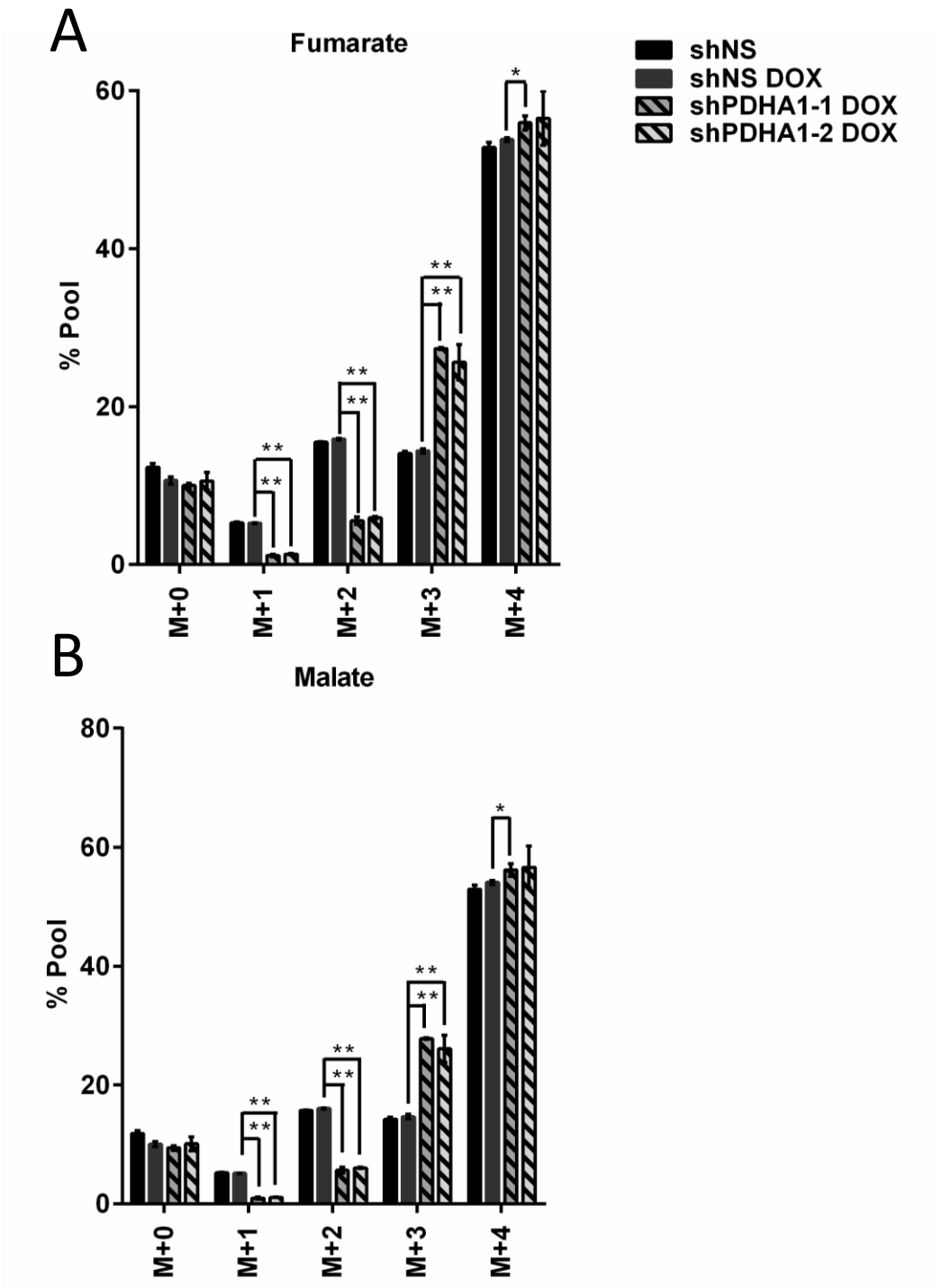

Figure 5.2 Reduction of PDHE1α alters MID of TCA metabolites fumarate and malate when labeled with [U-^{13}C] glutamine. H460 cells were incubated with 10 mM glucose and 4 mM [U-^{13}C] glutamine for 24 hours and metabolites were analyzed by GC-MS. **(A)** MID of fumarate is depicted, and **(B)** MID of malate is depicted. Values are biological triplicates with error bars representing SD. *P, <.05; **P<.005.

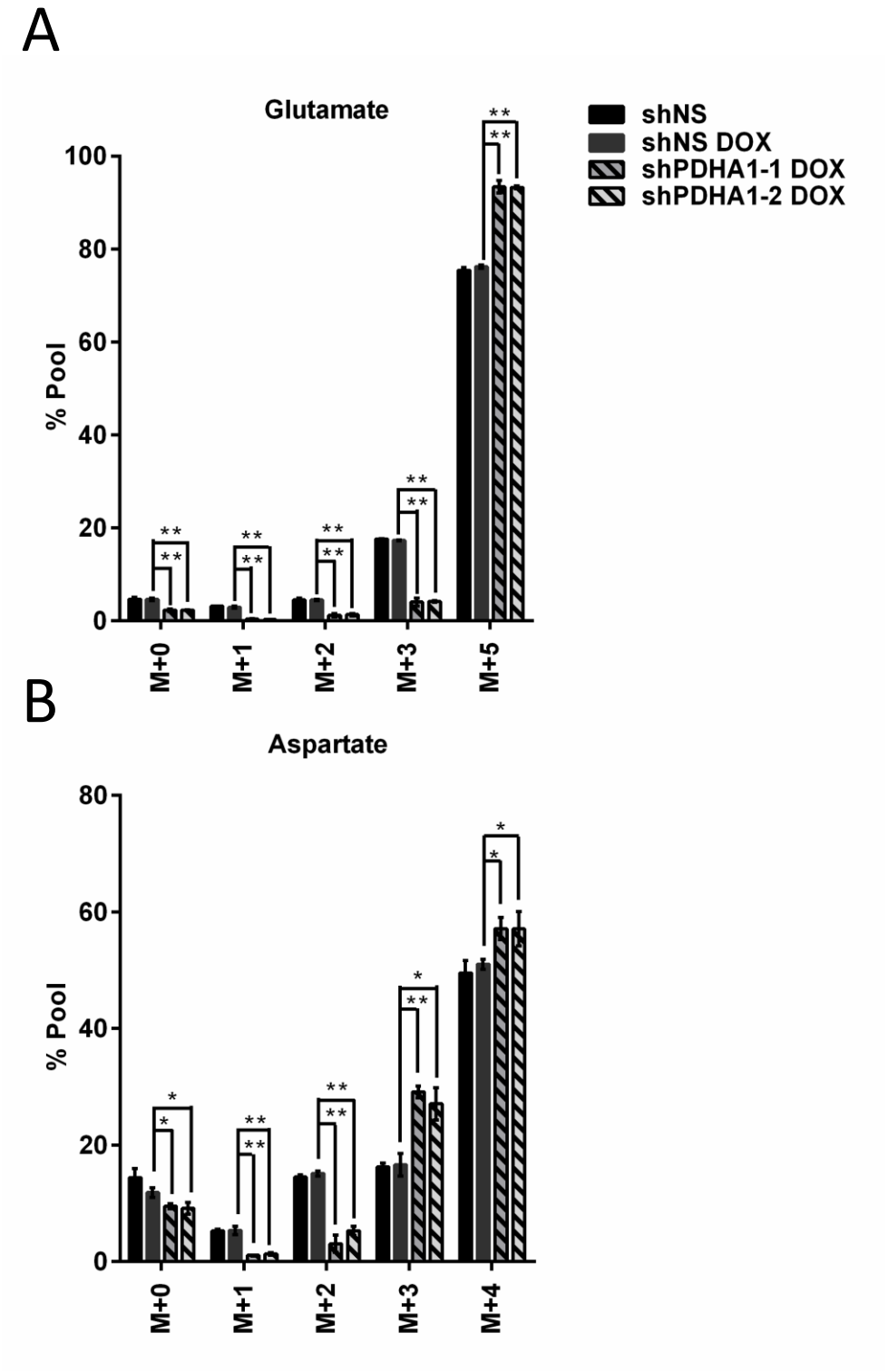

Figure 5.3 Reduction of PDHE1α alters MID of amino acids glutamate and aspartate when labeled with [U-^{13}C] glutamine. H460 cells were incubated with 10 mM glucose and 4 mM [U-^{13}C] glutamine for 24 hours and metabolites were analyzed by GC-MS. **(A)** MID of glutamate is depicted, and **(B)** MID of aspartate is depicted. Values are biological triplicates with error bars representing SD. *P, <.05; **P<.005.

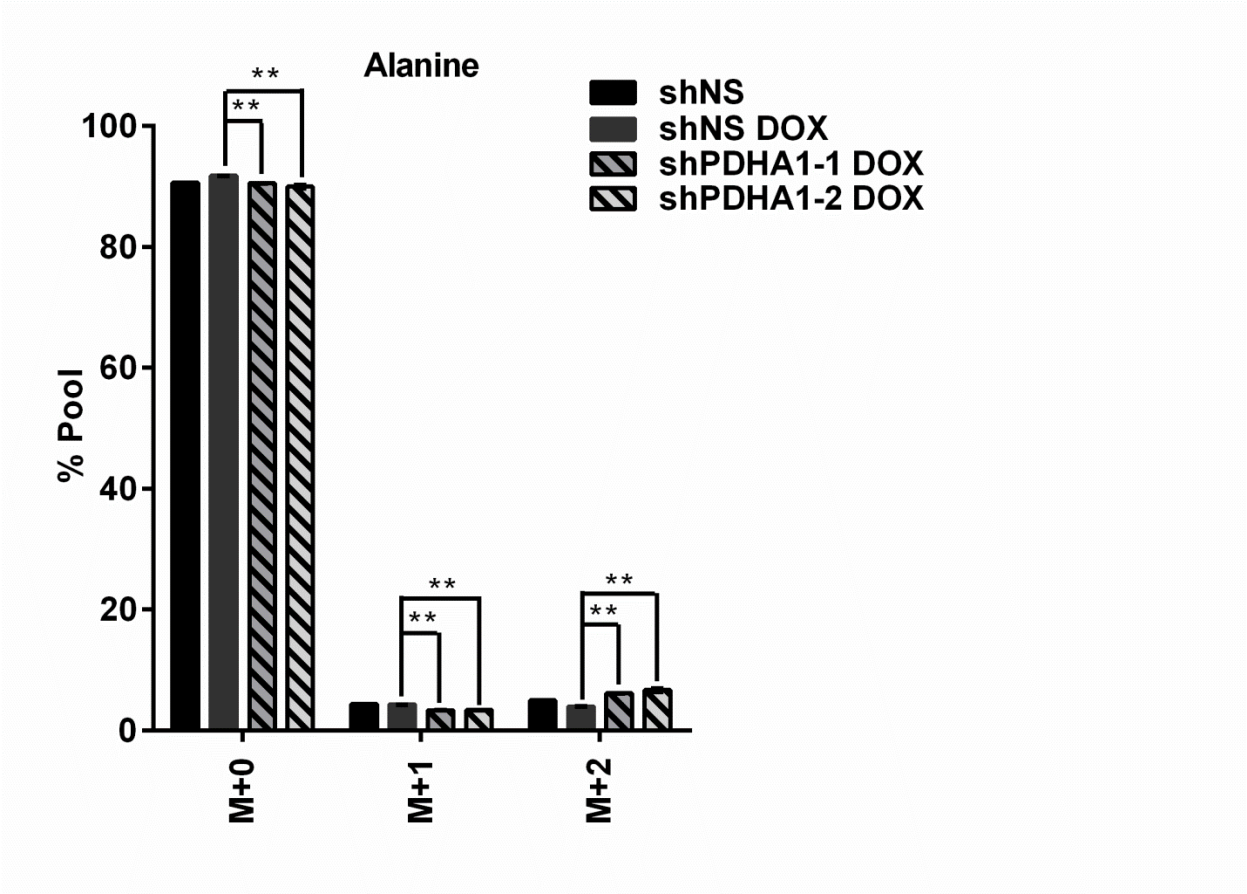

Figure 5.4 H460 cells do not show significant labeling in amino acid alanine when labeled with [U-^{13}C] glutamine. H460 cells were incubated with 10 mM glucose and 4 mM [U-^{13}C] glutamine for 24 hours and metabolites were analyzed by GC-MS. Two carbon fragment of alanine was selected for analysis due to MS interference for analysis of the entire molecule. MID of alanine is depicted. Values are the average of a biological triplicate with error bars representing SD. *P, <.05; **P<.005.

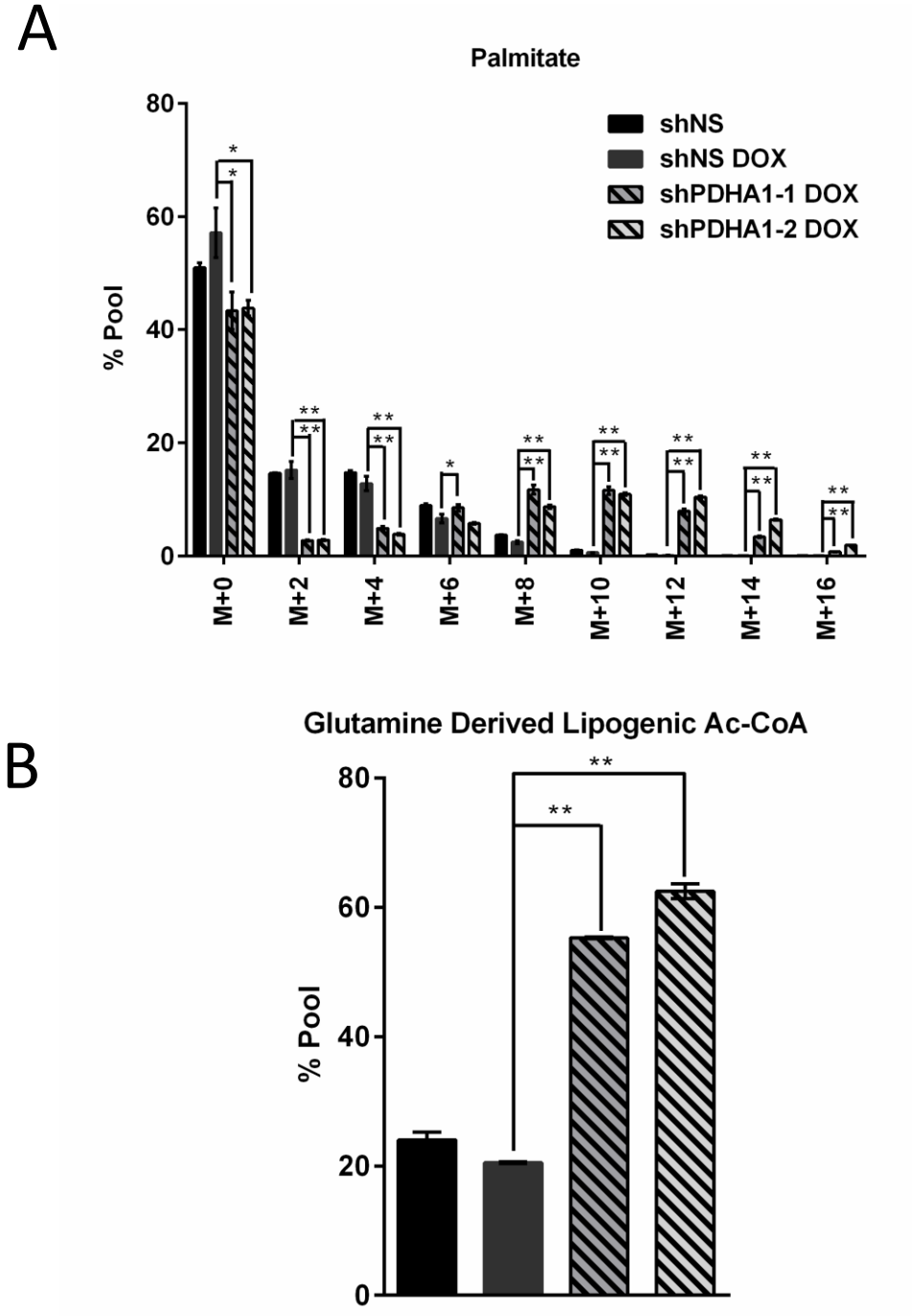

Figure 5.5 Reduction in PDHE1α increases contribution of glutamine carbon to fatty acid synthesis. H460 cells were incubated with 10 mM glucose and 4 mM [U-^{13}C] glutamine for 24 hours and metabolites were analyzed by GC-MS. **(A)** MID of palmitate is depicted. **(B)** Percent lipogenic acetyl-CoA derived from glutamine for palmitate synthesis. Values are the average of a biological triplicate with error bars representing SD. *P, <.05; **P<.005. *Abbreviations:* Ac-CoA, acetyl-CoA.

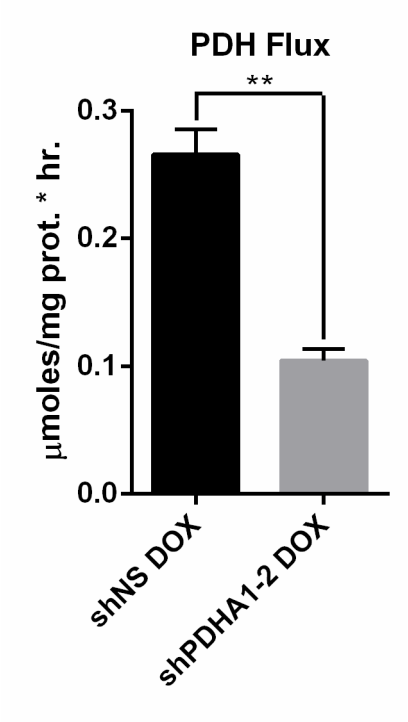

Figure 5.6 Metabolic flux analysis calculates an approximately 60% reduction in PDH flux in the shPDHA1-2 DOX condition. INCA software was used to model extracellular fluxes, growth rate, and MIDs from [U-^{13}C] glucose and [U-^{13}C] glutamine experiments to determine PDH flux. *P, <.05; **P<.005.

A

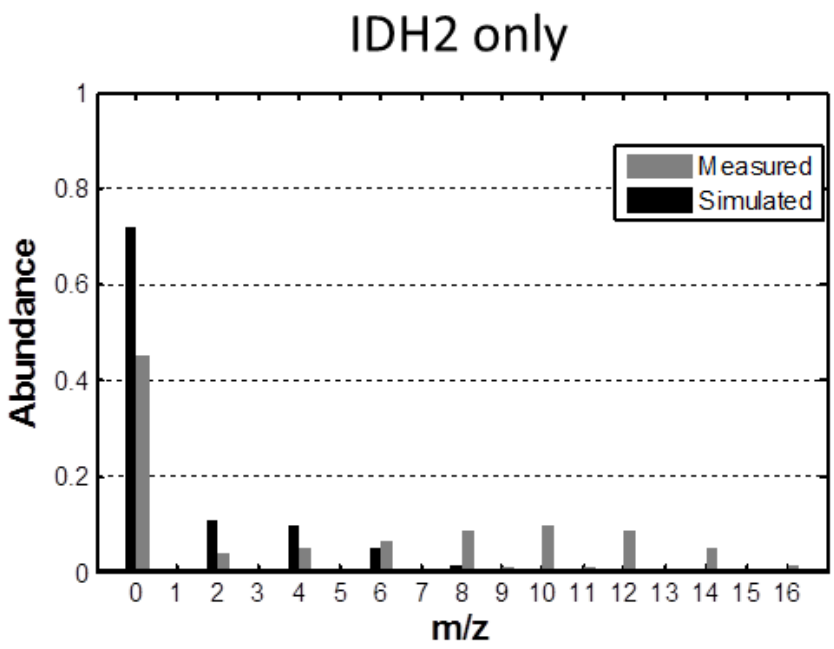

B

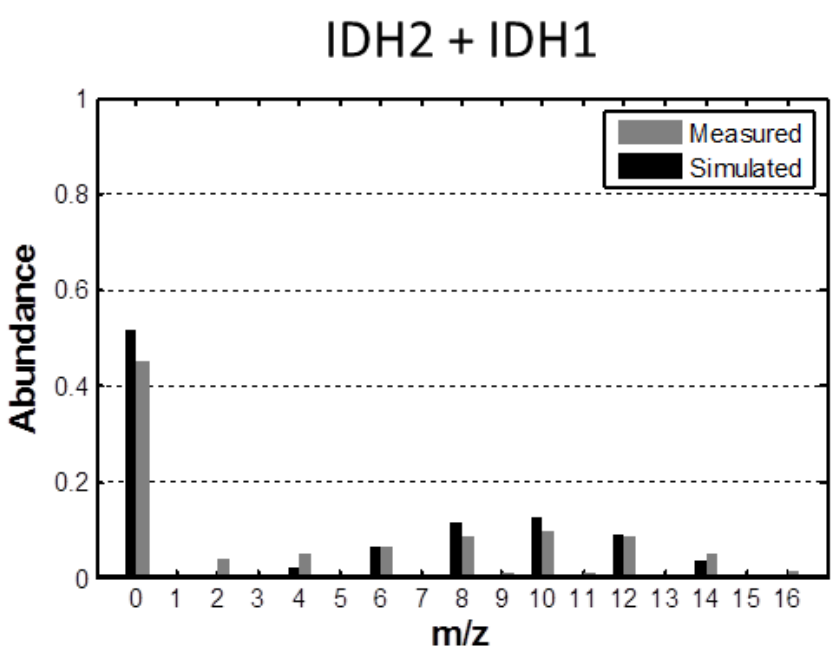

Figure 5.7 Addition of IDH1 in shPDHA1-2 DOX condition to simulation is able to best fit measured MID in palmitate based on metabolic flux analysis. (A) Measured MID of palmitate when labeled with [U-^{13}C] glutamine and in INCA simulation with exclusively IDH2. **(B)** Measured MID of palmitate when labeled with [U-^{13}C] glutamine and in INCA simulation with both IDH1 and IDH2. *Abbreviations:* IDH, isocitrate dehydrogenase. Figure adapted from the one by Robert Egnatchik.

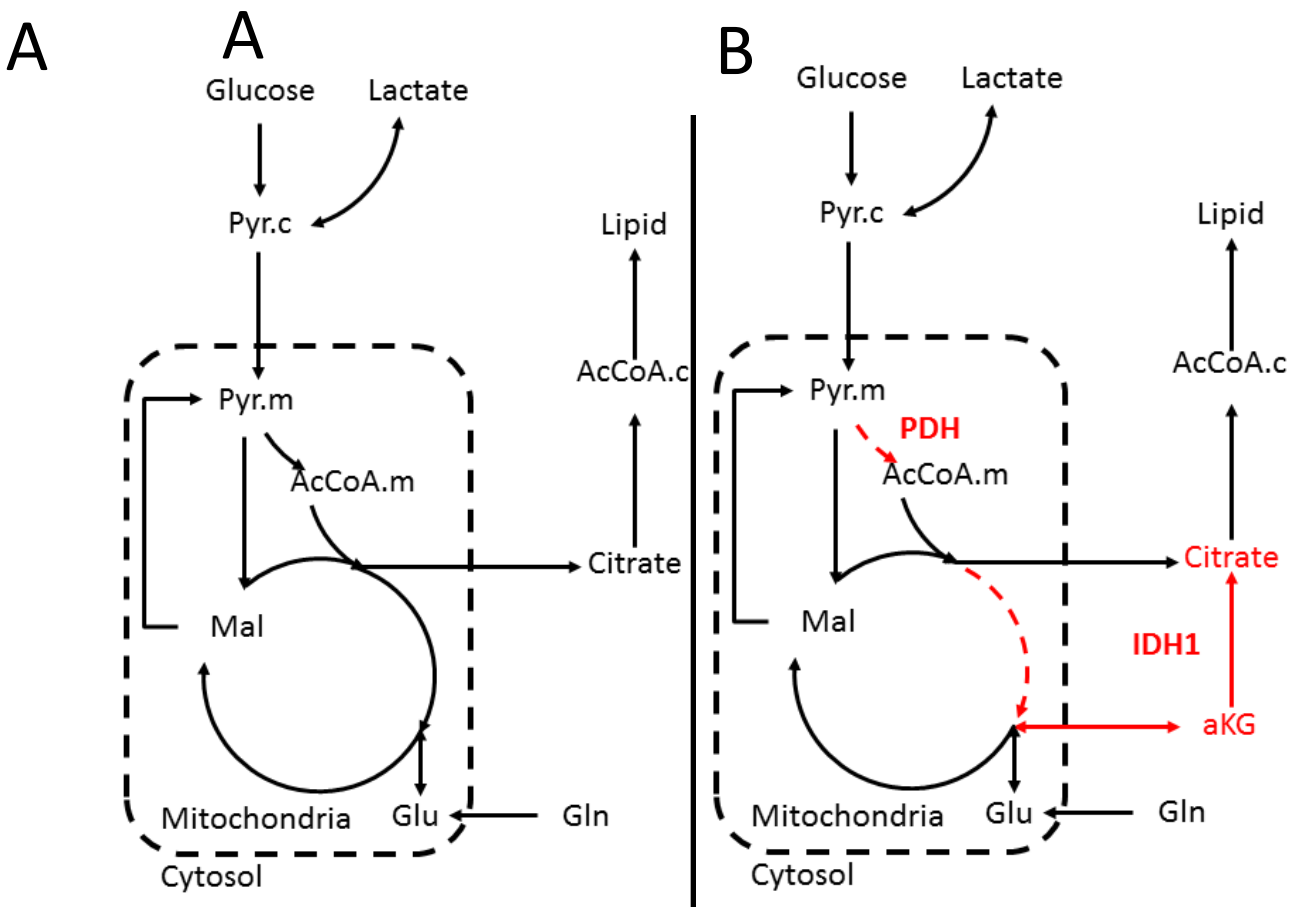

Figure 5.8 Metabolic flux analysis identifies a potential role for cytosolic IDH1 for lipid synthesis under suppression of PDH activity. Metabolic flux analysis was performed using the INCA software using [U-^{13}C] glucose and [U-^{13}C] glutamine MIDs along with extracellular fluxes and synthesis of biomass in **(A)** shNS DOX and **(B)** shPDHA1-2 DOX conditions. Reactions that change between the control and PDH suppressed network are displayed in red. *Abbreviations:* AcCoA.c, cytosolic acetyl-CoA; AcCoA.m, mitochondrial acetyl-CoA; aKG, α-ketoglutarate; Gln, glutamine; Glu, glutamate; IDH1, isocitrate dehydrogenase 1; Mal, malate; Pyr.c, cytosolic pyruvate; Pyr.m, mitochondrial pyruvate. Figure adapted from the one created by Robert Egnatchik.

CHAPTER 6

CLOSING REMARKS

6.1 Conclusion

Through this work, I attempted to determine whether mitochondrial glucose oxidation was required for cell proliferation. Previous work has shown that cells proliferating *in vitro* and tumors growing *in vivo* display enrichment of TCA cycle intermediates when fed isotopically labeled glucose (Cheng, Sudderth et al. 2011, Maher, Marin-Valencia et al. 2012, Marin-Valencia, Yang et al. 2012), thus indicating glucose oxidation. I used H460, a large cell adenocarcinoma cell line that rapidly proliferates *in vitro* to conduct my studies. To determine the role mitochondrial oxidation of glucose carbon played in metabolism and proliferation, I sought to intervene at the PDH complex, as this gates entry of glucose derived carbon into the TCA cycle. To this end, I devised genetic tools to abrogate this activity and then assayed cellular metabolism and growth using GC-MS based approaches and different growth assays.

My findings were significant in that they showed conclusively that PDH activity modulates glucose-derived carbon flux into the TCA cycle and importantly, that this flux is required for optimal *in vitro* growth when cells do not have access to exogenous lipids. Furthermore, in a setting in which flux through PDH is significantly suppressed, extracellular free fatty acids are sufficient to maintain optimal growth in lipid-depleted medium. The experiments also illustrated conclusively that suppression of PDH activity activates glutamine dependent fatty acid synthesis. Whether this pathway is dependent on reductive carboxylation of α-ketoglutarate by IDH remains to be tested. This work finds that a significant function of

PDH is to allow glucose dependent fatty acid synthesis, a function that is critical for maintaining rapid proliferation in settings when cells don't have access to exogenous lipids.

6.2 Future Experiments

6.2.1 Participation of IDH1 in Glutamine Derived Fatty Acid Synthesis

The flux modeling data discussed in chapter 5 indicates that during suppression of PDH activity, IDH1 is reductively carboxylating α-ketoglutarate derived from glutamine to generate citrate and ultimately, acetyl-CoA for the purposes of fatty acid synthesis. As depicted in figure 4.3(A), H460 cells with PDH suppression and lack of access to serum lipids still are able to proliferate. It is plausible that under these circumstances, glutamine carbon is providing the carbon necessary for fatty acid synthesis and proliferation. Future experiments in this area should first determine whether IDH1 activity is causing the "right-shift" in labeling of palmitate from glutamine during suppression of PDH. To this end, a chemical inhibitor of IDH1 will be used to see if this change in labeling can be altered. Additionally, H460 *IDH1* knockout cells can be used to determine if loss of IDH1 function causes toxicity when PDH is suppressed. Exogenous lipids can also be withdrawn under this context to further deprive cells of alternative compensatory pathways.

6.2.2 Generalizability of Findings to Other Cell Lines

Only one cell line, H460, was used in the studies in this dissertation. Alterations in different oncogenes and tumor suppressors alter metabolic pathways to sustain the energetic and biosynthetic demands rapid cell proliferation (Jones and Thompson 2009). As discussed in

chapter 4, tumorigenic mutations in *KRAS* enhances lipid scavenging pathways (Kamphorst, Cross et al. 2013). As H460 cells contain a canonical oncogenic mutation in *KRAS* (Piva, Ganzinelli et al. 2014), it is possible that they are protected from suppression of PDH by scavenging lipids from their surroundings. Infection and induction of the shRNA against the PDHA1 transcript in SF188 cells also causes reduction of PDHE1α protein levels. As SF188 cells have a vastly different oncogenic profile than H460 cells (mutations in *NF1*, *MYC*, *PIK3CA*, *RB1*) (Bax, Little et al. 2009) it is possible that suppression of PDH activity might have a more profound effect on their growth. This should be tested in normal conditions as well as conditions in which exogenous lipids are depleted.

6.2.2 Necessity of PDH for *In Vivo* Tumor Proliferation

The findings in this dissertation indicate that proliferating cells rely on PDH activity for optimal growth when they don't have access to exogenous lipids. *In vitro*, cells are cultured in growth medium that is supplemented with serum that contains lipids and contains supraphysiological concentrations of glucose and glutamine. It is plausible that tumor growth *in vivo* requires PDH activity for maximal proliferation as rapidly proliferating tumors are hindered in their access to nutrients due to poor perfusion. In order to test this, H460 cells can be subcutaneously implanted as xenograft tumors in the flanks of nude mice. Doxycycline can then be administered in the drinking water in order to suppress PDH activity and examine the effect on growth.

6.2.3 PDH Knockout Mouse Embryonic Fibroblasts

As illustrated in figure 3.1(B), when PDH activity is suppressed by using RNA interference to reduce levels of PDHE1α, there is still residual PDH activity. The flux modeling performed in the last chapter also indicates residual PDH activity. Thus, work in this dissertation has not conclusively determined PDH's role in cell proliferation because PDH activity was not totally ablated by our methods. It is critical to study the effect of PDH loss on cellular metabolism and proliferation by using gene knockout rather than knockdown. To this end, *Pdha1* knockout MEFs (mouse embryonic fibroblasts) were generated that preliminarily display growth retardation, even in lipid-replete medium (figure 6.1). Although this loss of PDH function is in a different background than the studies illustrated previously, this potentially indicates that suppression of PDH activity can be circumvented when cells have access to lipids but complete loss of PDH activity cannot. More studies to understand the metabolic phenotype caused by *Pdha1* knockout as well as growth studies should be conducted. Something particularly interesting, illustrated in figure 6.2, is the possibility that some metabolites that are derived from the PDH reaction, such as citrate and fatty acids, are secreted or released by cells. This work has shown how scavenging metabolites can play a role in maintenance of growth during PDH suppression. Thus, cells that are deficient in PDH might be able to scavenge and use these metabolites that are secreted by PDH-functional cells to maintain their growth. This would be an interesting paradigm of the metabolic heterogeneity of cancer, where cancer cells rely on non-cell autonomous metabolic interaction for growth.

6.3 Open Questions

6.3.1 Are there biological functions for pyruvate in hypoxia?

The data contained in this dissertation illustrate that when PDH activity is suppressed, pyruvate is transaminated to alanine by ALT. As mentioned earlier, unpublished work from the DeBerardinis Lab indicates that ALT is located inside the mitochondrion as treating cells with an inhibitor of the mitochondrial pyruvate carrier decreases alanine secretion. Taken together, these observations indicate that suppression of PDH activity by reducing levels of PDHE1α potentially causes some of the excess pyruvate to enter the mitochondrion. A recent study indicated that during hypoxia oxidative metabolism of glutamine continued and was the major source of ATP (Fan, Kamphorst et al. 2013). This observation is paradoxical because as described earlier, during hypoxia, Hif1α upregulates transcription of PDK1, which phosphorylates and inhibits pyruvate dehydrogenase. This effectively shunts glucose towards fermentation by LDH rather than oxidation in order to regenerate NAD+ to maintain glycolysis with a suppressed ETC due to lack of oxygen. However, if oxidation of glutamine carbon continues, perhaps the suppression of PDH activity is to provide the cell with mitochondrial pyruvate. Work done on HL-60 leukemia cells showed that pyruvate could be used as an antioxidant against reactive oxygen species (ROS) (Brand and Hermfisse 1997). As cellular ROS is increased during hypoxia, perhaps the entry of pyruvate into the mitochondrion is used to buffer against oxidative damage (Hamanaka and Chandel 2009).

6.3.2 Is PDH activity required for tumorigenesis *in vivo*?

The studies above indicate that exogenous lipids maintain maximal cell proliferation when PDH activity is suppressed. However, lipid scavenging might only be able to compensate for suppression of PDH activity, not complete loss of PDH activity. Briefly touched upon in the

last section, *Pdha1* knockout MEFs display growth retardation even when grown in media supplemented with serum containing lipids. It seems possible that a requirement for oxidative metabolism of glucose through PDH might be critical for tumor growth and development at early stages of tumorigenesis. Genetically engineered mouse models of cancer could be used to answer this question.

6.3.3 Is PDH a druggable target in cancer?

As mentioned in chapter 1, oxidation of glucose is far more energetically efficient for the cell. When cells are energetically stressed, they phosphorylate AMPK, which allows them to undergo a catabolic program to upregulate metabolic processes such as fatty acid oxidation and autophagy. Phosphorylation of AMPK is mediated by an upstream kinase, LKB1, which is required for the stress response (Hardie and Alessi 2013). For cells that are deriving a significant amount of their ATP from oxidative phosphorylation, a drug against PDH would decrease the ATP/ADP ratio and potentially trigger an AMPK response mediated by LKB1. As just discussed, this would trigger metabolic responses such as fatty acid oxidation designed to preserve ATP levels and cell viability. As LKB1 is frequently mutated in non-small cell lung cancer, it seems plausible that tumor cells with this mutation might have difficulty facing an energetic stress due to their inability to respond by phosphorylating AMPK. In fact, the ETC inhibitor phenformin is selectively toxic to LKB1 deficient lung cancer cells due to their inability to respond to energetic stress (Shackelford and Shaw 2009). Thus, it would seem as if therapies against PDH might be differentially toxic to LKB1 deficient cancer cells while normal cells would respond with a canonical stress pathway mediated by a wild-type LKB1. Additionally, the PDH

complex has been found to translocate from the mitochondria to the nucleus in response to growth signals and mediate histone acetylation that leads to cell cycle progression (Sutendra, Kinnaird et al. 2014). Thus, perhaps targeting this function of PDH will retard cancer growth.

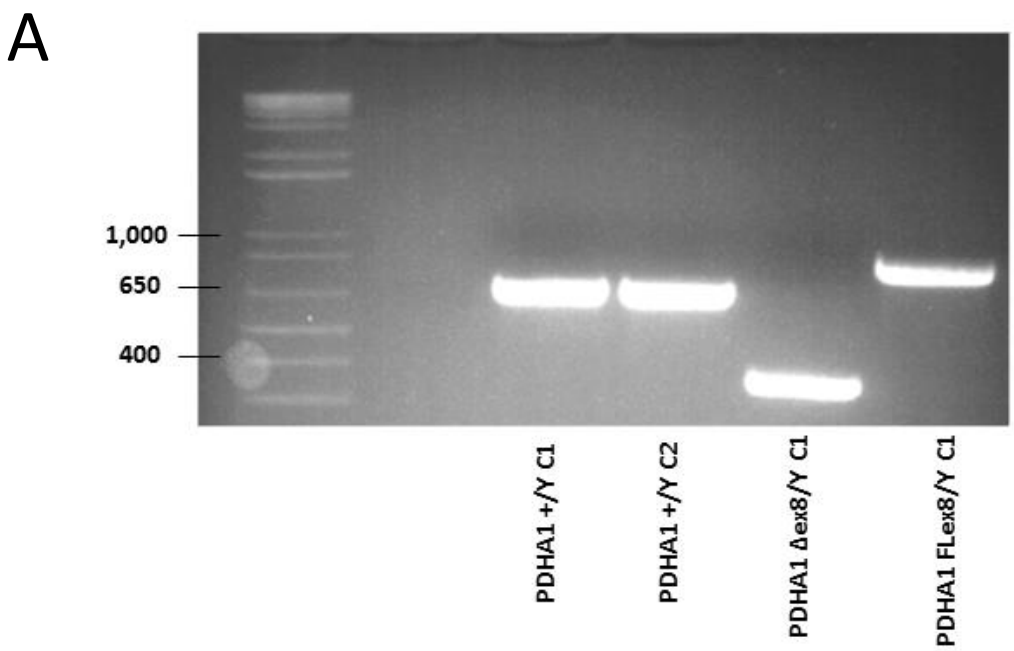

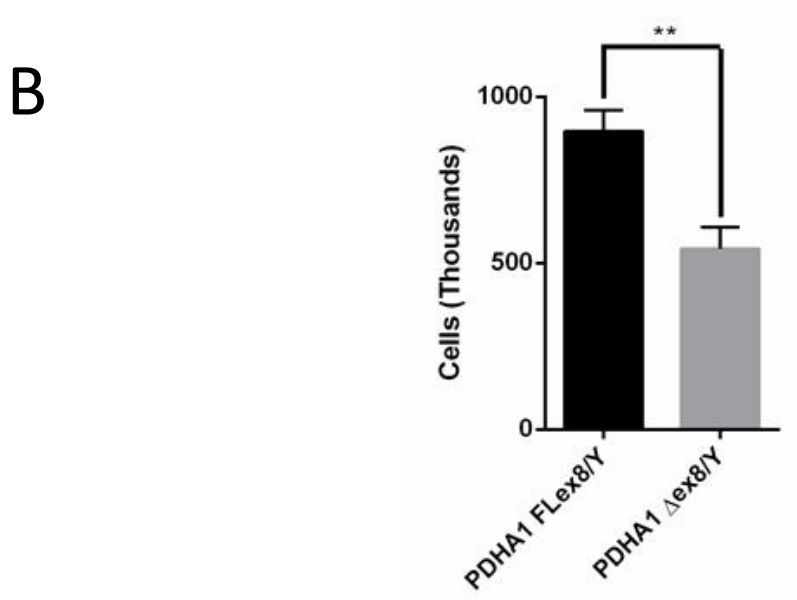

Figure 6.1 *PDHA1* knockout MEFs have a slowed proliferation rate in lipid-replete medium. MEFs expressing UBC-Cre/ERT2 were treated with 500 nM 4-hydroxytamoxifen. **(A)** Genotyping MEFs for *PDHA1*. Numbers on the left represent bases. **(B)** Growth after 60 hours starting with 100K cells. Values are the average of a biological triplicate with error bars representing SD. *P, <.05; **P<.005. *Abbreviations:* PDH, pyruvate dehydrogenase.

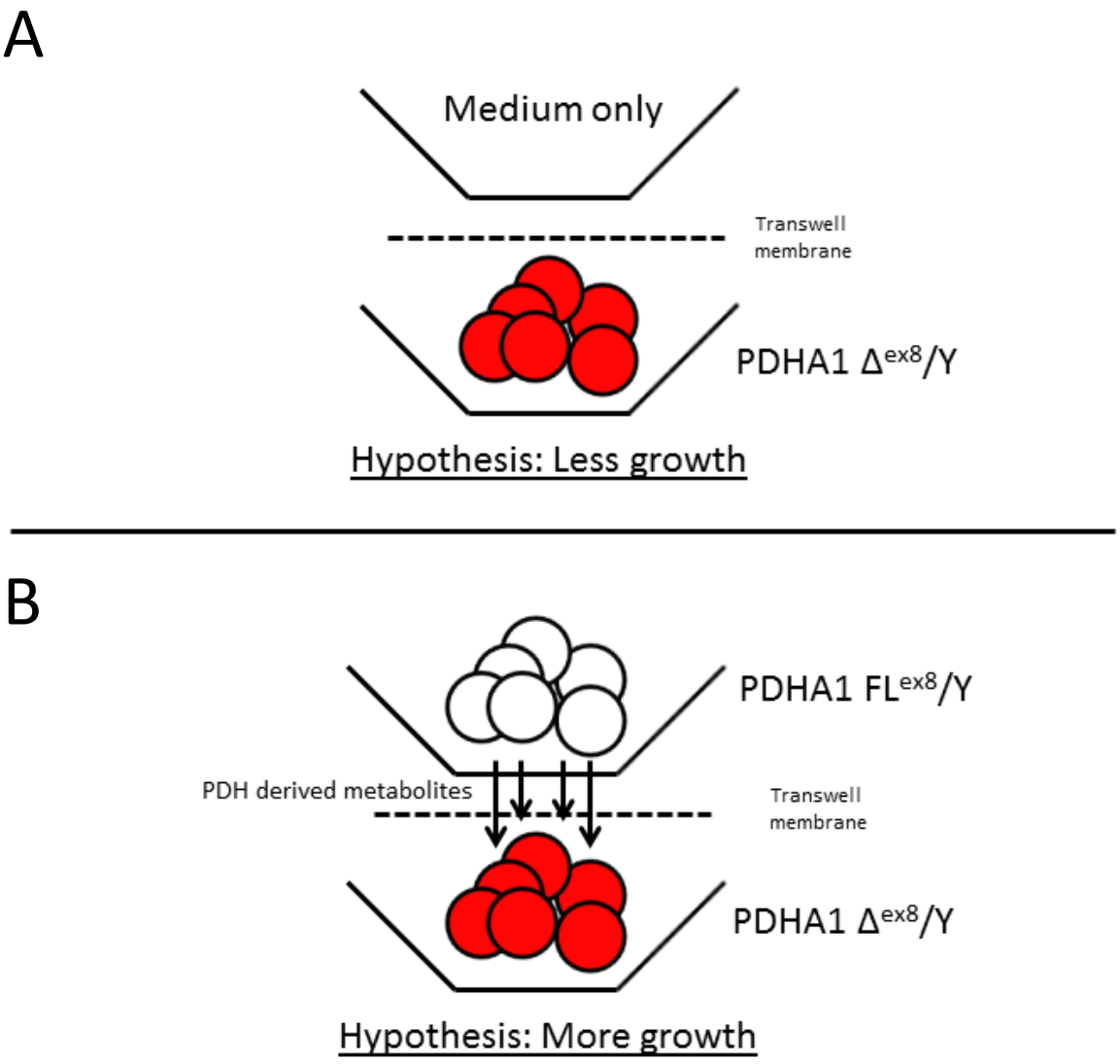

Figure 6.2 Experiment to determine if secreted metabolites derived from PDH can rescue PDH deficient cells. PDH deficient MEFs are plated on the bottom part of chambers with transwell membranes to allow diffusion of metabolites only. **(A)** Control condition is medium only on the top part. **(B)** Experimental condition is to plate MEFs with functional PDH in the top part.

APPENDIX A

HAIRPIN ID	SEQUENCE
Non-sense hairpin	TGCTGTTGACAGTGAGCGCCAACAAGATGAAGAGCACCAATGTGAAGCCACA GATGCGTTTGGTGCTCTTCATCTTGTTGTATCTACTGCCTCGGA
PDHA1 Hairpin #1	TGCTGTTGACAGTGAGCGCTTGCTCTAGCCTGTAAGTATATAGTGAAGCCACA GATGTATATACTTACAGGCTAGAGCAATTGCCTACTGCCTCGGA
PDHA1 Hairpin #2	TGCTGTTGACAGTGAGCGCAACGATTGGCAATTTGTTATATAGTGAAGCCACA GATGTATATAACAAATTGCCAATCGTTATGCCTACTGCCTCGGA
PDHA1 Hairpin #3	TGCTGTTGACAGTGAGCGCCACAGCATTCTACCAACCATATAGTGAAGCCACA GATGTATATGGTTGGTAGAATGCTGTGATGCCTACTGCCTCGGA
PDHA1 Hairpin #4	TGCTGTTGACAGTGAGCGCCACAGCATTCTACCAACCATATAGTGAAGCCACA GATGTATATGGTTGGTAGAATGCTGTGATGCCTACTGCCTCGGA
PDHA1 Hairpin #5	TGCTGTTGACAGTGAGCGATAGCCTGTAAGTATAATGGAATAGTGAAGCCACA GATGTATTCCATTATACTTACAGGCTAGTGCCTACTGCCTCGGA
PDHA1 Hairpin #6	TGCTGTTGACAGTGAGCGACCGAATGGAGTTGAAAGCAGATAGTGAAGCCACA GATGTATCTGCTTTCAACTCCATTCGGCTGCCTACTGCCTCGGA
PDHA1 Hairpin #7	TGCTGTTGACAGTGAGCGCTTGCTCTAGCCTGTAAGTATATAGTGAAGCCACA GATGTATATACTTACAGGCTAGAGCAATTGCCTACTGCCTCGGA
PDHA1 Hairpin #8	TGCTGTTGACAGTGAGCGCAGGGAAAGGAGGATCGATGCATAGTGAAGCCACA GATGTATGCATCGATCCTCCTTTCCCTTTGCCTACTGCCTCGGA
PDHA1 Hairpin #9	TGCTGTTGACAGTGAGCGCGAGGTCTGCCTGACTTTATATTAGTGAAGCCACA GATGTAATATAAAGTCAGGCAGACCTCATGCCTACTGCCTCGGA

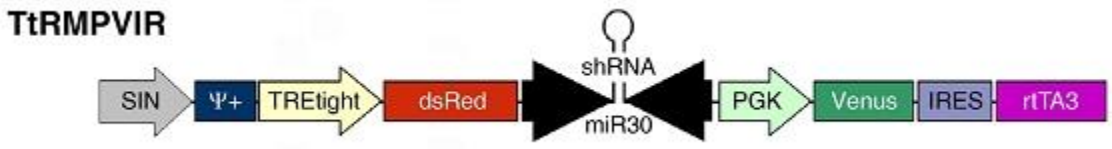

Appendix A. Hairpin sequences for knockdown of PDHA1 transcript. Ten hairpin sequences against the PDHA1 transcript (including a non-sense control) were screened to determine which silenced PDHE1α. The two that had the best silencing (hairpin #1 and hairpin #6) were cloned into a doxycycline inducible vector whose map is pictured below the chart. Vector image from (Zuber, McJunkin et al. 2011).

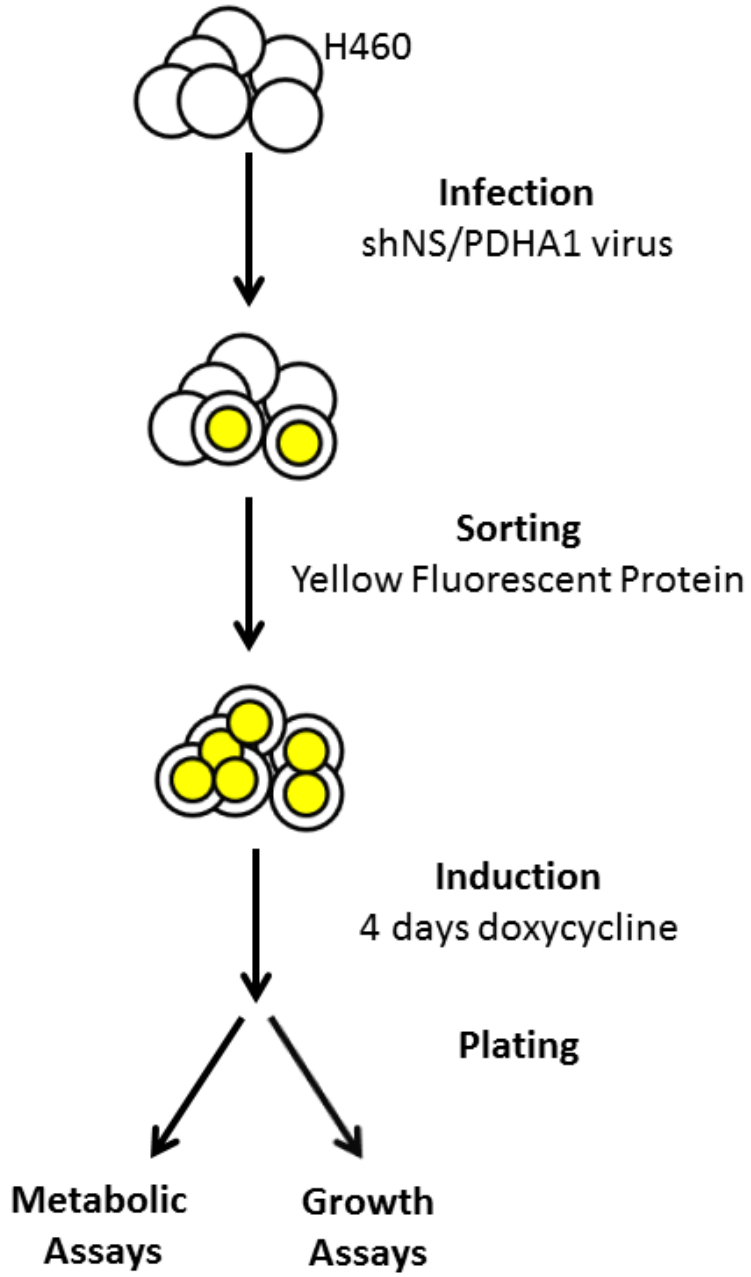

Appendix B. Experimental Approach. H460 cells were infected with virus with a control hairpin or one targeting the PDHA1 transcript. The virus constitutively expressed a YFP reporter. Cells were sorted for YFP to ensure high infection rates. Cells were then treated with doxycycline for 96 hours to ensure PDHE1α protein reduction. Metabolic and growth assays were then conducted. Cells were maintained in the un-induced state to prevent chronic metabolic changes from occurring.

BIBLIOGRAPHY

Bar-Sagi, D. and J. R. Feramisco (1986). "Induction of membrane ruffling and fluid-phase pinocytosis in quiescent fibroblasts by ras proteins." Science **233**(4768): 1061-1068.

Bax, D. A., S. E. Little, N. Gaspar, L. Perryman, L. Marshall, M. Viana-Pereira, T. A. Jones, R. D. Williams, A. Grigoriadis, G. Vassal, P. Workman, D. Sheer, R. M. Reis, A. D. Pearson, D. Hargrave and C. Jones (2009). "Molecular and phenotypic characterisation of paediatric glioma cell lines as models for preclinical drug development." PLoS One **4**(4): e5209.

Brand, K. A. and U. Hermfisse (1997). "Aerobic glycolysis by proliferating cells: a protective strategy against reactive oxygen species." FASEB J **11**(5): 388-395.

Brown, G. K., L. J. Otero, M. LeGris and R. M. Brown (1994). "Pyruvate dehydrogenase deficiency." J Med Genet **31**(11): 875-879.

Cantor, J. R. and D. M. Sabatini (2012). "Cancer cell metabolism: one hallmark, many faces." Cancer Discov **2**(10): 881-898.

Cham, B. E. and B. R. Knowles (1976). "A solvent system for delipidation of plasma or serum without protein precipitation." J Lipid Res **17**(2): 176-181.

Cheng, T., J. Sudderth, C. Yang, A. R. Mullen, E. S. Jin, J. M. Mates and R. J. DeBerardinis (2011). "Pyruvate carboxylase is required for glutamine-independent growth of tumor cells." Proc Natl Acad Sci U S A **108**(21): 8674-8679.

Ciszak, E. M., L. G. Korotchkina, P. M. Dominiak, S. Sidhu and M. S. Patel (2003). "Structural basis for flip-flop action of thiamin pyrophosphate-dependent enzymes revealed by human pyruvate dehydrogenase." J Biol Chem **278**(23): 21240-21246.

Dahl, H. H., R. M. Brown, W. M. Hutchison, C. Maragos and G. K. Brown (1990). "A testis-specific form of the human pyruvate dehydrogenase E1 alpha subunit is coded for by an intronless gene on chromosome 4." Genomics **8**(2): 225-232.

Dang, C. V. (2012). "Links between metabolism and cancer." Genes Dev **26**(9): 877-890.

DeBerardinis, R. J., J. J. Lum, G. Hatzivassiliou and C. B. Thompson (2008). "The biology of cancer: metabolic reprogramming fuels cell growth and proliferation." Cell Metab **7**(1): 11-20.

Deberardinis, R. J., N. Sayed, D. Ditsworth and C. B. Thompson (2008). "Brick by brick: metabolism and tumor cell growth." Curr Opin Genet Dev **18**(1): 54-61.

Fan, J., J. J. Kamphorst, R. Mathew, M. K. Chung, E. White, T. Shlomi and J. D. Rabinowitz (2013). "Glutamine-driven oxidative phosphorylation is a major ATP source in transformed mammalian cells in both normoxia and hypoxia." Mol Syst Biol **9**: 712.

Fendt, S. M., E. L. Bell, M. A. Keibler, B. A. Olenchock, J. R. Mayers, T. M. Wasylenko, N. I. Vokes, L. Guarente, M. G. Vander Heiden and G. Stephanopoulos (2013). "Reductive glutamine metabolism is a function of the alpha-ketoglutarate to citrate ratio in cells." Nat Commun **4**: 2236.

Halestrap, A. P., R. D. Scott and A. P. Thomas (1980). "Mitochondrial pyruvate transport and its hormonal regulation." Int J Biochem **11**(2): 97-105.

Hamanaka, R. B. and N. S. Chandel (2009). "Mitochondrial reactive oxygen species regulate hypoxic signaling." Curr Opin Cell Biol **21**(6): 894-899.

Hanahan, D. and R. A. Weinberg (2011). "Hallmarks of cancer: the next generation." Cell **144**(5): 646-674.

Hannah, V. C., J. Ou, A. Luong, J. L. Goldstein and M. S. Brown (2001). "Unsaturated fatty acids down-regulate srebp isoforms 1a and 1c by two mechanisms in HEK-293 cells." J Biol Chem **276**(6): 4365-4372.

Hardie, D. G. and D. R. Alessi (2013). "LKB1 and AMPK and the cancer-metabolism link - ten years after." BMC Biol **11**: 36.

Jones, R. G. and C. B. Thompson (2009). "Tumor suppressors and cell metabolism: a recipe for cancer growth." Genes Dev **23**(5): 537-548.

Kamphorst, J. J., J. R. Cross, J. Fan, E. de Stanchina, R. Mathew, E. P. White, C. B. Thompson and J. D. Rabinowitz (2013). "Hypoxic and Ras-transformed cells support growth by scavenging unsaturated fatty acids from lysophospholipids." Proc Natl Acad Sci U S A **110**(22): 8882-8887.
Kim, J. W., I. Tchernyshyov, G. L. Semenza and C. V. Dang (2006). "HIF-1-mediated expression of pyruvate dehydrogenase kinase: a metabolic switch required for cellular adaptation to hypoxia." Cell Metab **3**(3): 177-185.
Maher, E. A., I. Marin-Valencia, R. M. Bachoo, T. Mashimo, J. Raisanen, K. J. Hatanpaa, A. Jindal, F. M. Jeffrey, C. Choi, C. Madden, D. Mathews, J. M. Pascual, B. E. Mickey, C. R. Malloy and R. J. DeBerardinis (2012). "Metabolism of [U-13 C]glucose in human brain tumors in vivo." NMR Biomed **25**(11): 1234-1244.
Marin-Valencia, I., C. Yang, T. Mashimo, S. Cho, H. Baek, X. L. Yang, K. N. Rajagopalan, M. Maddie, V. Vemireddy, Z. Zhao, L. Cai, L. Good, B. P. Tu, K. J. Hatanpaa, B. E. Mickey, J. M. Mates, J. M. Pascual, E. A. Maher, C. R. Malloy, R. J. Deberardinis and R. M. Bachoo (2012). "Analysis of tumor metabolism reveals mitochondrial glucose oxidation in genetically diverse human glioblastomas in the mouse brain in vivo." Cell Metab **15**(6): 827-837.
Metallo, C. M., P. A. Gameiro, E. L. Bell, K. R. Mattaini, J. Yang, K. Hiller, C. M. Jewell, Z. R. Johnson, D. J. Irvine, L. Guarente, J. K. Kelleher, M. G. Vander Heiden, O. Iliopoulos and G. Stephanopoulos (2012). "Reductive glutamine metabolism by IDH1 mediates lipogenesis under hypoxia." Nature **481**(7381): 380-384.
Michelakis, E. D., G. Sutendra, P. Dromparis, L. Webster, A. Haromy, E. Niven, C. Maguire, T. L. Gammer, J. R. Mackey, D. Fulton, B. Abdulkarim, M. S. McMurtry and K. C. Petruk (2010). "Metabolic modulation of glioblastoma with dichloroacetate." Sci Transl Med **2**(31): 31ra34.
Mullen, A. R., Z. Hu, X. Shi, L. Jiang, L. K. Boroughs, Z. Kovacs, R. Boriack, D. Rakheja, L. B. Sullivan, W. M. Linehan, N. S. Chandel and R. J. DeBerardinis (2014). "Oxidation of alpha-ketoglutarate is required for reductive carboxylation in cancer cells with mitochondrial defects." Cell Rep **7**(5): 1679-1690.
Mullen, A. R., W. W. Wheaton, E. S. Jin, P. H. Chen, L. B. Sullivan, T. Cheng, Y. Yang, W. M. Linehan, N. S. Chandel and R. J. DeBerardinis (2012). "Reductive carboxylation supports growth in tumour cells with defective mitochondria." Nature **481**(7381): 385-388.
Nomura, D. K., J. Z. Long, S. Niessen, H. S. Hoover, S. W. Ng and B. F. Cravatt (2010). "Monoacylglycerol lipase regulates a fatty acid network that promotes cancer pathogenesis." Cell **140**(1): 49-61.
Patel, M. S. and L. G. Korotchkina (2001). "Regulation of mammalian pyruvate dehydrogenase complex by phosphorylation: complexity of multiple phosphorylation sites and kinases." Exp Mol Med **33**(4): 191-197.
Patel, M. S. and L. G. Korotchkina (2006). "Regulation of the pyruvate dehydrogenase complex." Biochem Soc Trans **34**(Pt 2): 217-222.
Patel, M. S., N. S. Nemeria, W. Furey and F. Jordan (2014). "The Pyruvate Dehydrogenase Complexes: Structure-based Function and Regulation." J Biol Chem **289**(24): 16615-16623.
Piva, S., M. Ganzinelli, M. C. Garassino, E. Caiola, G. Farina, M. Broggini and M. Marabese (2014). "Across the universe of k-ras mutations in non-small-cell-lung cancer." Curr Pharm Des **20**(24): 3933-3943.
Pliss, L., K. A. Hausknecht, M. K. Stachowiak, C. A. Dlugos, J. B. Richards and M. S. Patel (2013). "Cerebral Developmental Abnormalities in a Mouse with Systemic Pyruvate Dehydrogenase Deficiency." PLoS One **8**(6): e67473.
Prasad, C., T. Rupar and A. N. Prasad (2011). "Pyruvate dehydrogenase deficiency and epilepsy." Brain Dev **33**(10): 856-865.
Quehenberger, O., A. Armando, D. Dumlao, D. L. Stephens and E. A. Dennis (2008). "Lipidomics analysis of essential fatty acids in macrophages." Prostaglandins Leukot Essent Fatty Acids **79**(3-5): 123-129.
Rajagopalan, K. N. and R. J. DeBerardinis (2011). "Role of glutamine in cancer: therapeutic and imaging implications." J Nucl Med **52**(7): 1005-1008.

Shackelford, D. B. and R. J. Shaw (2009). "The LKB1-AMPK pathway: metabolism and growth control in tumour suppression." Nat Rev Cancer **9**(8): 563-575.
Sutendra, G., A. Kinnaird, P. Dromparis, R. Paulin, T. H. Stenson, A. Haromy, K. Hashimoto, N. Zhang, E. Flaim and E. Michelakis (2014). "A Nuclear Pyruvate Dehydrogenase Complex is Important for the Generation of Acetyl-CoA and Histone Acetylation." Cell **158**(1): 84-97.
Sutendra, G. and E. D. Michelakis (2013). "Pyruvate dehydrogenase kinase as a novel therapeutic target in oncology." Front Oncol **3**: 38.
Taylor, M. R., J. B. Hurley, H. A. Van Epps and S. E. Brockerhoff (2004). "A zebrafish model for pyruvate dehydrogenase deficiency: rescue of neurological dysfunction and embryonic lethality using a ketogenic diet." Proc Natl Acad Sci U S A **101**(13): 4584-4589.
Vander Heiden, M. G., L. C. Cantley and C. B. Thompson (2009). "Understanding the Warburg effect: the metabolic requirements of cell proliferation." Science **324**(5930): 1029-1033.
Warburg, O. (1956). "On the origin of cancer cells." Science **123**(3191): 309-314.
Young, J. D. (2014). "INCA: a computational platform for isotopically non-stationary metabolic flux analysis." Bioinformatics **30**(9): 1333-1335.
Zhou, Z. H., D. B. McCarthy, C. M. O'Connor, L. J. Reed and J. K. Stoops (2001). "The remarkable structural and functional organization of the eukaryotic pyruvate dehydrogenase complexes." Proc Natl Acad Sci U S A **98**(26): 14802-14807.
Zu, X. L. and M. Guppy (2004). "Cancer metabolism: facts, fantasy, and fiction." Biochem Biophys Res Commun **313**(3): 459-465.
Zuber, J., K. McJunkin, C. Fellmann, L. E. Dow, M. J. Taylor, G. J. Hannon and S. W. Lowe (2011). "Toolkit for evaluating genes required for proliferation and survival using tetracycline-regulated RNAi." Nat Biotechnol **29**(1): 79-83.